THE SLOW MANIFOLD AND THE PERSISTING GRAVITY WAVES

by

VENKATARAMANAIAH KRISHNAMURTHY

SUBMITTED TO THE DEPARTMENT OF
EARTH, ATMOSPHERIC, AND PLANETARY SCIENCES
IN PARTIAL FULFILLMENT OF THE REQUIREMENTS
FOR THE DEGREE OF

DOCTOR OF PHILOSOPHY

at the

MASSACHUSETTS INSTITUTE OF TECHNOLOGY

September 1985

Signature of Author _____
Department of Earth, Atmospheric, and Planetary Sciences
September, 1985

Certified by _____
Edward N. Lorenz
Thesis Supervisor

Accepted by _____
Theodore R. Madden
Chairman, Departmental Graduate Committee

THE SLOW MANIFOLD AND THE PERISISTING GRAVITY WAVES

by

VENKATARAMANAIAH KRISHNAMURTHY

Submitted to the Department of Earth, Atmospheric, and Planetary Sciences
in August 1985 in partial fulfillment of the requirements
for the Degree of Doctor of Philosophy

ABSTRACT

The slow manifold consists of states which are defined to be free of high-frequency gravity waves. Those solutions of primitive equations which consist of slow synoptic-scale motion with the complete absence of gravity waves must be contained in the slow manifold.

The low-order, nonlinear primitive equation (PE) model of Lorenz is studied to determine whether its solutions are embedded in a stable invariant slow manifold. The PE model consists of nine dependent variables and is derived from shallow water equations with bottom topography, forcing, and dissipation. The forcing in the model can be interpreted to be the Rossby number. An arbitrary trajectory of the model eventually approaches points of a bounded set called the attractor. The points on the three-dimensional slow manifold are determined by an algorithm based on complete separation of quasi-geostrophic (slow) and gravity waves frequencies. A low-order quasi-geostrophic (QG) model and a low-order balance equation (BE) model derived from the PE model are also studied. The QG and BE models consist of three equations which are obtained by replacing the divergence equations with the diagnostic geostrophic relation, or the classical balance equation, respectively.

All models have been studied as a function of forcing, or equivalently the Rossby number, for different values of topography. For the chosen values of the dissipation parameters, the attractors of the models are steady states for very weak forcing. As the forcing is increased, the attractors are found to be alternately chaotic and periodic. When the forcing is weak or slightly moderate, the attractors of the PE model consist of slow motion, varying on the order of a few days, with no apparent sign of the presence of gravity waves. The attractors of all the models are qualitatively similar in this range of forcing. The BE model reproduces the behavior of the PE model in a remarkably close manner for weak and slightly moderate forcing. The QG model, however, is not found to be a good approximation.

When the forcing is strong, the attractors of the PE model consist of persisting gravity waves, varying on a time scale of about six hours,

superimposed on slow motion with a few days' variation. The attractors with persisting gravity waves are predominently chaotic. The behaviors of the PE and BE models are completely different from each other in this range of forcing; this divergence is usually followed by a partiular bifurcation in the behavior. For certain values of topography, the PE model possesses a second attractor which is periodic and oscillates with gravity wave period. This periodic orbit is not superimposed on any slow motion.

The attractors of the PE model with the known presence of gravity waves for strong forcing are definitely not contained in any slow manifold defined with states found by the frequency separation algorithm. For moderate forcing, the states of the attractor and of the slow manifold are not too far apart. As the forcing decreases, the attractor gradually approaches the slow manifold. It is difficult to distinguish between the states of the slow manifold and the attractor for some values of weak forcing. The slow manifold thus does not contain the attractor. When a state in the slow manifold is used as an initial condition in the integration of the PE model the states of the subsequent evolution are not found to be contained in the slow manifold after a few days. The slow manifold is not invariant under the PE flow and the gravity waves reappear after just a few days. This initialization procedure is equivalent to a higher order nonlinear normal mode initialization scheme. The algorithm used to determine the states of the slow manifold does not yield convergent solutions at many points of the phase space of the attractor for moderate and strong forcing.

Thesis Supervisor: Edward N. Lorenz
Title: Professor of Meteorology

ACKNOWLEDGEMENTS

I would like to thank my advisor, Professor Edward Lorenz, for suggesting this problem and for his constant guidance.

I wish to thank Professors Kerry Emanuel, Paola Malanotte-Rizzoli, and Willem Malkus who served on my thesis committee. I am also thankful to Professor Mark Cane of Lamont-Doherty Geological Observatory who was my second advisor until he left M.I.T.

I would also like to thank Drs. Ronald Errico, Peter Gent, James McWilliams, and Joseph Tribbia of the National Center for Atmospheric Research and Professor James Curry and Mr. Douglas Winsand of the University of Colorado for many stimulating discussions during my visits to Boulder. I thank Dr. Piero Malguzzi of the University of Bologna with whom I had many interesting discussions when he was at M.I.T.

A very special thanks goes to Professor J. Shukla of the University of Maryland who introduced me to meteorology. His friendship and encouragement have been invaluable to me.

I wish to thank Jane McNabb and Laura Doughty for their cheerful help in every administrative matter, and Ellen Silverberg for her skillful editing of the thesis.

I was supported by the National Science Foundation grant 82-14582 ATM. All numerical computations for this thesis were performed on the computer system of the Vector Processing Facility of the Goddard Space Flight Center, Greenbelt, Maryland.

CONTENTS

Chapter 1 INTRODUCTION

The dynamics of the atmosphere is described by a set of nonlinear partial differential equations called the primitive equations. In general, the primitive equations are a combination of the equations of motion, the continuity equation, the thermodynamic equation and the equation of state. The solutions of the primitive equations are known to consist of low-frequency Rossby waves and high-frequency inertia-gravity waves. The Rossby waves, which vary on a time scale of a few days, are representative of the synoptic-scale weather patterns observed in the atmosphere. Though large-scale inertia-gravity waves are present in the atmosphere, they are considered to have very small amplitude in the troposphere. In the mid-latitudes, the large-scale motions in the atmosphere are observed to be approximately geostrophic, which means that the Coriolis force in the horizontal plane is nearly balanced by the pressure gradient force.

By performing a scale analysis of the observed large-scale motion, Charney (1948) showed that the atmosphere tends to be in a quasi-geostrophic (QG) state when the ratio of the inertial force to the Coriolis force is small compared to one. This ratio is of the same order of magnitude as the nondimensional Rossby number $\varepsilon = U/fL$, where U is a typical velocity scale, f the Coriolis parameter, and L a length scale. When ε is small, the quasi-geostrophic equations have been the most widely used approximation to the primitive equations in many theoretical studies aimed at understanding such atmospheric motions. In this approximation,

the horizontal acceleration terms are replaced by the acceleration of the geostrophic wind in the equations of motion. The quasi-geostrophic equations, whose solutions are completely free of gravity waves, were also used in the early days of numerical weather prediction.

Charney (1955) explained the geostrophic motion as the response of the atmosphere to the large horizontal and long time scales of the external energy source, the differential solar heating. Again his explanation was based on the scale analysis of the different components of atmospheric motion. Charney also suggested that the geostrophic flow was stable with respect to ageostrophic perturbations which may arise either directly from the external forcing or by nonlinear interactions. This question was examined by Errico (1981) who studied a nonlinear two-layer PE model. His results were in agreement with Charney's explanation of the quasi-geostrophic balance in the atmosphere. Errico found that the geostrophic motions were weakly unstable with respect to typical ageostrophic motions, and also discussed the importance of viscous and diabatic dissipation in restricting the amplitude of the ageostrophic modes.

Though quasi-geostrophic equations have helped to a great extent in advancing the understanding of the atmospheric dynamics, they are still a first approximation to the primitive equations in the limit $\varepsilon < 1$. The atmosphere is not always nearly geostrophic nor is the Rossby number small in many cases as U may be large or L may be small. Further, many studies that have tried to explain the quasi-geostrophic tendency of the atmosphere are linear analyses like the geostrophic adjustment and the

instability theory or are simple scale analyses. The atmosphere, however, is a forced dissipative nonlinear system with processes like advection as the source of nolinearity. The forcing is usually in the form of heat sources and sinks while dissipation can occur through mechanical and thermal means.

The importance of nonlinearity was clearly demonstrated in the pioneering studies of Lorenz (1960, 1963, 1964, 1965) who showed the existence of solutions with very interesting behavior like nonperiodicity that were completely unexpected from the studies of linear systems. In the last decade, considerable progress has been made in the mathematical understanding of the behavior of the nonlinear forced dissipative systems and quite a few of their interesting properties are now considered to be typical of many nonlinear systems regardless of what they represent. In view of these developments, an important problem is to know and understand the general solutions of the complete nonlinear primitive equations with forcing and dissipation. It is of interest to know if the solutions of the primitive equations tend to be approximately quasi-geostrophic or if inertia-gravity waves are present along with the slow motions. Following Errico's (1981) study, we can consider the primitive equations to represent nonlinear interaction between geostrophic an ageostrophic components. Whether these interactions along with the action of forcing and dissipation will render the system to be quasi-geostrophic when the Rossby number is small is an important problem to be explored. Any theoretical understanding of atmospheric dynamics by studying nonlinear primitive equations will also be quite useful in numerical weather prediction as primitive-equation (PE) models have been widely used in that

effort since the mid-60's.

Though PE models, either as general circulation models or as small models, have been used in many studies of dynamical meteorology, it was Lorenz (1980) who first studied the structure of the solutions of a nonlinear PE model with external forcing and dissipation. Lorenz was primarily interested in examining whether the solutions of the PE model tend to be near quasi-geostrophic equilibrium. His study consisted of not only comparing the solutions of the PE and the QG models but also of providing a precise quantitative characterization of the solutions without the presence of gravity waves in the PE models.

The PE model introduced by Lorenz is derived from shallow-water equations representing homogeneous, incompressible, hydrostatic, uniformly rotating flow over bottom topography. The system is forced by mass source and sink and damped diffusively by small scale motions. Since it is impossible to find analytical solutions to such nonlinear equations, the solutions are obtained by numerical integration with specified initial conditions. Since the primary purpose of Lorenz's study was to find the nature of all possible solutions of the PE model, he further simplified the model so as to obtain a large ensemble of solutions within a reasonable amount of computational time. The simplification consists of a procedure, introduced in an earlier work (Lorenz, 1960), in which the variables of the model are expressed as a linear combination of a finite number of spatially orthogonal functions. The coefficients of the linear combination become the dependent variables of the resulting set of ordinary differential equations (ODE's). Such low-order models have been

found useful in studying the effects of nonlinearity as demonstrated in many studies of Lorenz and others (see review by Lorenz, 1982). Low-order models enable us to obtain a large set of solutions or a solution on a long time scale with much less computational time than required by larger models, and to reproduce qualitative features of the atmospheric processes. In the PE model of Lorenz, the basis set of functions for spectral expansion consists of an interacting triad resulting in a set of nine ODE's. The corresponding QG model, a set of three ODE's, is constructed by neglecting certain small terms containing divergence. The QG model is equivalent in its form to the well-known convection model of Lorenz (1963).

Like the low-order models, a set of N ODE's describing the time evolution of N variables is known as a dynamical system. The states of the dynamical system can be represented by points in an N-dimensional phase space whose coordinates are just the N dependent variables. Therefore, a trajectory in the phase space is the time evolution initiating from a particular state. For a general class of forced dissipative dynamical systems discussed by Lorenz (1963), the volume in phase space usually contracts with the evolution of time. In such bounded dissipative systems, all the orbits will eventually enter a bounded region of phase space with zero volume. The set of all points encountered asymptotically by the orbits is the attractor of the forced dissipative dynamical system. The qualitative theory of ordinary differential equations is well discussed by Arnold (1973) and by Hirsch and Smale (1974) and the basic theory and the recent developments of dynamical systems are discussed by Guckenheimer and Holmes (1983). Familiar

examples of an attractor are the steady state and periodic solutions. The steady state solutions are fixed points in the phase space whereas the periodic solutions form closed orbits. However, as Lorenz (1963) discovered in his convection model, the most interesting behavior of a dynamical system involves solutions which vary nonperiodically with time. Such attractors have come to be known as strange or chaotic attractors and have very intricate geometrical structures. Strange attractors are unions of several unstable manifolds and when intersected with a curve transverse to the unstable manifolds, they reveal cantor-set structure. Since chaotic attractors consist of unstable orbits, they have extremely sensitive dependence on initial conditions (Lorenz, 1963, 1965). The nature of the attractor of a system may change as the external parameters, such as forcing, are varied. When such a change occurs, the system is said to undergo a bifurcation. Many of the bifurcations from steady state to periodic attractors, and from periodic to chaotic attractors found in Lorenz's convection model (Sparrow, 1982) are quite typical of the behavior of many dynamical systems (Guckenheimer & Holmes, 1983).

Thus, in the study of the nine-variable PE model, Lorenz's primary concern was to find its attractor and compare it to the attractor of the QG model. In order to find how the attractor looks like, it is necessary to generate a large number of solutions using different initial conditions and to integrate the model over long time. This point should help us appreciate the necessity of choosing to study one of the simplest low-order models. As Lorenz points out, in a dry PE model with 3N ODE's, all the geostrophic states are contained in an N-dimensional subspace.

However, the steady state and the periodic attractors are respectively zero- and one-dimensional. Therefore, Lorenz chose to study the PE model when the attractor is chaotic in order to provide a meaningful comparison with the QG attractor. The values of the physical parameters he used corresponded to large-scale motion in the mid-latitude atmosphere. The attention on the dynamical processes is thus focussed on Rossby motion, gravity waves and their interactions.

For a particular value of forcing, Lorenz found the attractor of the PE model to be chaotic. For an orbit starting from an arbitrary point, gravity wave oscillations are present initially but will disappear after a few days resulting in a motion with a slow time scale. The attractor of the PE model is shown to have good qualitative resemblance to the QG attractor, though not for the same value of forcing. Many states on the PE attractor are found to be in approximate geostrophic balance. On a more precise quantitative level, Lorenz showed that the PE attractor was embedded in a three-dimensional stable invariant manifold devoid of gravity waves. Here, the invariance is, of course, defined with respect to the flow determined by the primitive equations. By stable manifold, it is meant that an orbit emanating from a state not on the slow manifold will eventually reach the attractor and hence will be in the slow manifold in which the attractor is embedded. The states belonging to this invariant manifold can be determined using an algorithm devised by Lorenz based on separation of quasi-geostrophic and gravity wave frequencies. Lorenz termed the equation that would determine the invariant manifold as superbalanced equation, the explicit form of which is difficult to know.

In numerical weather prediction where large PE models are used, one of the difficult problems faced is the excitation of gravity waves of unrealistically large amplitudes. The generation of such gravity waves is due to the initial imbalances between the wind and pressure fields created by the errors in observed and analyzed data. This difficulty usually has been resolved by adopting some initialization procedure which specifies balanced initial fields, and the subsequent motion is expected to be free of gravity waves. When discussing the possibility of using PE models for weather prediction, Charney (1955) introduced the nonlinear balance equation as an initialization method to determine wind from pressure fields. The balance equation, which is a generalization of geostrophic approximation, was derived from the scale analysis of large-scale atmospheric motion. Using a simple model, Charney showed that the motion, initialized with the balance equation, continued to be approximately balanced for some time; the balance equation thus describes a nearly invariant manifold. Another method that has been used with some success is the nonlinear normal mode initialization scheme (Daley, 1981) developed independently by Machenhauer (1977) and Baer (1977) and generalized to some extent by Baer and Tribbia (1977). In this procedure, the model equations are expressed in terms of the normal linear modes (Rossby and gravity modes) and the time derivatives of the gravity modes are set to zero to obtain a nonlinear balance equation which can be solved iteratively. Machenhauer's scheme consists of finding the balanced initial fields by simply setting the first time derivatives of the gravity modes equal to zero.

Using a simple, f-plane Boussinesq model, Leith (1980) examined

the connection between Machenhauer's first-order normal mode scheme and the traditional quasi-geostrophic theory and showed that the two were equivalent. The equations of dynamics expressing the conservation of the pseudo-potential vorticity in the normal mode scheme, referred to as quasi-rotational dynamics by Leith, were shown to be identical to the quasi-geostrophic equations. For the initialization of the quasi-rotational dynamics, Leith derived a three-dimensional nonlinear balance equation which reduced to Charney's balance equation in two dimensions. Leith suggested that a higher order nonlinear normal mode scheme, an extension of the methods of Machenhauer and Baer, would produce a converged balance model with solutions identical to those of the corresponding PE model. The states determined by such a balance model belong to a nonlinear invariant manifold in the multidimensional phase space made up of linear Rossby and gravity manifolds. On this nonlinear manifold, which has been named slow manifold by Leith, any state would evolve in time slowly without the presence of high-frequency oscillations.

Whereas Leith introduced the slow manifold as a useful geometrical concept in the initialization problem, Lorenz actually demonstrated the existence of such an invariant manifold in which the attractor of the PE model was embedded. It is obvious that a higher order nonlinear normal mode initialization scheme is equivalent to the algorithm for determining Lorenz's superbalance states when the PE model is expressed in terms of the linear normal modes. Thus the ideal initialization scheme is one in which the data is projected onto the attractor using the superbalance equation provided the attractor is embedded in a stable slow manifold.

When the Rossby number ε is small ($\varepsilon < 1$), the quasi-geostrophic equations can be derived as order ε approximation in primitive equations by expanding the dependent variables in a power series in ε (Charney, 1973, ch. VII; Pedlosky, 1979, ch. 6). In view of Leith's result demonstrating the equivalence between the quasi-geostrophic and the quasi-rotational equations, it is interesting to know whether the higher order approximation in the Rossby number expansion would be an equation for the slow manifold. This problem is too complicated to be solved. However, using certain mathematical theorems of the invariant manifold theory of singularly perturbed systems, Kopell (1985) argues that there should exist a lower dimensional attracting invariant manifold for Lorenz's nine-variable PE model. In Kopell's discussion, the primitive equations are written in terms of variables rescaled with a small parameter like Rossby number ε and the quasi-geostrophic equations are obtained in the limit as $\varepsilon \to 0$. On the invariant manifold, the flow is described to be a regular perturbation of the QG flow for small ε. She also concludes that Lorenz's algorithm for finding the states on the invariant manifold is equivalent to the bounded derivative method of Kreiss (1979) (Kasahara, 1982) and that both the methods provide the correct asymptotic expansion for the invariant manifold in powers of ε.

Thus, for the value of the forcing considered by Lorenz, the points on the attractor of the PE model are approximately geostrophic and the attractor itself is embedded in a three-dimensional invariant manifold as found numerically. The existence of the slow manifold is claimed on theoretical grounds, by Kopell (1985), for a small Rossby number. However, the Rossby number is not always small in the atmosphere. The

forcing in Lorenz's PE model can be considered to be a measure of Rossby number when the dissipation parameters remain constant. For a value of forcing higher than that considered by Lorenz, it is interesting to know whether the gravity wave oscillations, if initially present, will vanish or will continue to be present when the attractor is reached. Though gravity wave oscillations are known to be part of the solutions of many PE models, as found in the studies of Errico (1981, 1982) and Hoffman (1981) for example, the nature of the entire attractor has not been studied. It is not known what the attractors with persisting gravity-wave oscillations look like in Lorenz's nine-variable PE model. Gent and McWilliams (1982) studied Lorenz's PE model as a function of forcing; however, their interest was focussed on the performance of the approximate models intermediate between PE and QG models. They have not studied the nature of the attractors of the PE or other models in any detail, and are uncertain about the persistence of gravity waves in the solutions of PE model for moderate to strong forcing. Their study did not include any discussion of the slow manifold.

For the case studied by Lorenz, all the states of the PE attractor are either approximately geostrophic or are nearly satisfied by the balance equation. For a higher value of forcing, if the solutions consist of high-frequency gravity waves, it is interesting to know if quasi-geostrophic states are also part of the attractor. If the attractor is chaotic, we would like to understand how the system visits quasi-geostrophic states from time to time and moves into ageostrophic regions of the phase space.

In his numerical comparisons, Lorenz found that the points on the attractor agreed with the corresponding states determined by superbalance algorithm to five decimal places. It is not known whether the agreement is better than Lorenz's result. Therefore it is also not clear whether the slow manifold determined by Lorenz's alogrithm is exactly invariant under the PE flow for the value of forcing used by Lorenz. An appropriate question to address is whether the forcing corresponds to a "small" Rossby number, in the sense Kopell uses, so that the attractor is identical to the states of an invariant slow manifold. We would like to know whether there exists an attracting invariant slow manifold for any value of the forcing for which the attractors are either periodic or chaotic. According to the definition of Lorenz's superbalance equation, steady state solutions belong to the slow manifold. For a range of values of forcing smaller than the one studied by Lorenz, the PE model has steady states as attractors. Therefore, it is necessary to reexamine more precisely the solutions of the superbalance algorithm and to compare the superbalanced state with the attractor, which are not fixed points, for small value of forcing.

For a higher value of forcing or, equivalently Rossby number, it is interesting to find what the initialization procedure with the superbalance algorithm would produce. If the attractor contains gravity waves, it should not be expected to be embedded in a slow manifold even if the "dimension" of the chaotic attractors were less than three. However, it is still interesting to find the solutions of the superbalance algorithm for all the regions of the phase space of the attractor. The convergence of the solutions of the algorithm is itself a matter of great

importance. If it is possible to obtain a converged solution, the difference between the states of the attractor and the corresponding superbalance states will provide an estimate of the amount of deviation from quasi-geostrophic equilibrium. The initialization procedure with a converged superbalanced state will determine whether or not the slow manifold is invariant under the PE flow. If any points on the attractor are different from the superbalance states and if there exists an invariant slow manifold, then the slow manifold is unstable. However, if the slow manifold is not invariant, then the initialization procedure using some converged superbalance state may damp the gravity waves for some time initially, but eventually the system should reach the attractor.

The aim of this thesis is to determine whether there exists an invariant slow manifold in which the attractor is embedded for any small value of the Rossby number, and to investigate the stability and invariance of the slow manifold as the Rossby number is varied. It must be emphasized that the slow manifold is defined here strictly as consisting of states determined by Lorenz's superbalance algorithm. We intend to study the nature of the attractor as far as its relation to quasi-geostrophic equilibrium is concerned and to find whether persisting gravity waves are present in the attractor of the PE model as the Rossby number is increased. If possible, we would like to obtain a picture of the attractor of the PE model containing the gravity waves and compare it with the attractors of the BE and QG models. To this end, Lorenz's nine-variable PE model will be studied numerically as a function of forcing which can be considered to be a measure of the Rossby number.

The attractors of the PE model will be determined and will be compared with attractors of the BE and QG models in order to gain a qualitative understanding of the extent to which the solutions PE model do not contain gravity waves. The solutions of the PE model will be examined for the presence of the gravity waves as the forcing is increased. The various bifurcations in the forcing parameter space will be determined for all the models and the results will be compared. When a nonlinear system undergoes a bifurcation, a drastic change occurs in the nature of its attractor. Therefore, we would like to know the extent to which the bifurcations of the PE and BE or QG models are similar. We also wish to find if the behavior of the two models will be completely different following any particular bifurcation. We will investigate whether any bifurcation of the PE model coincides with the appearance of persisting gravity waves in the attractor and whether such an event could be detected.

For all the values of forcing to be studied, the superbalnce algorithm will be applied for many points on the PE attractors and the solutions will be tested for convergence. The superbalance states will be compared with the points on the attractor to determine whether or not the attractor is embedded in a slow manifold. By integrating the PE model using superbalnce state as initial condition, and comparing the evolved states with their corresponding superbalance states, the invariance of the slow manifold will be determined. The stability of any invariant slow manifold that is found to exist will also be tested. Employing these various procedures, we will try to determine if there exists an attracting invariant slow manifold for any value of forcing for which the attractor

is not a fixed point. If such an attracting invariant slow manifold exists, we will investigate its existence as the forcing is increased. Even if the invariant slow manifold exists for all values of forcing, the attractor may not be contained in the slow manifold for all the values. If such is the case, we would like to know if the change occurs suddenly or whether it is gradual in the forcing parameter space, and whether there is any relation to the regular bifurcations of the PE model.

The outline of the thesis is as follows. In Chapter 2, we present a physical description of the model and derive the equations for the low-order PE, BE and QG models. The numerical methods used in obtaining the solutions of the model are given and some properties of the equations are discussed. The choice of the numerical values of various parameters used are also given.

In Chapter 3, we will discuss the behavior of all the models, found numerically, as a function of forcing. The attractors and the bifurcations of the PE model are compared with those of the BE and the QG models, and similarities and differences are discussed. These studies are also performed for different values of the topography to demonstrate the existence of different kinds of attractors of the PE model and show major differences with the BE model. The nature of the attractors of the PE model and its relation to quasi-geostrophic equilibrium, and the existence of persisting gravity waves are discussed.

Chapter 4 is devoted to the discussion of the slow manifold. The numerical results of the application of Lorenz's superbalance algorithm

are presented. The initialization procedure is used to determine the existence of the invariant slow manifold. The states belonging to the attractor are compared to those of the slow manifold. All the experiments are performed as as a function of forcing and the change in the behavior of the attractor and its relation to the slow manifold are discussed. Finally, in Chapter 5, a summary of the results is presented and certain conclusions on the existence of the slow manifold and on the attractors with persisting gravity waves are stated.

Chapter 2 THE MODELS

2.1. PRIMITIVE EQUATIONS (PE)

The primitive equation model studied by Lorenz (1980) is derived from the shallow water equations representing a flow of homogeneous, incompressible fluid of average depth H on a rotating plane with constant Coriolis parameter f. The fluid moves over a surface of infinite horizontal extent and topographic height h(r), and its upper surface is at height H + z(r,t) where r is a horizontal position vector and t is time. The fluid is assumed to obey hydrostatic conditions and its vertical velocity is determined from the continuity of mass. The horizontal velocity V(r,t) of the fluid is independent of height. The forcing for the flow is in the form of a mass source and sink F(r), while small scale motions are assumed to damp the flow diffusively with coefficients κ and ν. The governing equations are

$$\partial V/\partial t = -(V.\nabla)V - fk \times V - g\nabla z + \nu\nabla^2 V, \tag{2.1}$$

$$\partial z/\partial t = -(V.\nabla)(z - h) - (H + z - h)\nabla.V + \kappa\nabla^2 z + F, \tag{2.2}$$

where g is the acceleration due to gravity and k is a unit vector in the vertical direction.

The horizontal velocity can be separated into divergent and rotational parts as

$$V = \nabla\chi + k \times \nabla\psi \tag{2.3}$$

where χ is the velocity potential for the divergent part and ψ is the streamfunction. Then, from (2.1), the equations for divergence $\nabla^2\chi$ and vorticity $\nabla^2\psi$ are given by

$$\partial\nabla^2\chi/\partial t = -1/2\nabla^2(\nabla\chi.\nabla\chi) - (\nabla\chi.\nabla(\nabla^2\psi) \times k + \nabla^2(\nabla\chi.\nabla\psi \times k) + \nabla.(\nabla\psi\nabla\psi) - 1/2\nabla^2(\nabla\psi.\nabla\psi) + \nu\nabla^4\chi + f\nabla^2\psi - g\nabla^2 z, \quad (2.4)$$

$$\partial\nabla^2\psi/\partial t = -1/2\nabla.(\nabla^2\psi\nabla\chi) - \nabla\psi.\nabla(\nabla^2\psi) \times k - f\nabla^2\chi + \nu\nabla^4\psi, \quad (2.5)$$

and, from (2.2), we have

$$\partial z/\partial t = -\nabla.(z - h)\nabla\chi - \nabla\psi.\nabla(z - h) \times k - H\nabla^2\chi + \kappa\nabla^2 z + F. \quad (2.6)$$

By introducing three dimensionless horizontal vectors α_1, α_2, and α_3, whose sum is zero, (2.4) - (2.6) can be converted into a low-order model. With a horizontal length scale L, the model variables are expanded in a basis set of orthogonal functions

$$\phi_i = \cos(\alpha_i.r/L), \qquad i=1,2,3. \quad (2.7)$$

Certain constants are defined as

$$a_i = \alpha_i.\alpha_i,$$
$$b_i = \alpha_j.\alpha_k,$$
$$c_i = \alpha_j \times \alpha_k.k = (b_1b_2 + b_2b_3 + b_3b_1)^{1/2} = c, \quad (2.8)$$

for (i,j,k) in cyclic order. The nondimensional variables are defined as

$$t = f^{-1}\tau,$$
$$\chi = 2L^2f \sum x_i\phi_i,$$
$$\psi = 2L^2f \sum y_i\phi_i,$$
$$z = 2L^2f^2g^{-1} \sum z_i\phi_i$$

$$h = 2L^2f^2g^{-1} \sum h_i\phi_i,$$
$$F = 2L^2f^3g^{-1} \sum F_i\phi_i, \tag{2.9}$$

where the summations are from 1 to 3.

The nondimensional variables in (2.9) are substituted in (2.4) - (2.6), and, after neglecting the parts of the nonlinear terms which do not project onto the basis functions, the equations of the low-order PE model are obtained as

$$a_i dx_i/d\tau = a_i b_i x_j x_k - c(a_i - a_k)x_j y_k + c(a_i - a_j)y_j x_k - 2c^2 y_j y_k - \nu_0 a_i{}^2 x_i + a_i y_i - a_i z_i, \tag{2.10}$$

$$a_i dy_i/d\tau = - a_k b_k x_j y_k - a_j b_j y_j x_k + c(a_k - a_j)y_j y_k - a_i x_i - \nu_0 a_i{}^2 y_i, \tag{2.11}$$

$$dz_i/d\tau = - b_k x_j (z_k - h_k) - b_j (z_j - h_j)x_k + cy_j(z_k - h_k) - c(z_j - h_j)y_k + g_0 a_i x_i - \kappa_0 a_i z_i + F_i, \tag{2.12}$$

where $g_0=ghL^{-2}f^{-2}$, $\nu_0=\nu L^{-2}f^{-1}$, $\kappa_0=\kappa L^{-2}f^{-1}$, and (i,j,k) = (1,2,3), (2,3,1) or (3,1,2). By assuming α_1 to be pointing northward, the variables with subscript 1 will denote zonally uniform fields, whereas the superposed waves are denoted by those with subscripts 2 and 3.

2.2. QUASI-GEOSTROPHIC (QG) EQUATIONS AND BALANCE EQUATIONS (BE)

As discussed by Charney (1948), the geostrophic approximation can be used in the equations of motion in a dynamically consistent manner by

omitting the terms containing the horizontal divergence and by replacing the horizontal wind with the geostrophic wind. Thus, the QG model is constructed, as Lorenz (1980) has shown, by neglecting all the terms containing the x's and all the nonlinear terms in (2.4), and all the nonlinear or topographic terms with the x's in (2.5) and (2.6). After eliminating the x's and the z's, we obtain the QG equations as

$$y_i = z_i, \tag{2.13}$$

$$(a_i g_0 + 1)dy_i/d\tau = g_0 c(a_k - a_j)y_j y_k - a_i(a_i g_0 \nu_0 + \kappa_0)y_i - ch_k y_j + ch_j y_k + F_i. \tag{2.14}$$

The derivation of the balance equation (Charney, 1955) is based on the observation that the horizontal divergence is small in some cases even if the Rossby number is not small and that the vertical advection terms are smaller than the other advection terms in the horizontal equations of motion. The vertical advection terms do not appear in the divergence equation (2.10) or the vorticity equation (2.11). Therefore, in the divergence equation (2.4), all the terms containing the horizontal divergence are neglected to obtain the balance equation as

$$\nabla.(\nabla^2\psi\nabla\psi) - 1/2\nabla^2(\nabla\psi.\nabla\psi) + f\nabla^2\psi = g\nabla^2 z, \tag{2.15}$$

or, equivalently, from (2.10), we obtain

$$a_i y_i - 2c^2 y_j y_k = a_i z_i. \tag{2.16}$$

Since the vorticity and height equations do not require any modifications, (2.11) or (2.12) along with (2.16) constitute the BE model. We note that

the balance equation (2.16) reduces to the geostrophic relation (2.13) if the nonlinear terms in (2.16) are small.

The quasi-geostrophic equations (2.14) can be derived in a more systematic manner, as has been demonstrated by Charney (1973, ch. VII), Pedlosky (1979) and McWilliams and Gent (1980), as a first-order approximation in a Rossby number expansion of the primitive equations. For this purpose, the variables of (2.4) - (2.6) can be nondimensionalized in a manner different from (2.9) by introducing a velocity scale U and by defining

$$
\begin{aligned}
t &= UL^{-1}\tau \\
\chi &= 2UL \sum x_i \phi_i \\
\psi &= 2UL \sum y_i \phi_i \\
z &= 2UfLg^{-1} \sum z_i \phi_i \\
h &= 2UfLg^{-1} \sum h_i \phi_i \\
F &= 2Uf^2Lg^{-1} \sum F_i \phi_i
\end{aligned}
\tag{2.17}
$$

When (2.17) are substituted in (2.4) - (2.6), the Rossby number $\varepsilon = U/fL$ appears explicitly in the nondimensional PE model that is equivalent to (2.10) - (2.12). By expanding the variables x_i, y_i and z_i in a power series in ε, for small ε, the quasi-geostrophic equations identical in form to (2.14) can be obtained as order ε approximation provided κ_0, ν_0 and F_i are proportional to ε and g_0 is an order 1 quantity. Thus F_i can be interpreted to be the Rossby number when κ_0 and ν_0 are chosen to be of order ε. Gent and McWilliams (1982) note that F_i should be proportional to the square of the Rossby number in such an analysis.

Since they have not shown this explicitly, the origin of the discrepancy is unknown.

2.3. GENERAL PROPERTIES OF THE MODELS

The QG model (2.14), in the absence of forcing and dissipation, possesses a positive definite quadratic invariant quantity

$$E_q = 1/2 \sum_i (a_i g_0 + 1) y_i^2 \tag{2.20}$$

which may be treated as the total energy of the model. When the forcing and dissipation are included, we have, from (2.14),

$$dE_q/d\tau = - \sum_i a_i (a_i g_0 \nu_0 + \kappa_0) y_i^2 + \sum_i F_i y_i . \tag{2.21}$$

If E_1 is an ellipsoid whose surface is represented by $dE_q/dt = 0$ in (2.21), then, outside E_1, the dissipation dominates the forcing in such a way that $dE_q/dt < 0$. If an ellipsoid E_2 represented by (2.20) contains E_1 in its interior, then each orbit will eventually be trapped in E_1.

The truncated PE model (2.10) - (2.12), however, does not conserve any positive definite quantity with quadratic terms when the forcing and dissipation are not present because the energy in the continuous model (2.1) - (2.2) is not quadratic. Therefore, when the forcing is strong, all the orbits of the PE model may go to infinity. If we define

$$E_p = 1/2 \sum_i [a_i (x_i^2 + y_i^2) + g_0^{-1} z_i^2] \tag{2.22}$$

as the energy of the PE model, then, as Lorenz (1980) has explained, it is possible that $dE_p/dt < 0$ between two spheres R_1 and R_2. Outside the

outer sphere R_2, all the orbits will go to infinity, while all the orbits within R_2 will ultimately be trapped in R_1. For the same reason as in the PE model, the BE model does not possess any quadratic energy invariant quantity, but will have bounded solutions for a sufficient range of values of forcing.

In all three models, the volume of the phase space V_0 changes with time according to the equation

$$dV_0/d\tau = -V_0 \sum_i b_i, \tag{2.23}$$

where

$$b_i = (2\nu_0 + \kappa_0)a_i \qquad \text{for PE model,}$$

$$= a_i(a_i g_0 \nu_0 + \kappa_0)/(a_i g_0 + 1) \qquad \text{for QG model.}$$

The explicit expression of b_i for the BE model is difficult to find, but still involves terms containing ν_0 and κ_0. Since $\sum b_i$ is positive definite, the volume V_0 decreases exponentially and hence the attractor is is a bounded set of zero volume. Thus, for a range values of forcing, the attractors for all the models can be found by numerical integration with suitable initial conditions.

2.4. METHOD OF SOLUTION AND CHOICE OF NUMERICAL VALUES

The solutions of all the models are obtained by numerical integration using Taylor series scheme which consists of calculating the first n time derivatives of each variable at time τ. At time $\tau + \Delta\tau$, where $\Delta\tau$ is a small increment, any variable s is evaluated as

$$s(\tau + \Delta\tau) = \sum_{k=0}^{n} [d^k s(\tau)/d\tau^k]\Delta\tau^k/k!. \tag{2.18}$$

If the expression for $ds/d\tau$ is known, then any higher order time derivative, $d^k s/d\tau^k$, can be evaluated easily, and the summation in (2.18) can be extended to any desired n. Therefore, it is straightforward to integrate PE and QG models since the expressions for the first derivatives of all the dependent variables are known explicitly.

The integration of the BE model, however, involves an inversion of a matrix to evaluate x_i at each time step. Substituting (2.11) and (2.12) in (2.16) after differentiating once, the diagnostic equation for x_i is obtained as

$$\begin{aligned}
&\{a_i a_j a_k(1 + g_0 a_i) - 2c^2(a_j{}^2 b_j y_j{}^2 + a_k{}^2 b_k y_k{}^2)\}x_i \\
&- \{a_j a_k[y_k(2c^2 - a_k b_k) + (a_i b_k(z_k - h_k)] + 2c^2 a_i a_j b_i y_i y_j\}x_j \\
&- \{a_j a_k[y_j(2c^2 - a_j b_j) + (a_j b_j(z_j - h_j)] + 2c^2 a_i a_k b_i y_i y_k\}x_k \\
&\quad = a_j a_k\{c(a_k - a_j)y_j y_k + ca_i[(z_j - h_j)y_k - y_j(z_k - h_k) \\
&\qquad + a_i[a_i(\kappa_0 z_i - \nu_0 y_i) - F_i]\} + 2c^2[ca_j(a_j - a_i)y_i y_j{}^2 \\
&\qquad + ca_j(a_i - a_k)y_i y_k{}^2 - \nu_0 a_j a_k(a_j + a_k)y_j y_k].
\end{aligned} \tag{2.19}$$

Thus, at each time step of the integration of the BE model, the values of z_i are first found from the balance equation (2.16) for given y_i and then the values of x_i are determined from (2.19) by inverting a matrix. We then use the vorticity equation (2.11) and the Taylor series scheme (2.18) to advance y_i in time. A problem unique to the BE model is the possible singularity of the matrix in (2.19). This singularity, which has been referred to as the solvability condition by Gent and McWilliams

(1982), for the BE and other intermediate models is discussed in detail by Curry and Winsand (1985). The solvability condition is not relevant to this thesis as long as the attractor of the BE model can be found.

The numerical values of most of the physical constants will be chosen to be those used by Lorenz (1980) corresponding to large-scale motion in the midlatitude atmosphere. We shall let

$$L = 1080 \text{ km}, \qquad H = 8 \text{ km},$$

$$f^{-1} = 3 \text{ h}, \qquad g = 10 \text{ m s}^{-2}$$

and $\kappa = \nu = 2.25 \times 10^6 \text{ m}^2 \text{ s}^{-1}$.

Thus, the numerical values of the nondimensionalized parameters become

$$g_0 = 8, \qquad \kappa_0 = \nu_0 = 1/48,$$

and, we also choose

$$a_1 = a_2 = 1, \quad a_3 = 3.$$

The values of κ_0 and ν_0 mean that the variables with subscripts 1 and 2 have 6-day diffusive damping time while those with subscript 3 have 2-day damping time. The forcing and the topography will be zonally uniform by letting

$$F_2 = F_3 = 0, \qquad h_2 = h_3 = 0.$$

With such a choice of numerical values, Lorenz (1980) has shown that the QG model (2.14) can be transformed into a form identical to his well known three-variable convection model (Lorenz, 1963). In order that the QG

model exhibit interesting behavior, it is necessary to choose negative values for h_1 and positive values for F_1. Such a choice will also ensure that they are physically relevant representation of the atmosphere. In this thesis, all the models have been studied with different values of F_1 and h_1.

For the Taylor series scheme (2.18) used in the numerical integration, we shall choose n = 4 and $\Delta\tau$ = 1/12 (=15 min.) for most of the cases. For the BE and the QG models, whose solutions do not contain gravity waves, we can use $\Delta\tau$ = 1 (=3 h) for small values of forcing. These values of n and $\Delta\tau$ ensure sufficient numerical accuracy and computational stability. When the forcing is stronger, we must decrease the value of $\Delta\tau$ for stability. In such cases, for the PE model, we shall use $\Delta\tau$ = 1/24. However, in some of the more precise calculations, we shall be employing a higher value for n and a very small time step $\Delta\tau$ depending on the accuracy required. The exact values of these will be specified when discussing such cases in the next two chapters.

With the choice of the forcing and topography to be zonally uniform, the equations of all three models remain unchanged if all the variables with subscripts 2 and 3 change sign. This symmetry exists for all values of F_1 and h_1. The solutions which remain invariant under the symmetry operation will be referred to as symmetric solutions. Therefore, non-symmetric solutions will always occur in pairs.

Chapter 3 BEHAVIOR OF THE MODELS

In this chapter we will discuss the behavior of the models as the forcing F_1 is varied for different values of the topography h_1. The zonally uniform topography simulates the effects of the β-term which would result from a variable Coriolis parameter f and is responsible for the excitation of topographic Rossby waves. We will first describe the solutions of the PE model for h_1=-1.0 which is the value used in Lorenz's study. The behavior of the PE model will then be compared to those of the BE and QG models. The results of similar studies for different values of h_1 will also be described. Finally, we will discuss the persistence of gravity waves in the solutions for different cases.

3.1. PE MODEL WITH $h_1 = -1.0$

For all values of forcing F_1, the PE model possesses a steady state solution which is purely zonal and nearly geostrophic. This stationary solution, which has been referred to as the Hadley solution by Lorenz (1980), is given by

$$\begin{aligned} x_1 &= -\nu_0 a_1 y_1 \\ y_1 &= F_1/a_1\nu_0(\nu_0^2 a_1^2 + g_0 a_1 + 1) \\ z_1 &= (1 + \nu_0^2 a_1^2) y_1 \\ x_2 &= y_2 = z_2 = x_3 = y_3 = z_3 = 0. \end{aligned} \tag{3.1}$$

The Hadley solution (H) is stable for small values of F_1; a linear stability analysis shows that H becomes unstable at F_1=0.015. The loss of

stability of the Hadley fixed point coincides with two new steady state solutions coming into existence. These fixed points, which will be called B_1 and B_2, on the new branches are not zonally uniform (i.e., the variables with subscripts 2 and 3 are nonzero). Each of these two solutions is an image of the other under the symmetry of the equations of the model (see Sec. 2.4).

The bifurcation involving the instability of the Hadley fixed point and the simultaneous appearance of B_1 and B_2 is a pitchfork bifurcation. The numerical determination of the steady states B_1 and B_2 is based on Newton's method with good initial guesses. In Appendix A, we discuss Newton's method of determining the fixed points and the different types of bifurcations of steady states.

As F_1 is increased, B_1 and B_2 continue to be stable for a while, and both loose stability at F_1=0.0533 due to a Hopf bifurcation (see Appendix A). The imaginary parts of the complex conjugate pair of eigenvalues of the linearized flow which cross the imaginary axis at the bifurcation indicate that a small perturbation over B_1 or B_2 oscillates with a period of about 11 days.

Apart from the steady states H, B_1 and B_2, we have determined the existence of other (at least six) fixed points using Newton's method. However, all these other fixed points are found to be unstable and are located in regions of phase space which are of no relevance to atmospheric conditions.

A second bifurcation of the already unstable Hadley fixed point occurs at F_1=0.0774. This is a Hopf bifurcation and the imaginary parts of the complex pair of eigenvalues which crosses the imaginary axis correspond to an instability with gravity wave period (about 6 hours). The consequences of this Hopf bifurcation will be discussed later.

When the steady states B_1 and B_2 become unstable at F_1=0.0533, the solutions of the PE model are found to be nonperiodic. These solutions have been obtained by numerical integration with many different initial conditions which include small departure from Hadley solution, a value of 0.1 for all the variables and other arbitrary points. The model is usually integrated for a long time so that the transients damp out and the orbits reach the attractor. In all the cases, we have examined the time series of different variables and the Poincare cross-sections which are merely the intersections of the orbits with some specifically chosen surface transverse to the flow. If the orbits are periodic, the Poincare cross-sections consist of a few points which are visited by the orbits in a particular order at regular intervals. However, when the attractor is chaotic, the cross-sections will have complicated structures and could be without any order. We have studied the solutions of the PE model as a function of F_1 and have found that the solution goes to infinity at $F_1 \approx 0.68$ due to the reasons discussed in Sec. 2.3. The behavior of the model is shown schematically in Fig. 3.1 and the values of F_1 corresponding to the different regimes of behavior are listed in Table 3.1.

The Hopf bifurcation at F_1=0.0533 is found to be subcritical,

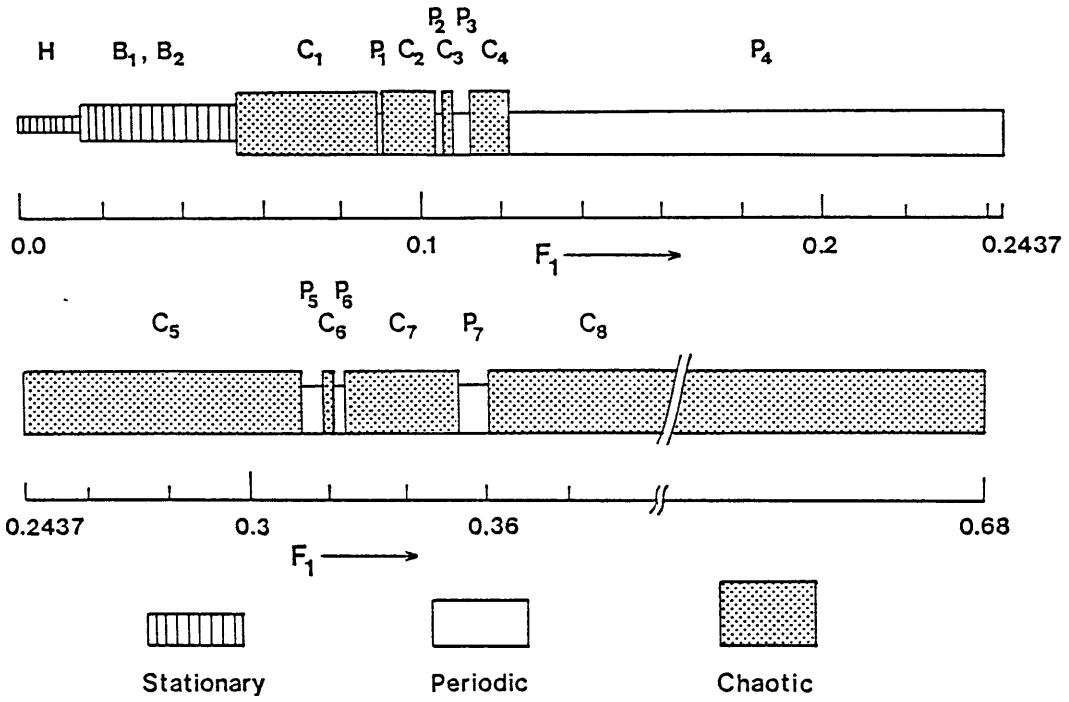

Figure 3.1. Behavior of the PE model ($h_1 = -1.0$)

Regime	Range of F_1
Hadley fixed point (H)	0.00.. - 0.0149
Fixed points B_1 and B_2	0.0150 - 0.0533
Chaotic C_1	0.054 - 0.0908
Periodic P_1 (x^2y)	0.0909 - 0.091
Chaotic C_2	0.0911 - 0.1052
Periodic P_2 (x^2yxy^2xy)	0.1053 - 0.106
Chaotic C_3	0.1061 - 0.1091
Periodic P_3 (x^2y^2)	0.1092 - 0.115
Chaotic C_4	0.116 - 0.1233
Periodic P_4 (xy)	0.1234 - 0.2437
Chaotic C_5	0.2438 - 0.312
Periodic P_5 (x)	0.313 - 0.318
Chaotic C_6	0.319 - 0.321
Periodic P_6 (x^3)	0.322 -
Chaotic C_7	0.323 - 0.352
Periodic P_7 (x)	0.353 - 0.359
Chaotic C_8	0.360 - 0.680

Table 3.1. PE model (h_1=-1.0): F_1 for different regimes

meaning that the steady states B_1 and B_2 become unstable by absorbing an unstable periodic orbit. We have confirmed the existence of this unstable periodic orbit in the range $0.047 < F_1 < 0.053$. The numerical technique for finding such periodic orbits is based on Newton's method and is described in Appendix B. The definition and numerical determination of the stability of the periodic orbits are also discussed there. The period of the unstable periodic orbit is of the order of a few days and increases rapidly as F_1 decreases from 0.053. Before the transition to chaotic behavior at $F_1 \approx 0.054$ occurs, as F_1 is increased with the same initial conditions, the model requires increasingly longer time to reach its steady state attractor.

As shown in Fig. 3.1, the behavior of the PE model consists of alternate chaotic and periodic regimes at irregular intervals in F_1. The schematic representation in Fig. 3.1 is based on studying the model with an interval in F_1 not exceeding 0.001. In some regimes, especially when a transition takes place, the interval in F_1 is less than 0.0001. It is possible that a more complex behavior might be revealed if the parameter space were spanned with a finer structure. However, such a detailed study is irrelevant to the purpose of this thesis and we are certain that the model has revealed a rich structure to answer some of the questions we posed earlier.

We will now discuss in some detail the solutions of the model in the different regimes of Fig. 3.1. Figure 3.2 shows the behavior of x_1, y_1 and z_1 for 80 days starting from an arbitrary initial condition at $F_1=0.055$ in the chaotic regime C_1. This is the smallest value of F_1 that

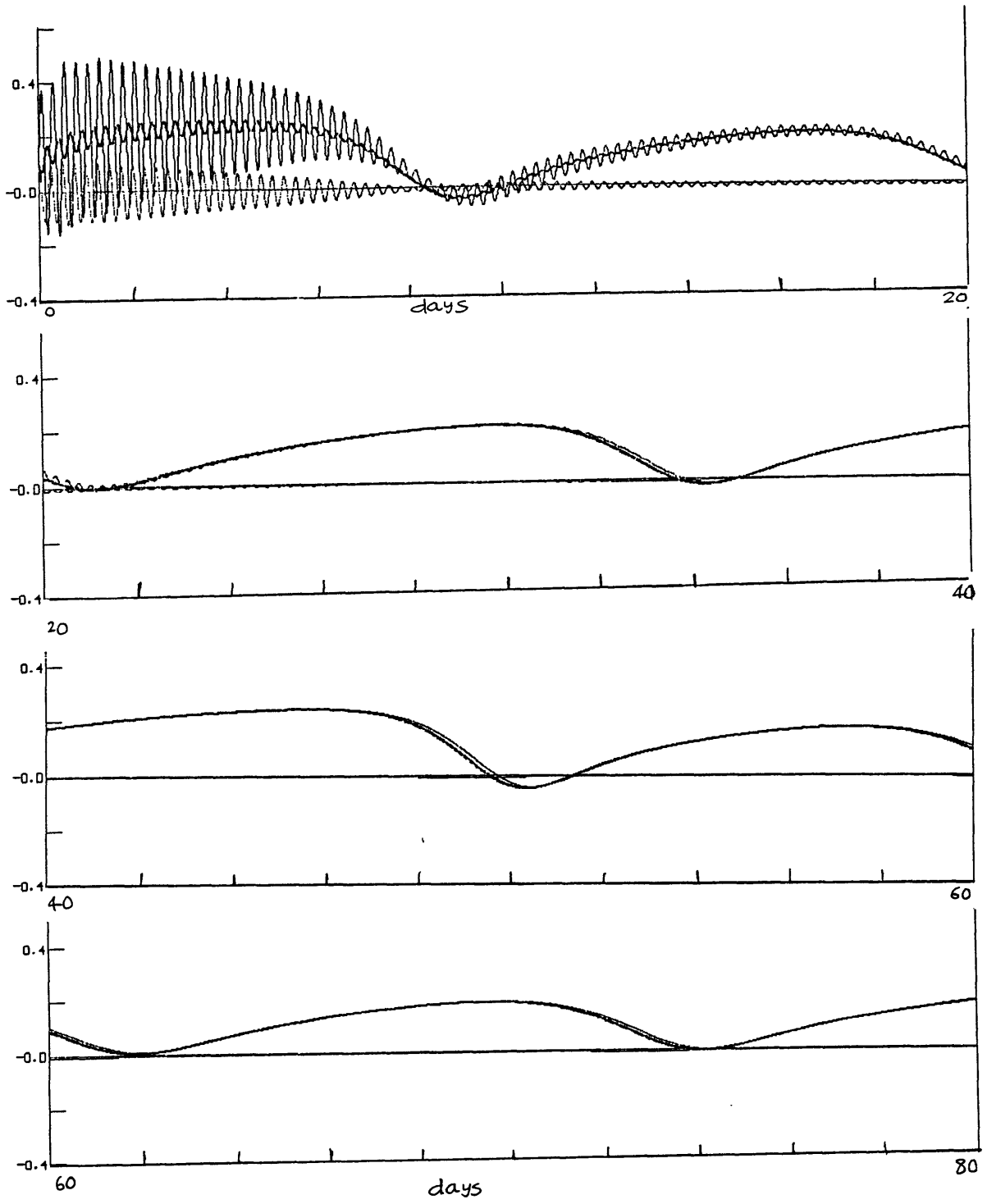

Figure 3.2. PE model (h_1=-1.0): Variations of x_1 (dotted line), y_1 (heavy solid line), z_1 (thin solid line) at F_1=0.055.

we have studied for which the attractor is chaotic. The gravity waves present initially damp out completely after about 40 days and the solution varies nonperiodically forever. We notice that, after 40 days, the solution varies on a slow time scale of about 10 days and y_1 and z_1 are nearly indistinguishable most of the time. Similar behavior was revealed with an examination of the variation of the other variables, thereby implying that the solutions are quasi-geostrophic. As F_1 is increased within the chaotic regime C_1, the amplitudes of the variables increase while the time scale of their variation decreases. The attractors are found to be still free of gravity waves and have approximately geostrophic states.

The periodic attractors in the regime P_1 do not contain any gravity waves. Figure 3.3 shows a projection of the stable periodic on the $y_1 - y_3$ subspace at F_1=0.091. This periodic orbit spirals around the two steady states B_1 and B_2. We will adopt the symbolic description used by Sparrow (1982) and call the periodic orbit in Fig. 3.3 xy^2 orbit. Here x refers to the orbit spiralling each time in $y_3 > 0$ and y to the spiralling of the orbit each time in $y_3 < 0$. This description is quite helpful in distinguishing the orbits in different periodic regimes. Because of the symmetry of the model equations, there is also a stable x^2y orbit which is an image of the xy^2 orbit about the y_3-axis.

The attractor studied by Lorenz (1980) at F_1=0.1 falls in the chaotic regime C_2. The structure of the strange attractor at F_1=0.1 is discussed in detail by Lorenz and will not be repeated here. However, the behavior of x_1, y_1 and z_1 for 40 days, after the model has reached the

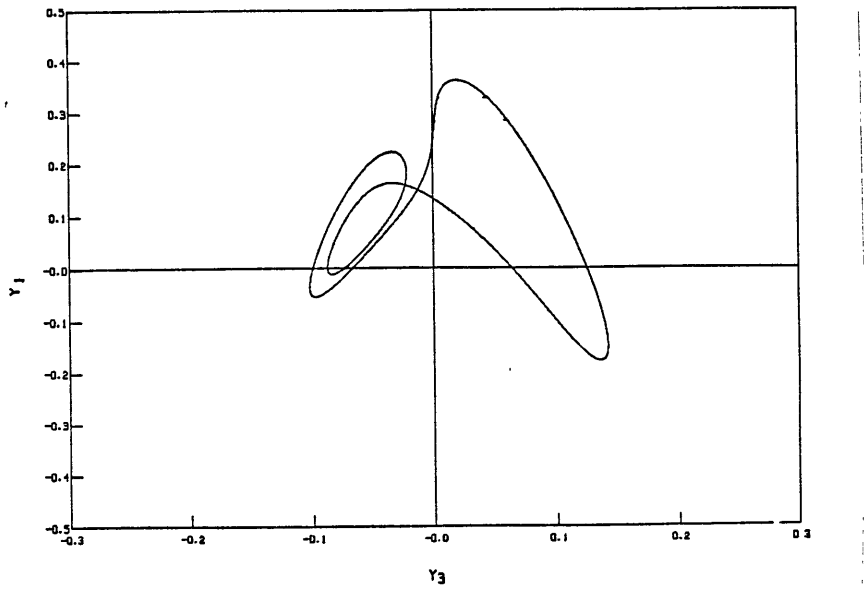

Figure 3.3. Projection of x^2y orbit at F_1=0.091 on y_1 - y_3 plane.

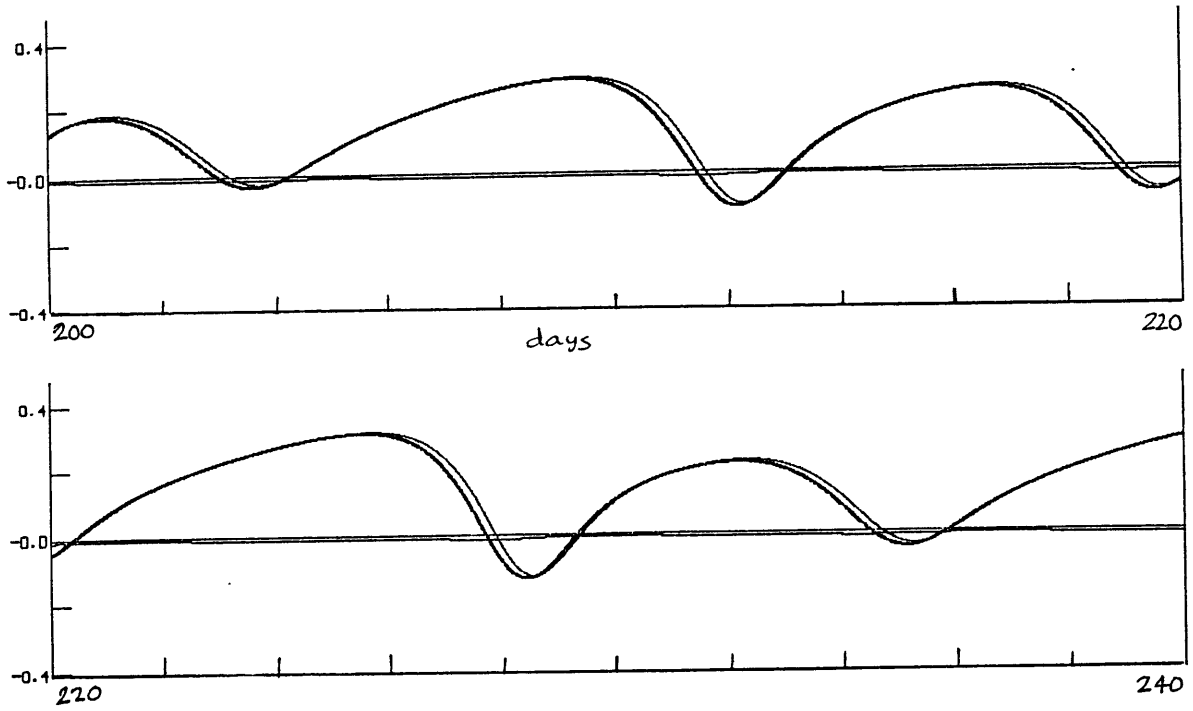

Figure 3.4. Variation of x_1, y_1, and z_1 at F_1=0.1 (as in Fig. 3.2).

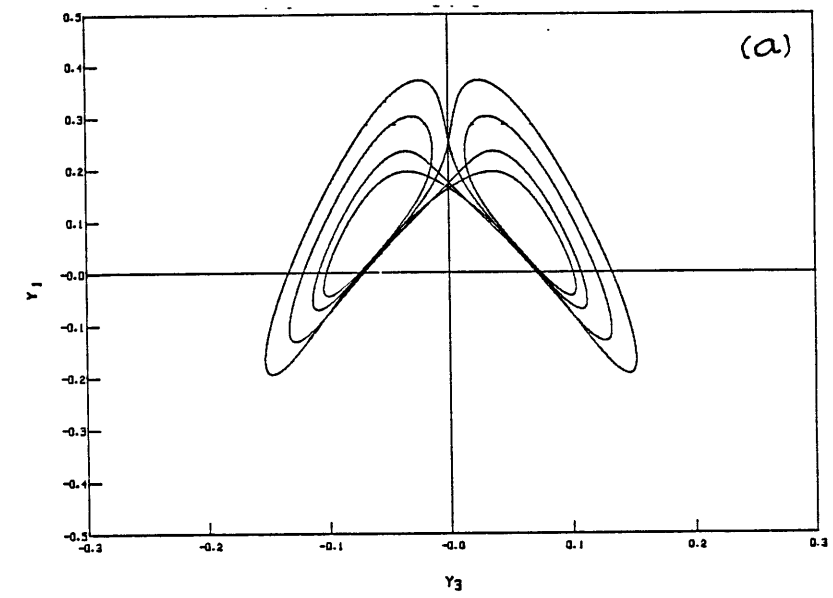

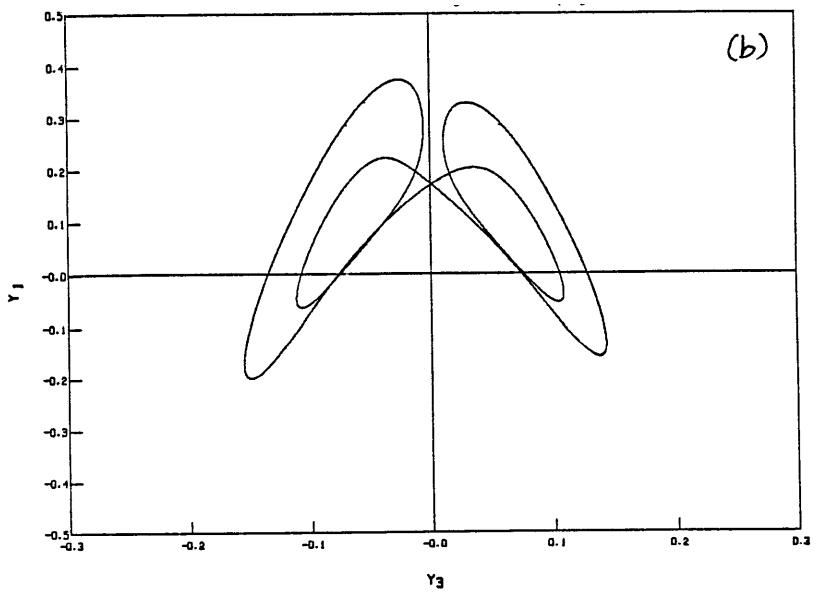

Figure 3.5 Projection of (a) x^2yxy^2xy orbit at F_1=0.106 and (b) x^2y^2 orbit at F_1=0.11.

attractor, is presented in Fig. 3.4 in order to compare the chaotic attractors at different values of F_1. Comparing Figs. 3.1 and 3.4, we notice that, as F_1 increases, the amplitude increases and the time scale of the variation decreases. As discussed by Lorenz, the states of the attractor are quasi-geostrophic and free of gravity waves.

The periodic regime P_2 consists of stable symmetric x^2yxy^2xy orbits; one such orbit at F_1=0.106 is shown in Fig. 3.5. After P_2, there is a narrow range of values of F_1, represented by C_3, for which the attractors are chaotic. As F_1 is increased, the model enters the periodic regime P_3 in which attractors are x^2y^2 orbits. In Fig. 3.5, we have plotted the nonsymmetric x^2y^2 orbit at F_1=0.11.

With the further increase of F_1, the behavior of the model changes over to the chaotic regime C_4. The behavior of the model at F_1=0.12 is illustrated in Fig. 3.6 showing the variation of x_1, y_1, and z_1 for 80 days within the attractor. In Figs. 3.1 - 3.5 we notice that the gravity waves seem to disappear completely once the orbits reach the attractors. Even at F_1=0.12, the variables y's and z's are in phase and their differences are small most of the time. We have examined the solutions at F_1=0.12 for a long period of time without detecting any high-frequency oscillations in the solutions. In addition, we present a picture of the attractor at F_1=0.12 in the form of a few Poincare cross-sections in Fig. 3.7. This picture is similar to that presented by Lorenz for F_1=0.1. The chaotic attractor at F_1=0.12 has a structure similar to that at F_1=0.1.The states of the attractor are either nearly geostrophic or well approximated by the balance equation 2.16. The chaotic attractor is

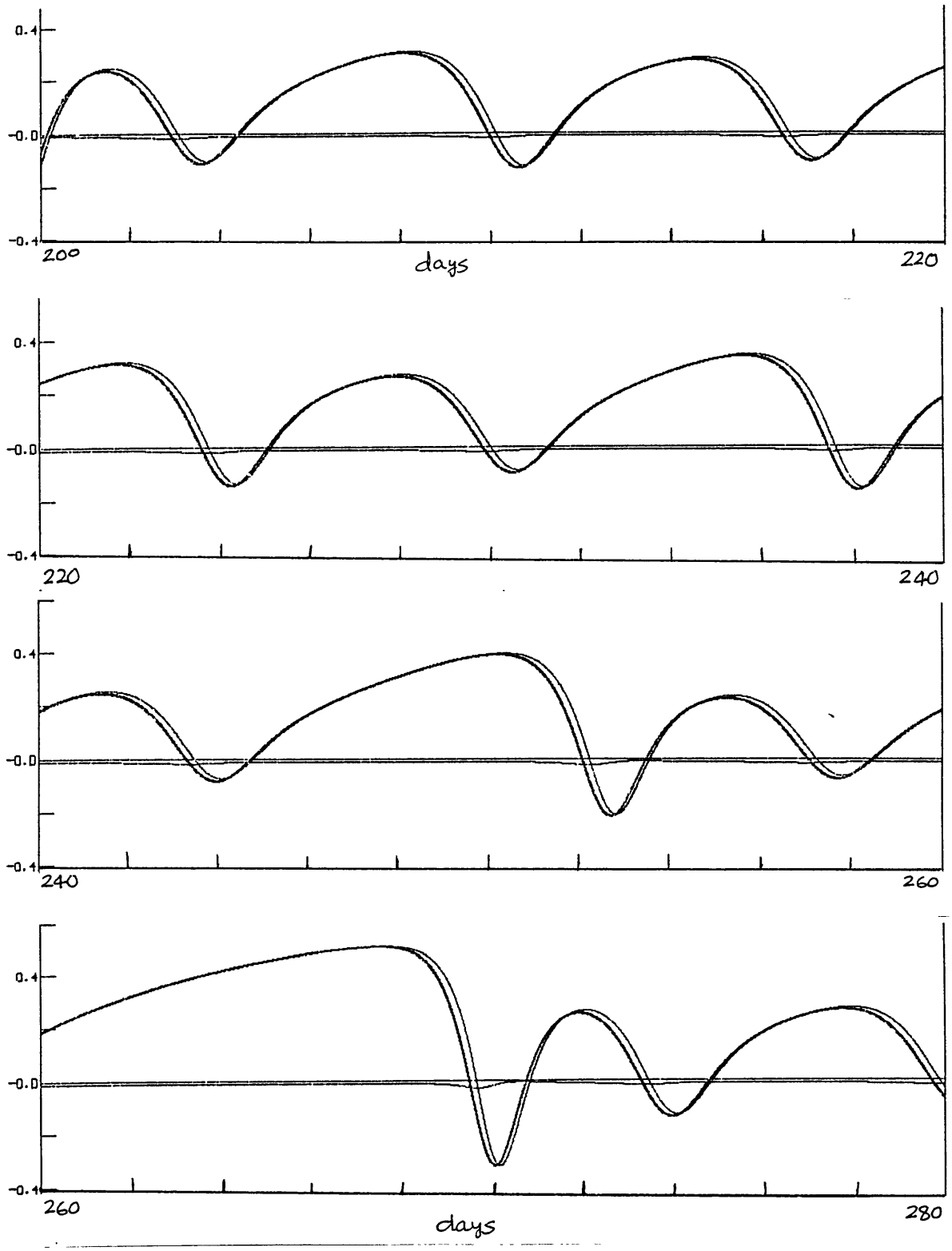

Figure 3.6. Variations of x_1, y_1, and z_1 at F_1=0.12 (as in Fig. 3.2).

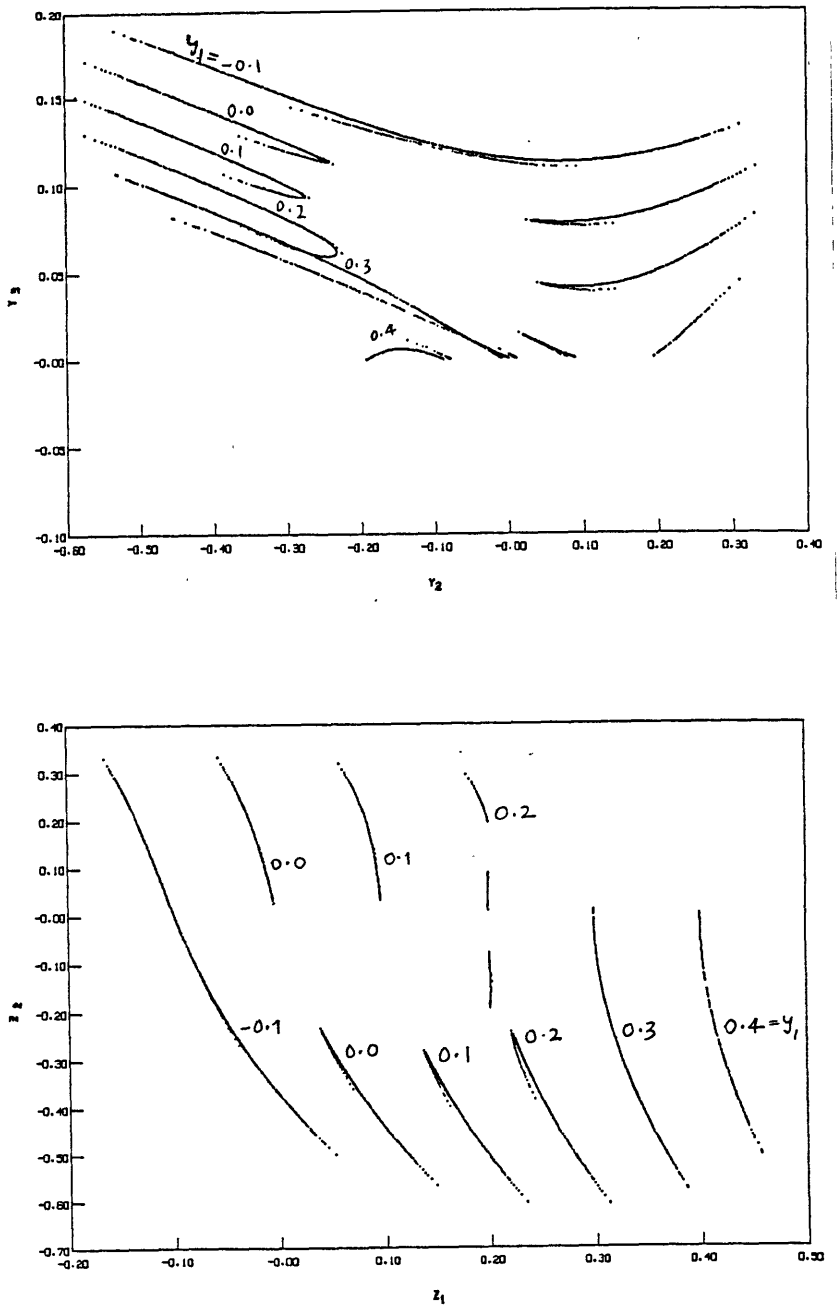

Figure 3.7. Projection of the chaotic attractor at F_1=0.12:
(a) y_1 cross-sections on y_2-y_3 plane and
(b) y_1 cross-sections on z_1-z_2 plane.

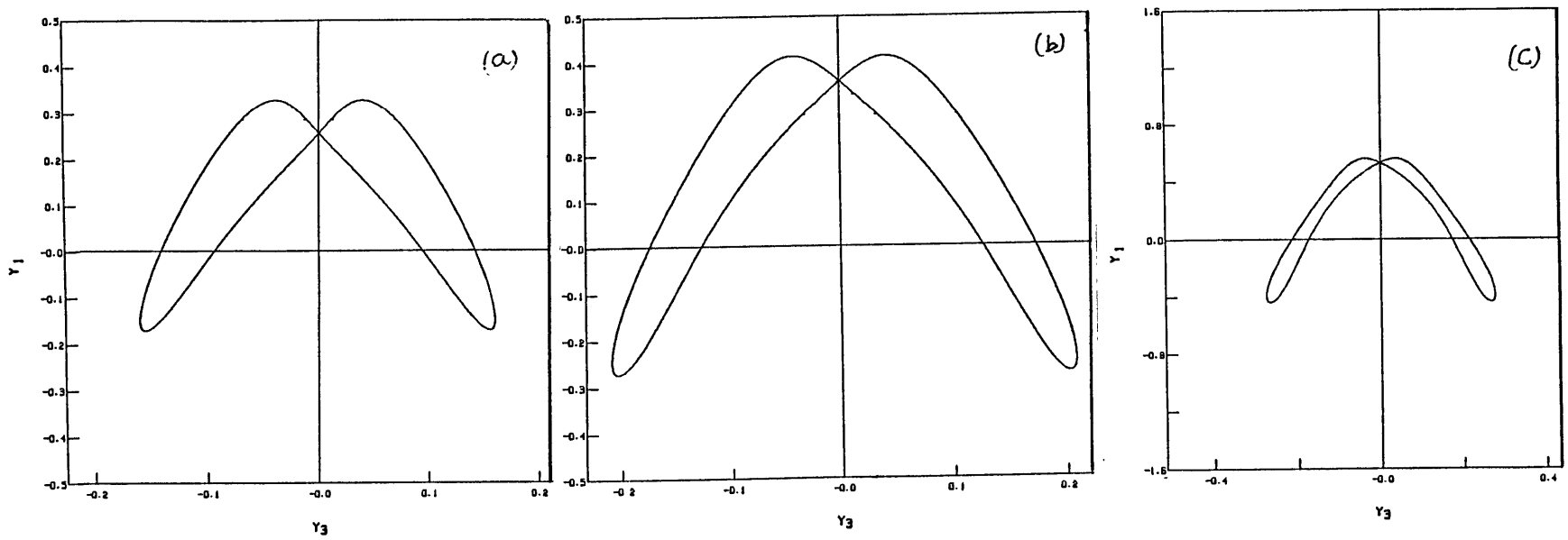

Figure 3.8. Symmetric xy orbit at (a) F_1=0.15, (b) F_1=0.2, and (c) F_1=0.24.

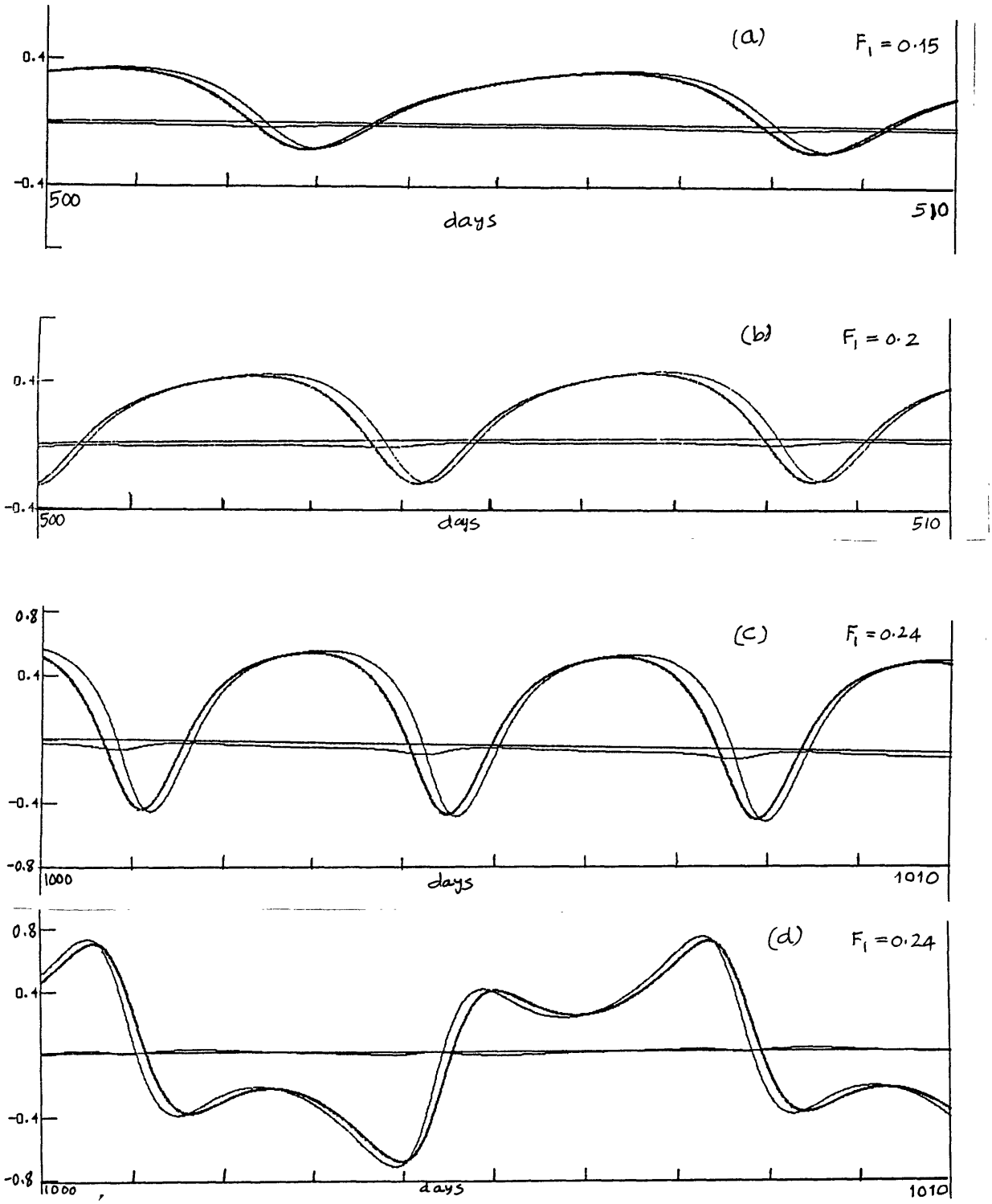

Figure 3.9. Variations of x_1, y_1, and z_1 at (a) F_1=0.15, (b) F_1=0.2, and (c) F_1= 0.24. (d) Variations of x_2, y_2, and z_2 at F_1=0.24.

approximated by two surfaces in the various three dimensional subspaces onto which it is projected.

After the chaotic regime C_4 ends, the attractors of the PE model become periodic as F_1 is increased and remain so for a long range of values between F_1=0.1234 and F_1=0.2437. In this periodic regime, P_5, there are xy orbits. The projection of the xy orbits at F_1=0.15, 0.2, and 0.24 are as shown in Fig. 3.8, and the corresponding behavior of x_1, y_1, and z_1 for ten days within the attractor is presented in Fig. 3.9. From these figures, it is clear that there is no visible sign of the presence of the gravity waves in the attractors. The variables y's and z's are still very close at some points along the orbit and are not too far away at other points. The divergences x's are also small most of the time. A close examination of the numerical values of the maxima of y_1 or z_1 has also not revealed any high-frequency oscillations in the entire P_5 regime except at F_1=0.24. At F_1=0.24, superposed on the slow oscillation of z_1, there are two maxima separated by an interval of about six hours. However, the amplitudes of these high-frequency oscillations are too small to be resolved in Fig. 3.9. The period of the xy orbit has decreased from about 11 days at F_1=0.15 to about seven days at F_1=0.24. In order to verify that the period at F_1=0.24 is indeed seven days, we must examine the variation of y_2 or z_2 which is shown in Fig. 3.9.

Before studying the behavior of the PE model for $F_1 > 0.2437$, we wish to summarize the nature of the attractors for $F_1 < 0.2437$ and discuss the transitions from the periodic to chaotic attractors. The attractors of the PE model between F_1=0.054 and F_1=0.2437 are either chaotic or

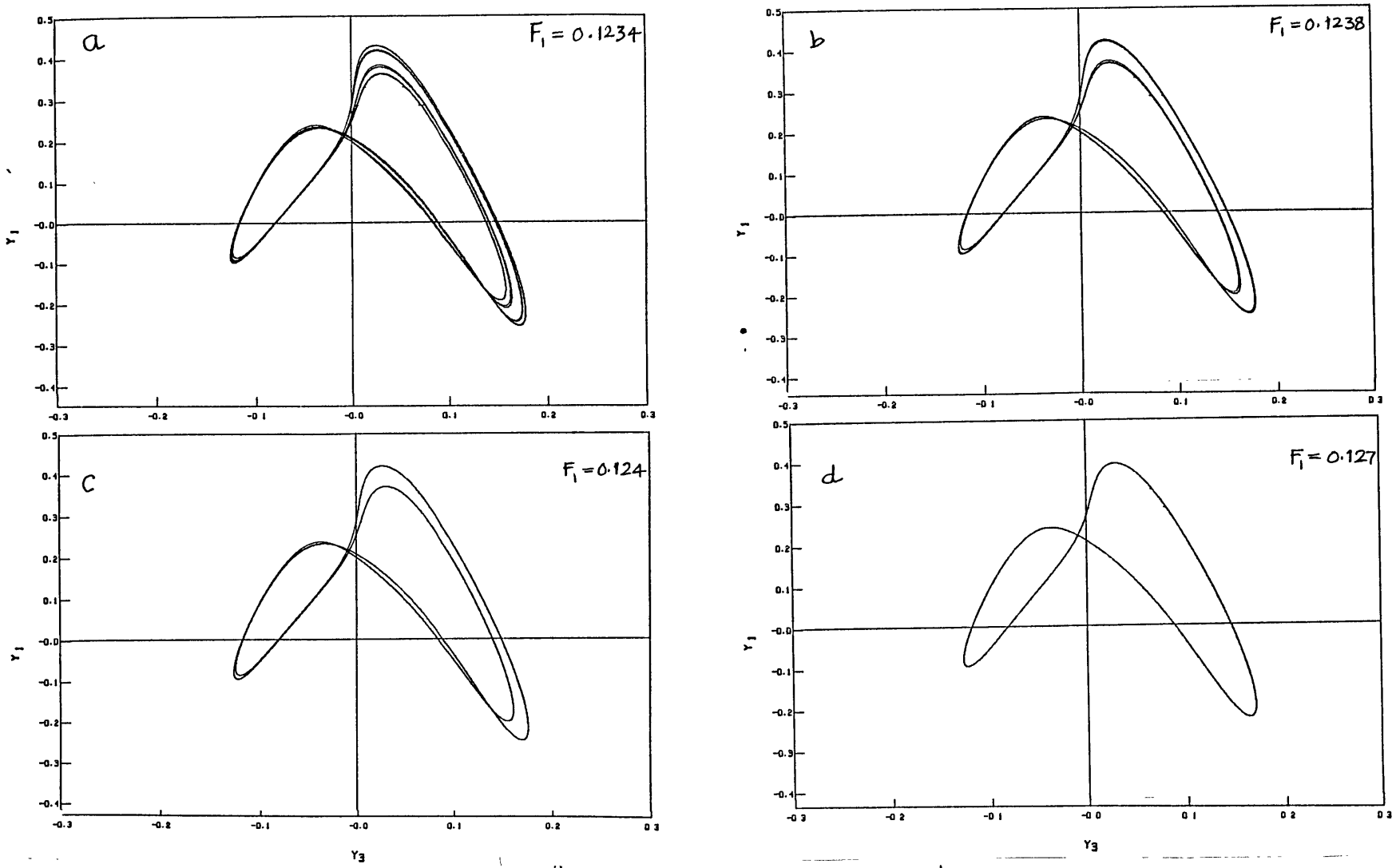

Figure 3.10. (a) $(xy)^8$ orbit at F_1=0.1234, (b) $(xy)^4$ orbit at F_1=0.1238, (c) $(xy)^2$ orbit at F_1=0.124 and (d) nonsymmetric xy orbit at F_1=0.127.

periodic and their orbits consist of variations on a time scale of a few days. The high-frequency oscillations do not seem to be present and the states of the attractors are either quasi-geostrophic or nearly approximated by the balance equation. For many of these attractors, we have compared the states of the attractor with z's determined by the balance equation 2.16. The agreement between the two is extremely close at almost all the points along the orbits for small values of F_1. Even in the periodic regime P_4, the disagreement occurs in about the third decimal place. At a particular value of F_1, there is always better agreement when y_1 or z_1 are positive rather than negative. Whether these attractors are embedded in a three-dimensional invariant manifold will be addressed in Chapter 4.

The transitions from periodic to chaotic regimes will now be discussed beginning with P_4 and we will describe the change in the behavior as F_1 is decreased. The different ways in which the periodic orbits loose their stability are discussed in Appendix B. In the P_4 regime, between F_1=0.149 and F_1=0.2437, the stable xy orbits are symmetric as shown in Fig. 3.8. At F_1=0.148, a symmetric saddle-node bifurcation occurs when the symmetric xy orbit looses stability and a pair of nonsymmetric xy orbits come into existence. One such nonsymmetric xy orbit, at F_1=0.127, is shown Fig. 3.10. As F_1 decreases, the nonsymmetric xy orbit becomes unstable because of a period doubling bifurcation forming a nonsymmetric $(xy)^2$ orbit. This will be followed by a sequence of such period doubling bifurcations involving nonsymmetric $(xy)^n$ (n = powers of 2) orbits. We have presented the nonsymmetric $(xy)^2$ orbit at F_1=0.124, the $(xy)^4$ orbit at F_1=0.1238, and the $(xy)^8$ orbit at F_1=0.1234 in Fig.

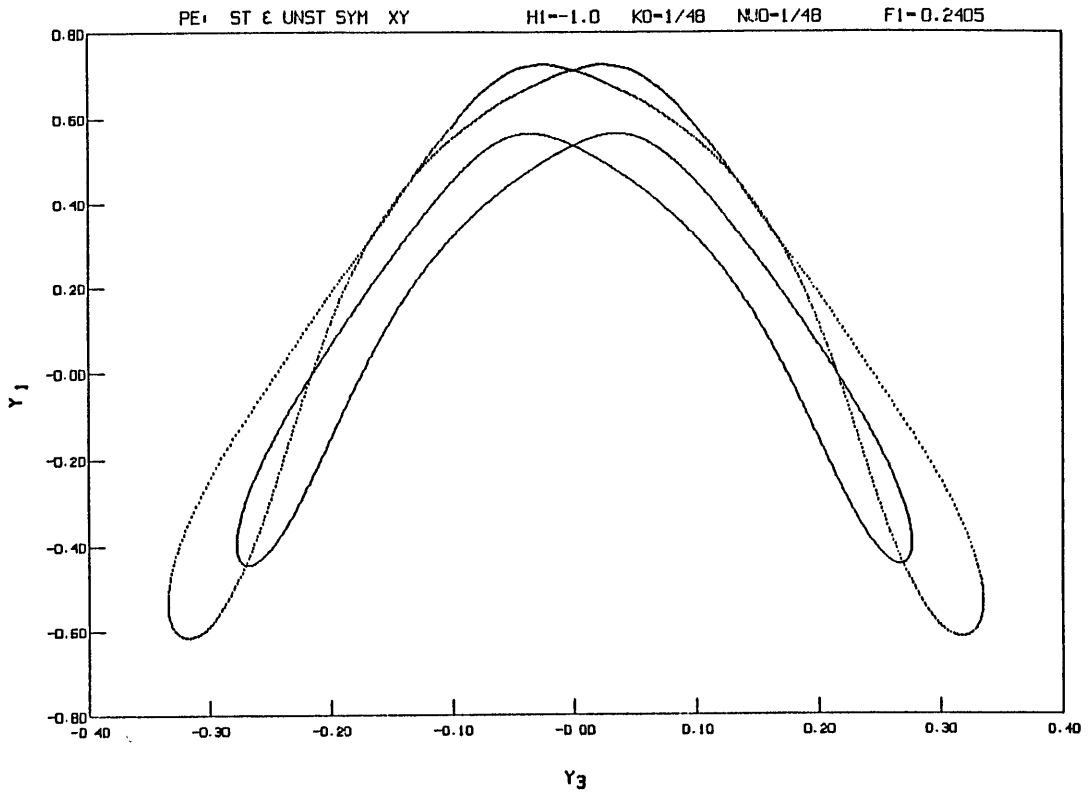

Figure 3.11. Stable (solid) and unstable (dotted) xy orbits at F_1=0.2405.

3.10. It is expected that this infinite sequence of doubling tends to a limit where the attractor becomes chaotic and the model makes a transition to the chaotic regime C_4.

The symmetric xy orbit which becomes unstable at F_1=0.148, however, continues to exist as an unstable solution as F_1 is decreased. In fact, using the periodic orbit-finding method of Appendix B, we have traced its existence all the way upto F_1=0.0464 where it appears to become a homoclinic orbit of the Hadley fixed point. A homoclinic orbit tends to a particular unstable fixed point both forwards and backwards in time. Similarly, the nonsymmetric xy orbit is born as a homoclinic orbit at about F_1=0.0992.

At the other end (higher value of F_1) of the periodic regime P_4, the symmetric xy orbit goes out of existence at F_1=0.2437 in a saddle-node bifurcation (Appendix B) by merging with an unstable symmetric xy orbit. The existence of the unstable symmetric xy orbit has been determined numerically. Both the stable and unstable symmetric xy orbits, with different periods, at F_1=0.2405 are shown in Fig. 3.11. As F_1 increases, the period of the stable orbit decreases while that of the unstable orbit increases. When the bifurcation occurs, the periods of the two orbits approach a common value.

The entire bifurcation diagram involving the P_4 regime is schematically shown in Fig. 3.12. The bifurcation diagram for the periodic regimes P_2 and P_3 is similar to that of the P_4 regime. However, since x^2y is nonsymmetric, the bifurcation diagram for the P_1 regime is

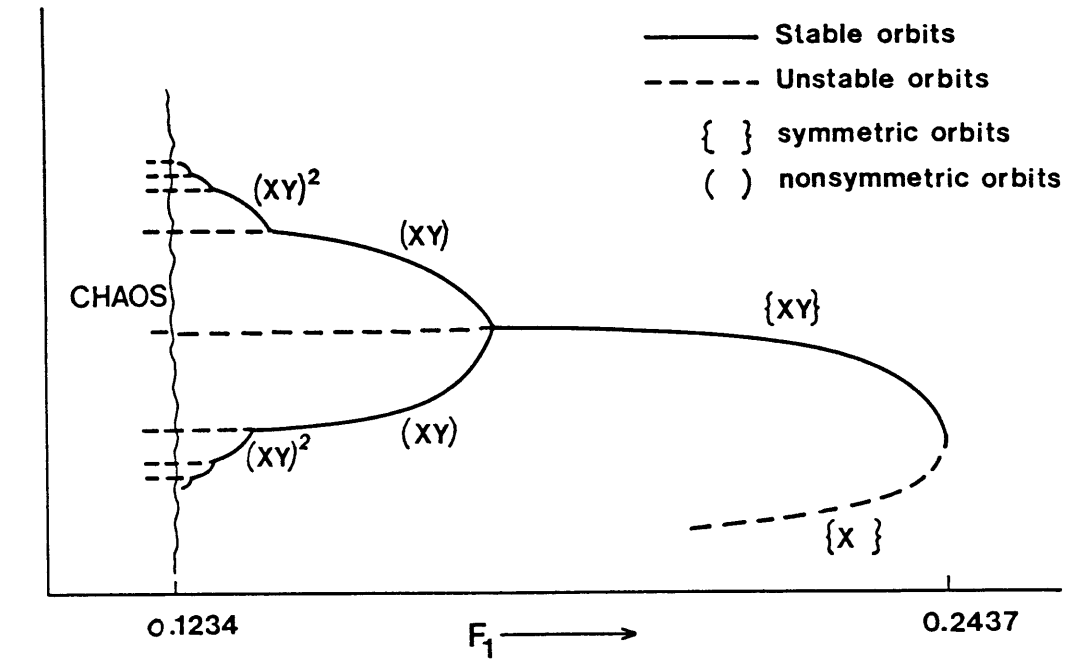

a.

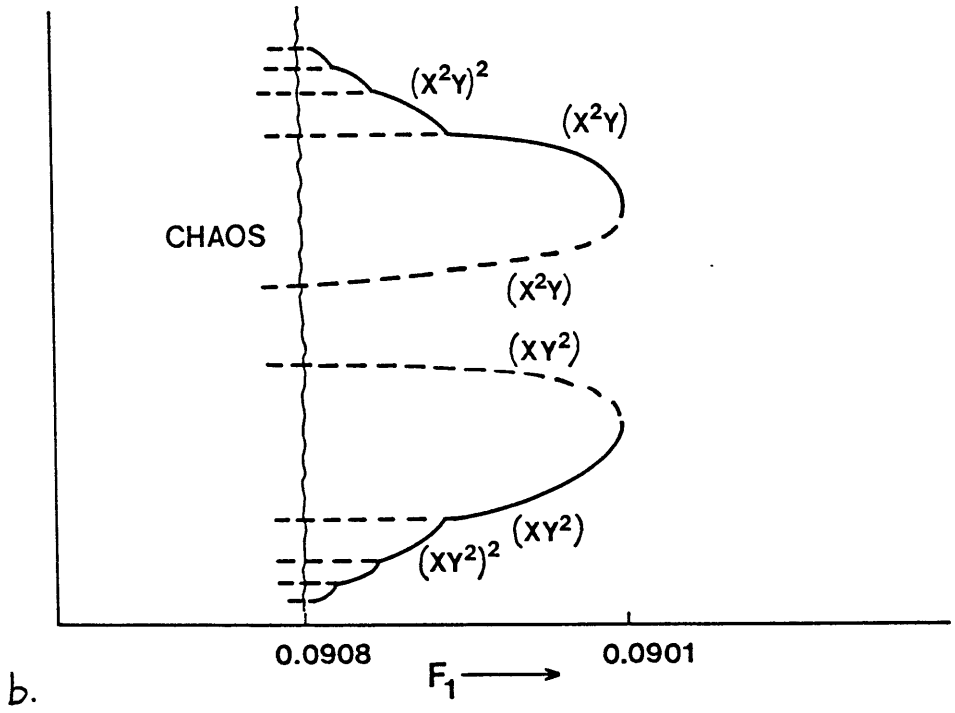

b.

Figure 3.12. Bifurcation diagram for (a) regime P_4 and (b) regime P_1.

slightly different as shown in Fig. 3.12. The entire sequence of behavior from the Hadley fixed point to the periodic regime P_4 and the associated bifurcations in the PE model are similar to those of Lorenz's convection model (Sparrow, 1982). However, in the convection model, the stable symmetric xy orbit never goes out of existence. Many unstable periodic orbits are part of different chaotic attractors. Since different periodic orbits are created and destroyed at different values of F_1, one difference between the different chaotic regimes is the types of the periodic orbits that will be part of them. The important features of the PE model to note in Figs. 3.1 and 3.12 are the annihilation of the xy orbit at F_1=0.2437 and the apparent absence of persisting gravity waves in the attractors.

We now discuss the behavior of the PE model when $F_1 > 0.2437$ beginning with a description of the transition from the periodic regime P_4 to the chaotic regime C_5. If F_1 is increased by a very small value after the end of P_4 (i.e., after the saddle-node bifurcation), though the periodic xy orbit has ceased to exist, the trajectories seem to move near it in an almost periodic manner. Then they vary chaotically with high-frequency gravity waves superposed on a slow variation for a short period of time before returning to an almost periodic behavior. This behavior is repeated at irregular intervals of time indefinitely. In Fig. 3.13, we show such behavior of the model at two different intervals when F_1=0.2439. The intervals of chaotic behavior with gravity waves are short and occur irregularly. This behavior is known as intermittent chaos (Manneville and Pomeau, 1978) and the near periodic intervals are referred to as laminar behavior. In fact, intermittent chaos is also observed just after the

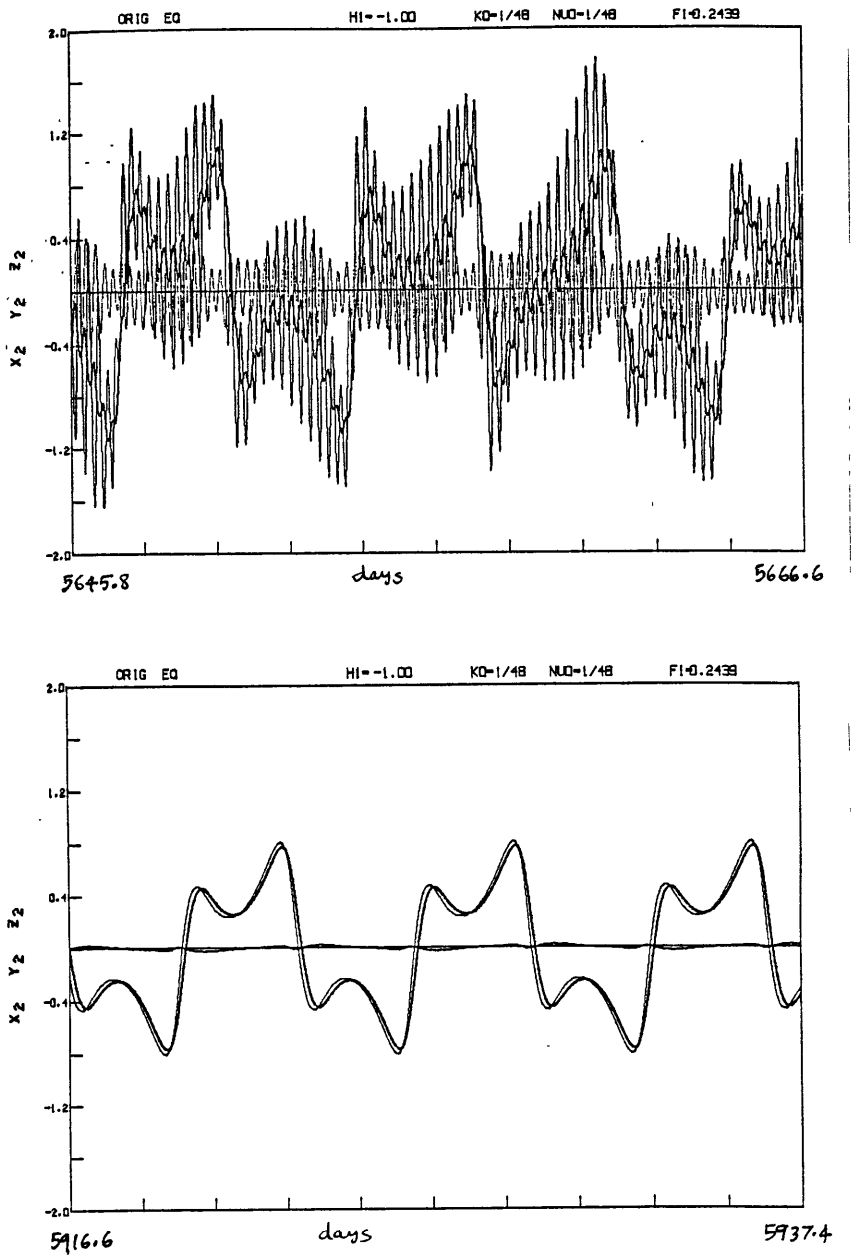

Figure 3.13. Variations of x_2, y_2, and z_2 at F_1=0.2439

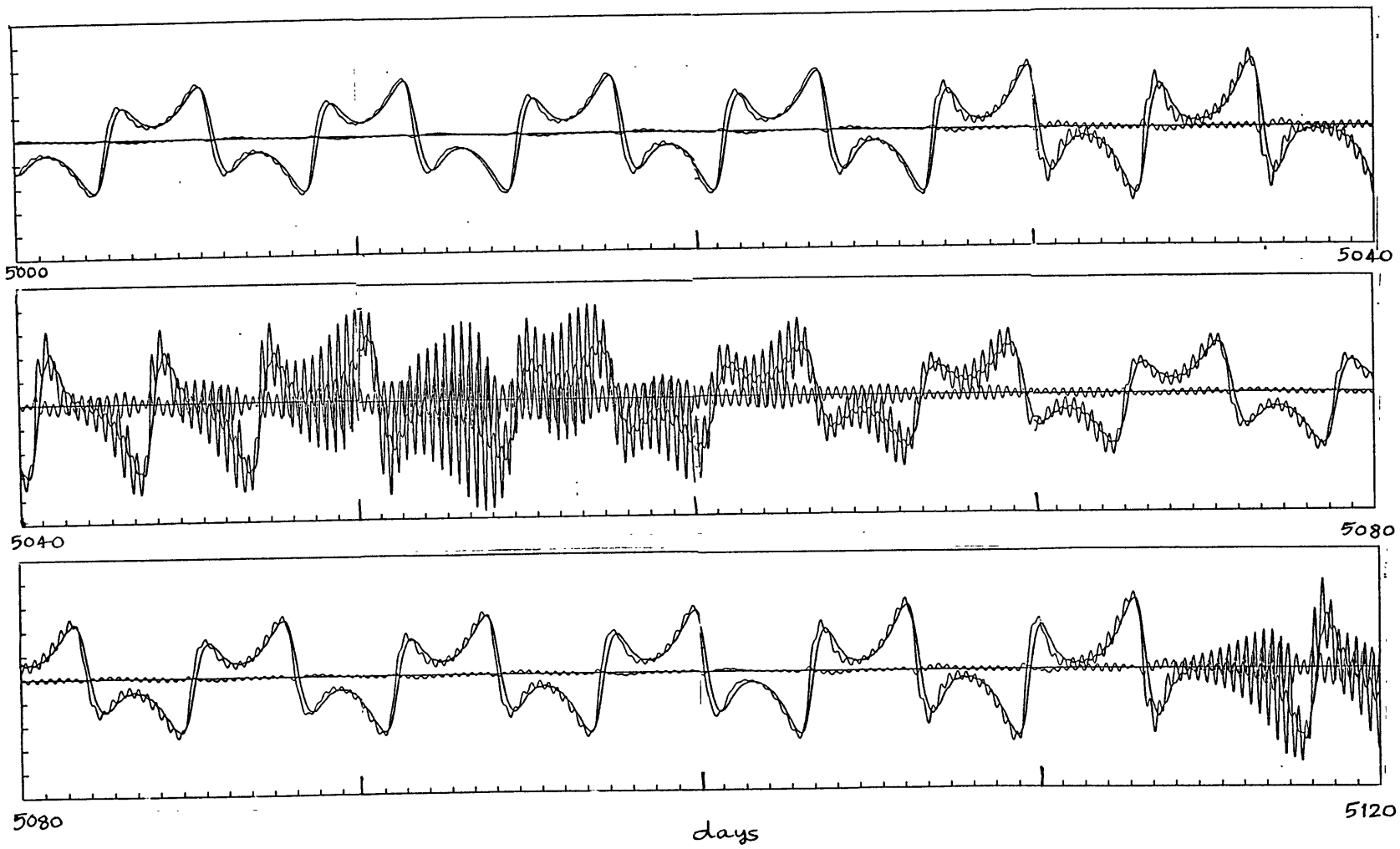

Figure 3.14a. Time series continued on next page

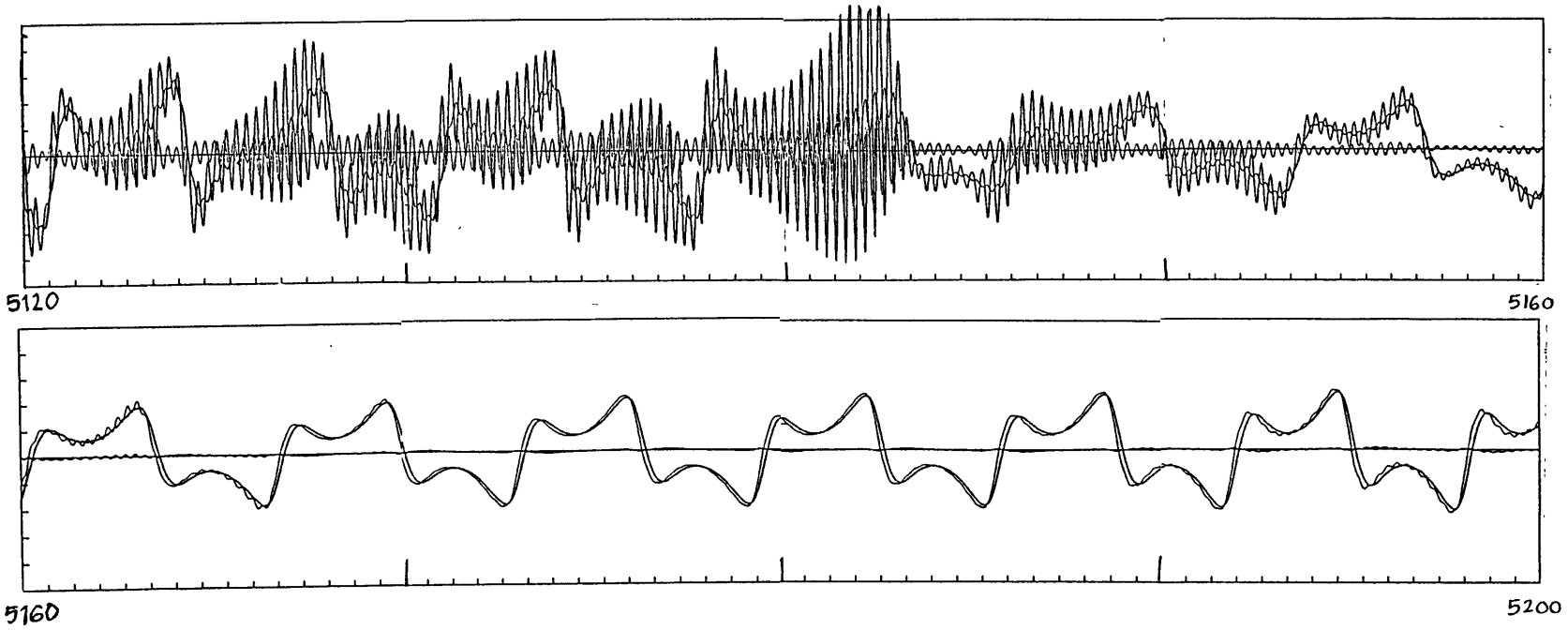

Figure 3.14a. Variations of x_2, y_2 and z_2 at F_1=0.25 for 200 days in the attractor.

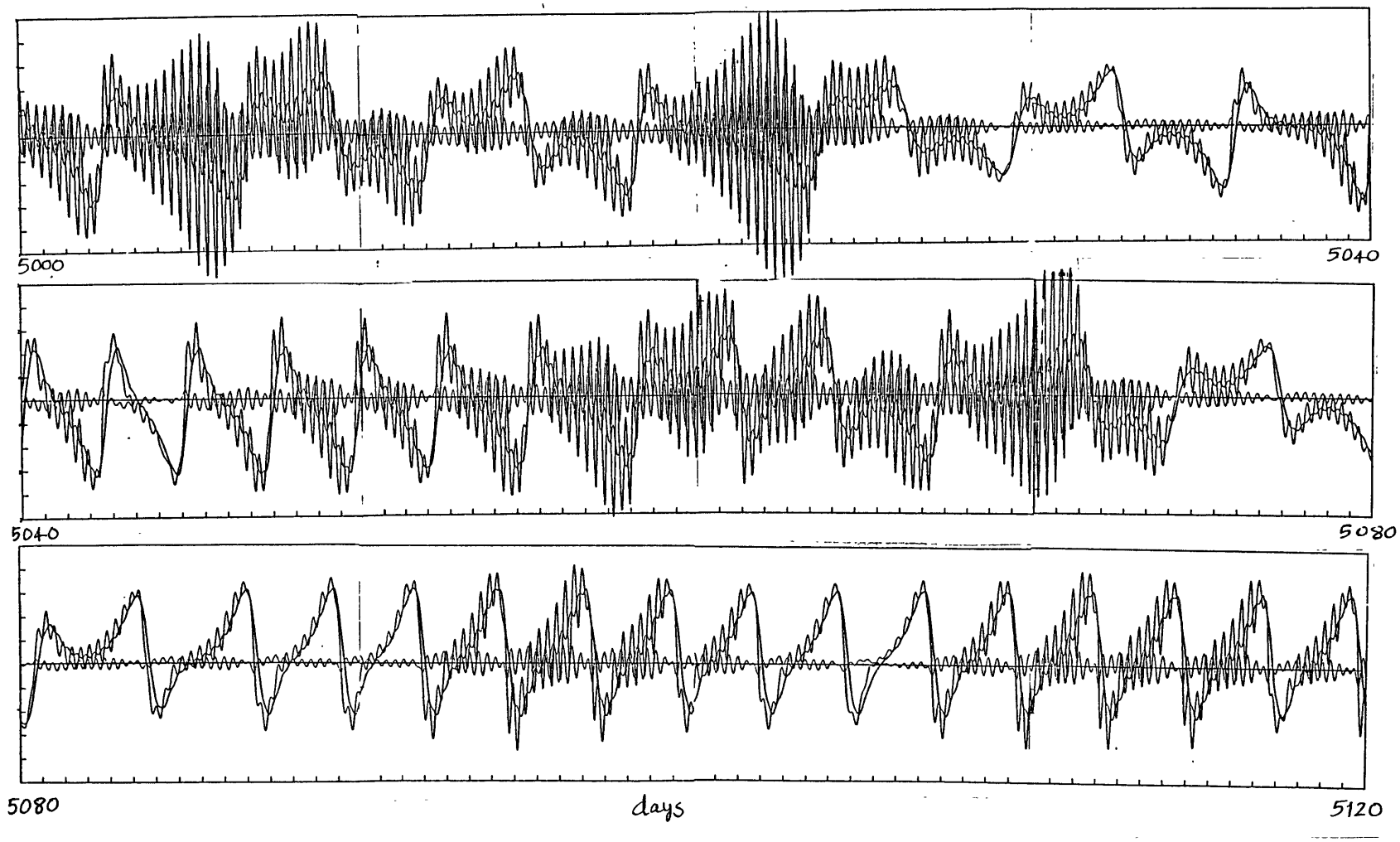

Figure 3.14b. Time series continued on next page.

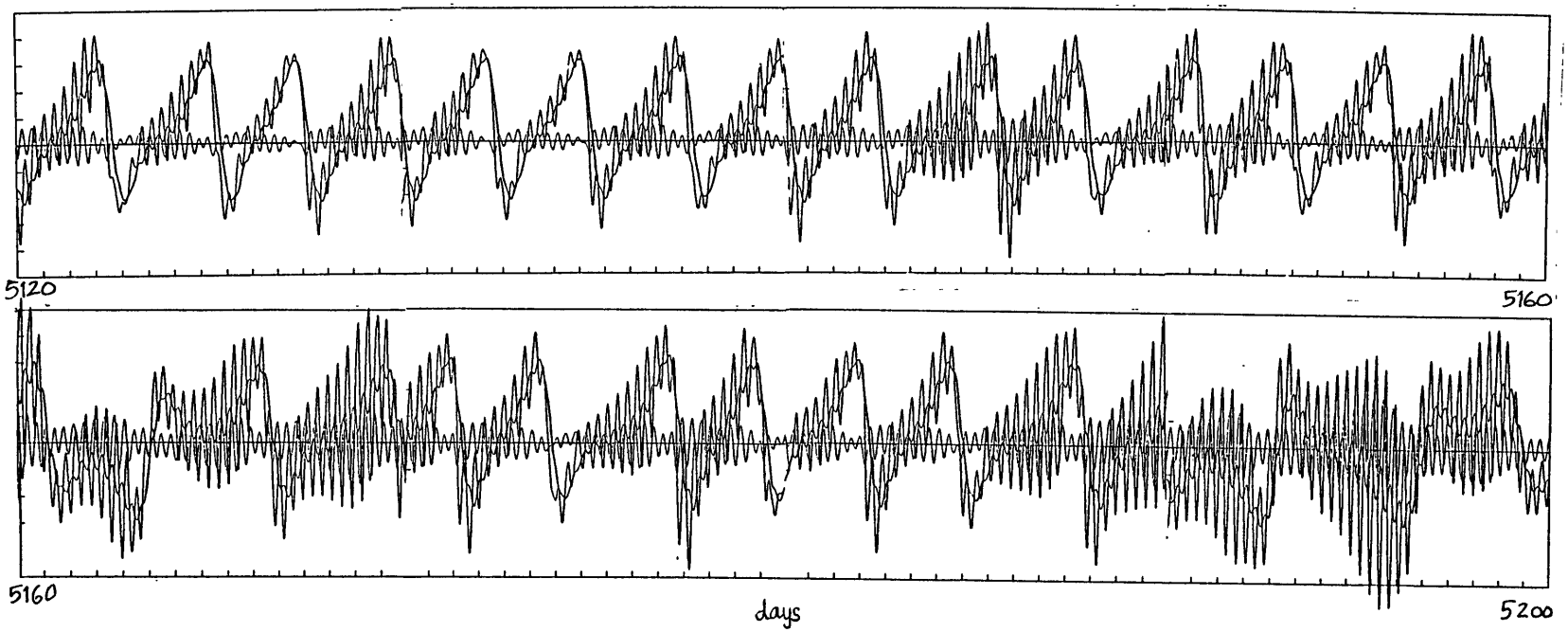

Figure 3.14b. Variations of x_2, y_2 and z_2 at F_1=0.3 for 200 days in the attractor.

periodic regimes P_1, P_2, and P_3 cease to exist. However, in those cases, neither the chaotic bursts nor the laminar intervals contain any gravity waves.

As F_1 is increased further, within the C_5 regime, the periods of chaotic behavior with gravity waves increase in length and the laminar behavior decreases until the motion appears to be completely chaotic. In Fig. 3.14 we have presented the behavior of model at F_1=0.25 and F_1=0.3 in the C_5 regime. Figure 3.14 consists of the variations of x_2, y_2 and z_2 for 200 days after the model has been integrated for a very long time. The time series of y_2 and z_2, rather than y_1 and z_1, clearly shows that during the laminar phases the orbit moves like an xy orbit. As seen in Fig. 3.14, when F_1=0.25, the superposed gravity waves during the laminar intervals have very small amplitude and, sometimes, the high-frequency oscillations do not seem to be present even. During such intervals, an examination of the differences between y's and z's indicate that such states may be in quasi-geostrophic equilibrium. The chaotic bursts, however, contain very high amplitude gravity waves. At F_1=0.3 (Fig. 3.14), we notice that the orbits are more chaotic and the gravity waves are present all the time. The slow components during certain intervals appear to be moving around an x or a y orbit.

Between F_1=0.2437 and F_1=0.68 (Fig. 3.1) the attractors of the PE model consist of persisting gravity waves superposed on slow motions. In this range, the attractors are mostly chaotic except for the periodic regimes P_5, P_6 and P_7. In the regimes P_5 and P_7, the attractors consist of x orbits (and y orbits by symmetry) in which the gravity waves and the

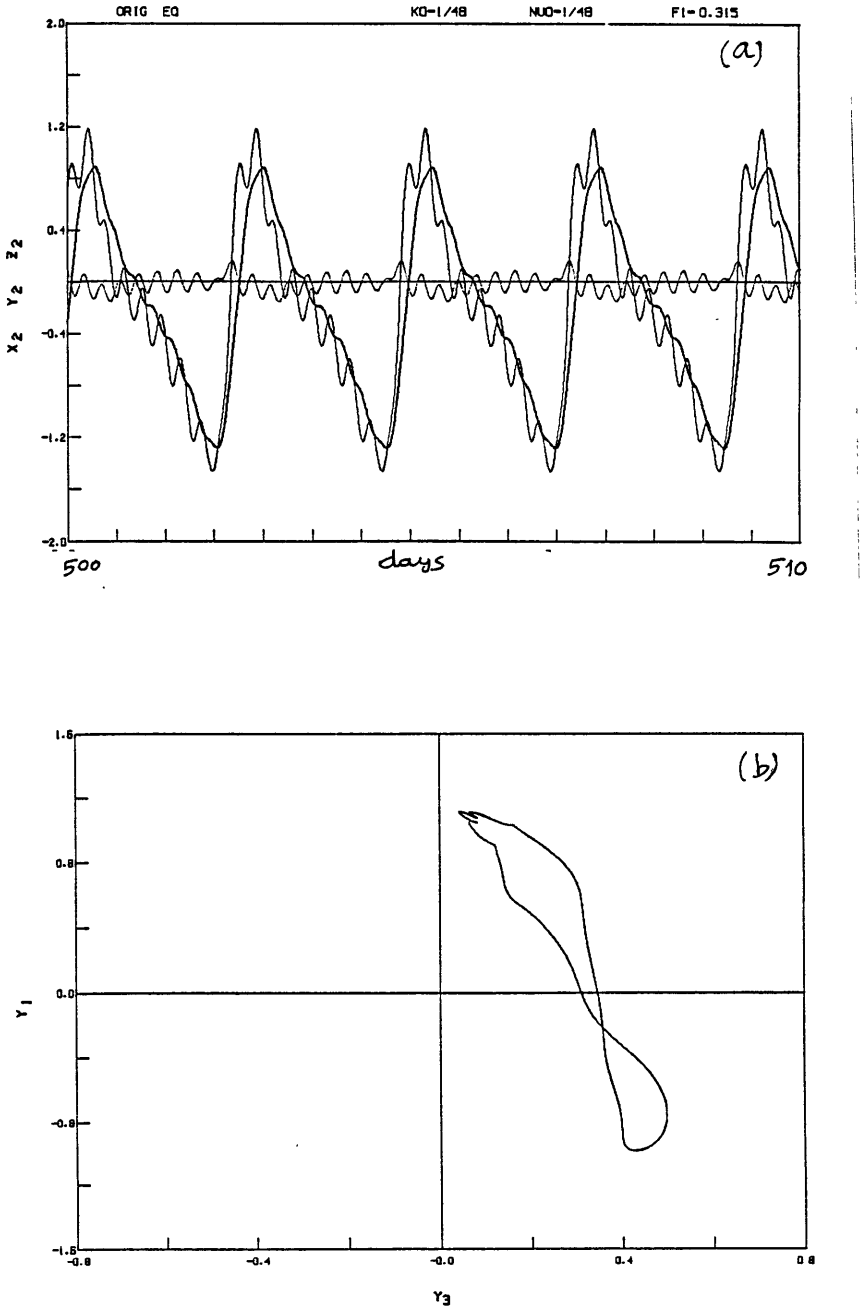

Figure 3.15. x orbit at F_1=0.315.

F_1	λ_1	λ_2	λ_3	λ_4	λ_5	λ_6	λ_7	λ_8	λ_9	d
0.055	0.006	0.0	-0.019	-0.020	-0.020	-0.020	-0.063	-0.063	-0.114	2.32
0.08	0.007	0.0	-0.019	-0.020	-0.020	-0.020	-0.063	-0.063	-0.115	2.37
0.1	0.005	0.0	-0.019	-0.019	-0.020	-0.020	-0.063	-0.063	-0.113	2.29
0.244	0.010	0.0	-0.009	-0.012	-0.025	-0.028	-0.062	-0.062	-0.125	3.08
0.25	0.017	0.001	0.0	-0.008	-0.026	-0.033	-0.061	-0.063	-0.139	4.38
0.3	0.042	0.008	0.0	-0.006	-0.027	-0.043	-0.058	-0.062	-0.166	5.40

Table 3.2. Spectra of Lyapunov exponents (λ's) and Fractal dimensions (d) ($h_1 = -1.0$)

slow motion are phase locked in some manner. Figure 3.15 shows the x orbit at F_1=0.315. The x orbits in P_5 and P_7 become unstable, at both the lower and the higher ends of F_1, by Hopf bifurcation of the periodic orbits (see Appendix B). The x orbits of those regimes continue to exist as unstable periodic solutions for a long range of values of F_1. The periodic orbits in P_6 are x^3 orbits and the transition from P_6 to the chaotic regime C_7 is through a period doubling bifurcation. As F_1 is decreased, the x^3 orbit becomes unstable near C_6 by Hopf bifurcation.

The chaotic attractors with persisting gravity waves when $F_1 >$ 0.2437 appear to be more chaotic than the attractors in C_1, C_2, C_3 or C_4. If the attractors in C_5 or C_6 are projected onto a three-dimensional subspace, it will result in a region of phase space being completely filled up. The projections will not resemble in any way the cross-sections presented in Fig. 3.7 for F_1=0.12. A quantitative estimate of the differences among the various chaotic attractors in C_1 - C_6 can be obtained by evaluating their spectra of Lyapunov exponents and fractal dimensions. Lyapunov exponents are a measure of the average exponential rate of divergences of nearby orbits and are used in defining fractal dimensions. These are discussed in Appendix C. In Table 3.2 we present the spectra of Lyapunov exponents and the fractal dimensions corresponding to several chaotic attractors. The chaotic attractors in the regimes C_1 - C_4 have only one positive exponent in each spectrum and their fractal dimensions are less than three. However, for the chaotic attractors with known persisting gravity waves, there are more positive exponents and their fractal dimensions are also higher.

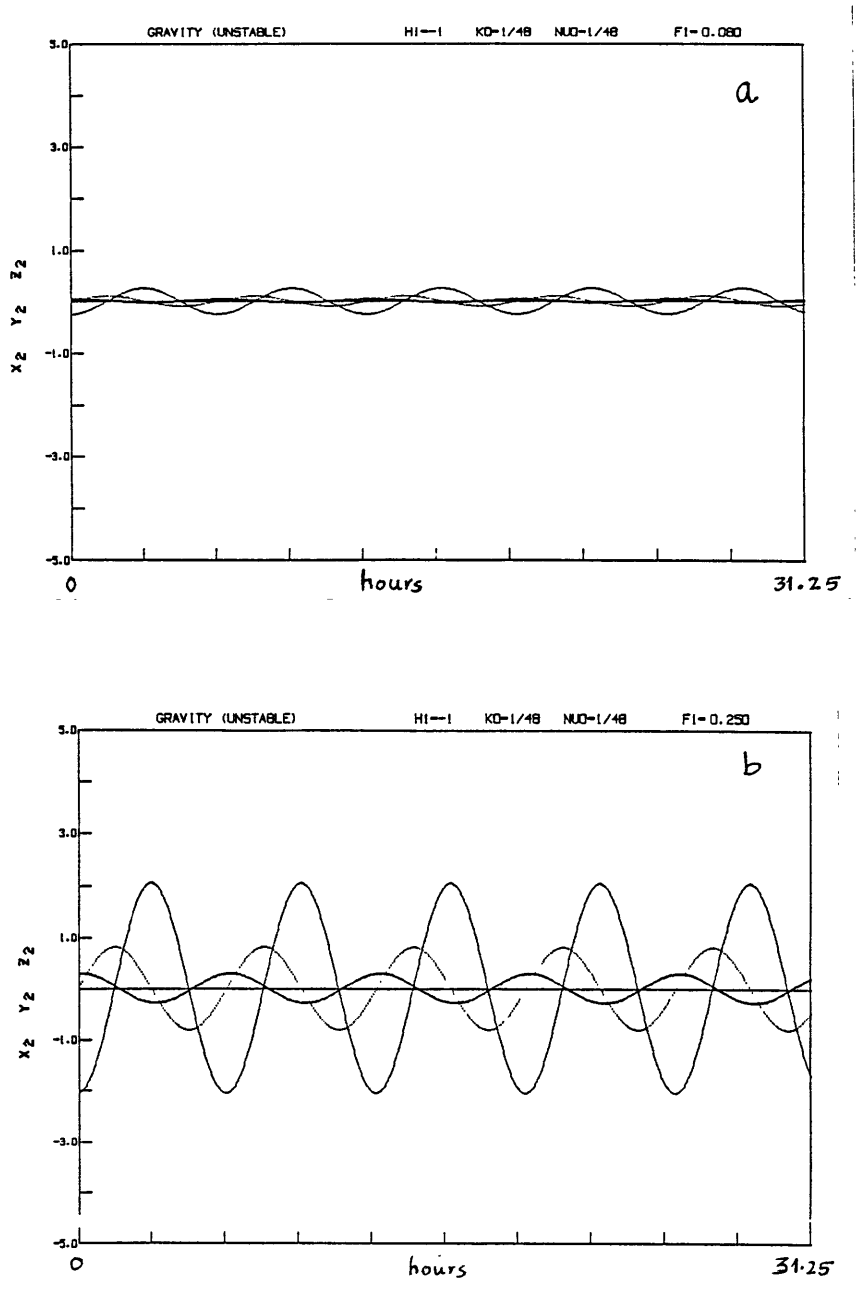

Figure 3.16. Unstable periodic orbit G (a) F_1=0.08, (b) $F_1$0.25.

Apart from the different solutions of the PE model represented in Fig. 3.1, there is another branch of solution which is related to the Hopf bifurcation of the Hadley fixed point at F_1=0.0775. As a result of this Hopf bifurcation, a periodic orbit oscillating with gravity wave period (about 6 hours) comes into existence. We have found numerically the existence of such a gravity periodic orbit, and it is unstable for all values of $F_1 > 0.0775$. This regime will be referred to as the periodic regime G. The orbit in G at all values of F_1 are centered around the Hadley fixed point of F_1=0.0775. As F_1 is increased, the amplitudes of certain variables, notably x_2 and z_2, increase considerably and the period of the orbit shows a very small steady increase. In Fig. 3.16 we present the variations of some variables at F_1=0.08 and F_1=0.25. These oscillations do not seem to be superposed on any slow motion.

3.2. QG AND BE MODELS WITH $h_1 = -1.0$

The behavior of the QG and BE models as the forcing F_1 is varied is summarized schematically in Fig. 3.17. Table 3.3 lists the values of F_1 corresponding to the different regimes given in Fig. 3.17.

The QG and BE models both possess Hadley steady solution H which is given by

$$y_1 = F_1/a_1\nu_0(1 + a_1g_0)$$
$$y_2 = y_3 = 0 \qquad (3.2)$$

For small values of F_1, the Hadley fixed point is stable in both models.

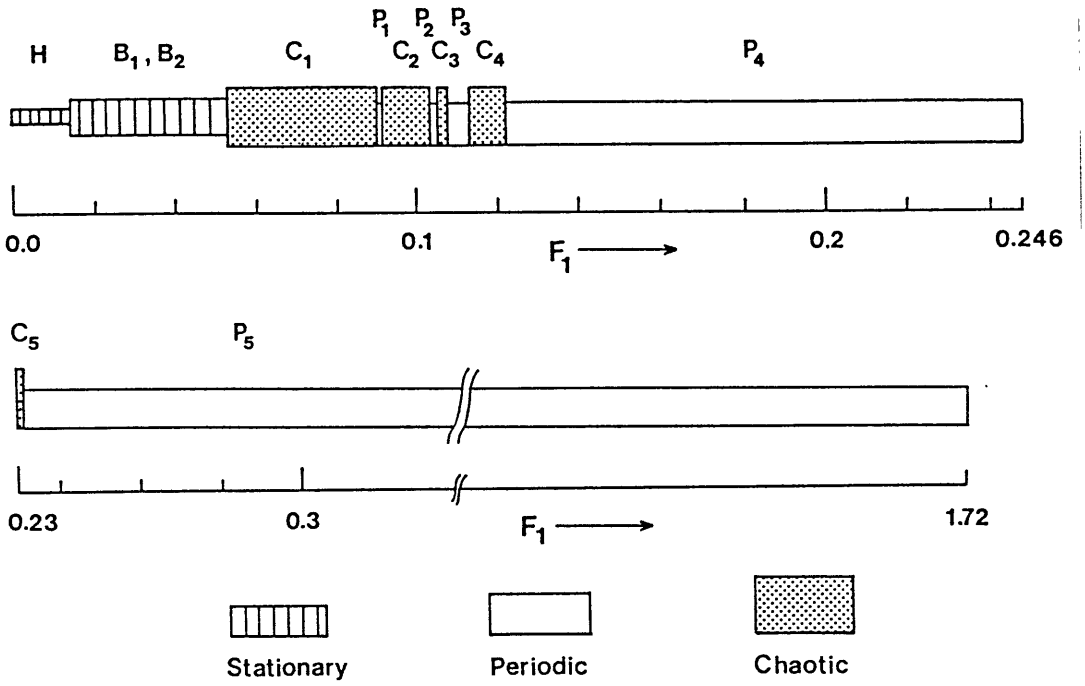

Figure 3.17a. Behavior of the BE model (h_1=-1.0)

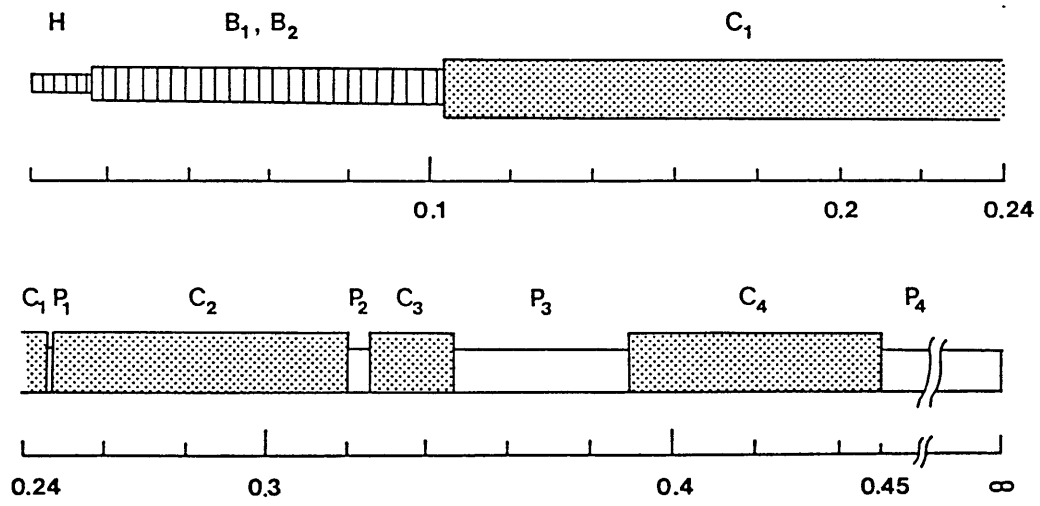

Figure 3.17b. Behavior of the QG model (h_1=-1.0)

Regime	Range of F_1 (BE)	Range of F_1 (QG)
Hadley fixed point (H)	0.00.. - 0.0149	0.00.. - 0.0163
Fixed points B_1 and B_2	0.0150 - 0.0533	0.0164 - 0.1031
Chaotic C_1	0.054 - 0.0908	0.104 - 0.246
Periodic P_1 (x^2y)	0.0909 - 0.091	0.247 - 0.248
Chaotic C_2	0.0911 - 0.1053	0.249 - 0.321
Periodic P_2 (x^2yxy^2xy)	0.1054 - 0.1601	0.322 - 0.325
Chaotic C_3	0.1062 - 0.1092	0.326 - 0.347
Periodic P_3 (x^2y^2)	0.1093 - 0.115	0.348 - 0.388
Chaotic C_4	0.116 - 0.1234	0.389 - 0.451
Periodic P_4 (xy)	0.1235 - 0.246	0.452 - ∞
Periodic P_5 (x)	0.247 - 1.720	
P_5 + C_5 (Hysterisis)	0.2293 -	

Table 3.3. BE and QG models (h_1=-1.0): F_1 for different regimes

In the QG model, the Hadley fixed point looses stability in a pitchfork bifurcation at F_1=0.0163 when the branch points B_1 and B_2, similar to those in the PE model, come into existence. The fixed points B_1 and B_2 become unstable at F_1=0.103 undergoing a Hopf bifurcation. Similarly, in the BE model, the pitchfork bifurcation of H occurs at F_1=0.015 and the branch points B_1 and B_2 loose stability in a Hopf bifurcation at F_1=0.054. Thus, the BE model reproduces the behavior of the PE model in an extremely close manner, and much better than the QG model does. It is obvious that the Hadley fixed point does not undergo the Hopf bifurcation involving gravity wave frequency of the type found in the PE model.

After all the steady states have become unstable, as F_1 is increased, the solutions of the QG and BE models follow the same sequence of chaotic and periodic regimes as found in the PE model (Figs. 3.1 and 3.17). The similarity in their behavior does not extend beyond the periodic regime P_4. The periodic orbits in P_1, P_2, P_3 and P_4 of the QG and BE models are qualitatively similar to those of the corresponding regimes in the PE models. For example, the P_4 regime in the QG and BE models also have xy orbits. We have also found similar qualitative resemblances in the attractors of the different chaotic regimes; specific examples will be discussed in some detail later. The different sequences of bifurcations occuring between C_1 and P_4 regimes are the same for all the models.

In the QG model, the xy orbit in the periodic regime is a solution for all values of $F_1 > 0.451$ and does not undergo any bifurcation as $F_1 \to \infty$. The behavior of the QG model is equivalent to that of Lorenz's

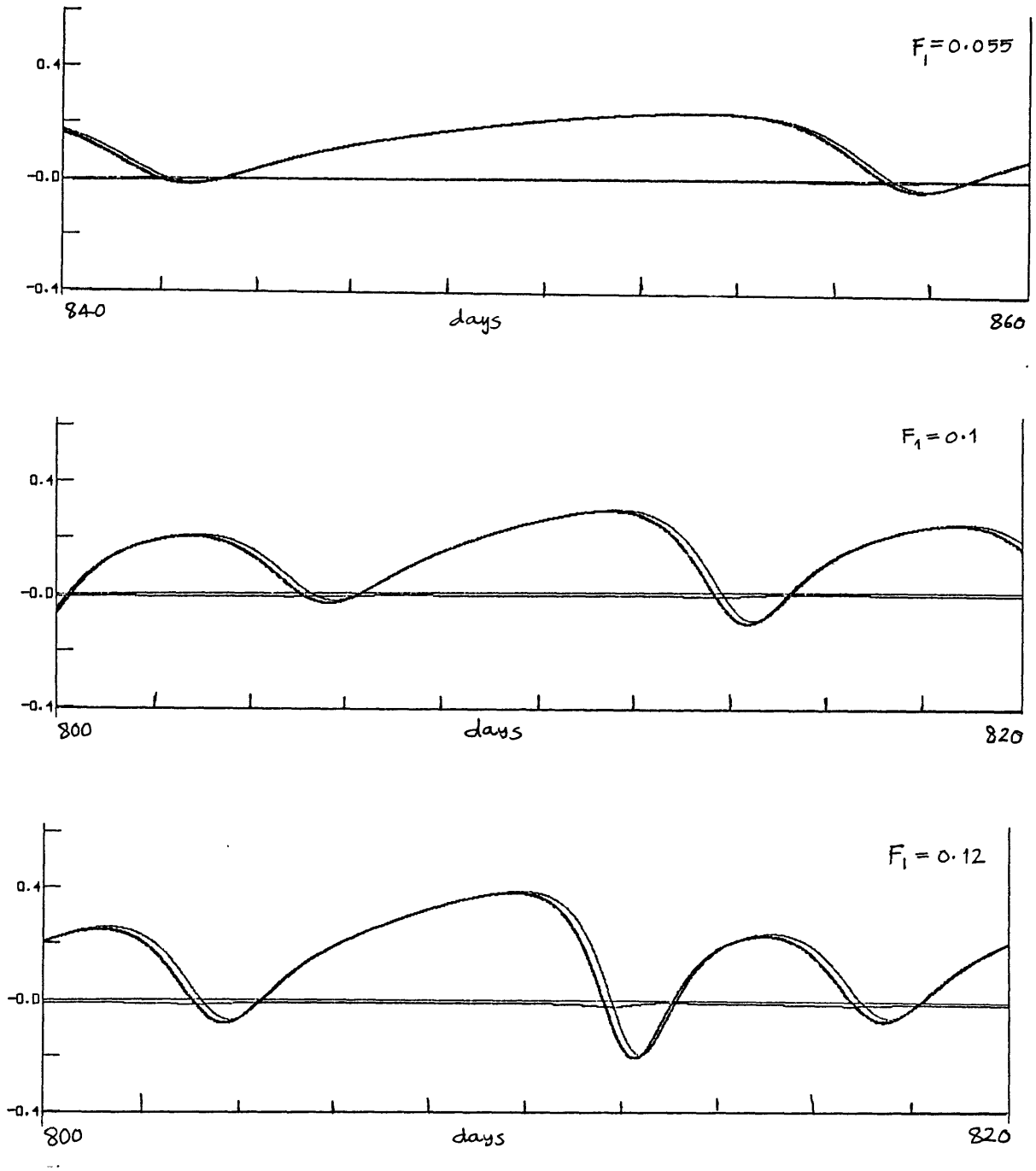

Figure 3.18. BE model: Variations of x_1, y_1, z_1 at F_1=0.055, 0.1, 0.12

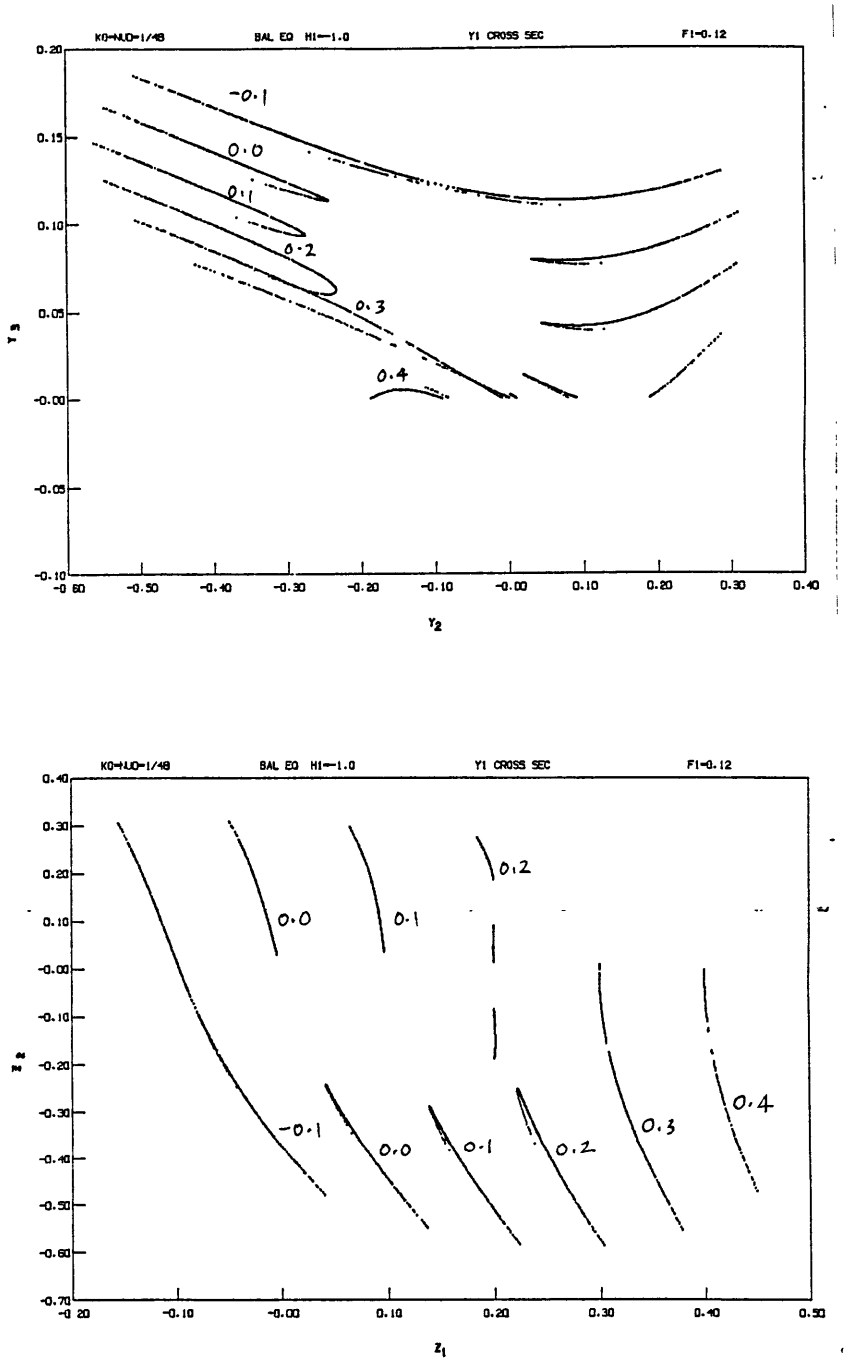

Figure 3.19. Poincare cross-sections of the attractor of the BE model at F_1=0.12 (compare with the PE model in Fig. 3.7).

convection model (Sparrow, 1982). A comparison of Tables 3.1 and 3.3 reveals that there is a large difference in the range values of F_1 of different regimes between the PE and QG models. For instance, the x^2y periodic orbit comes into existence at F_1=0.091 in the PE model and at F_1=0.247 in the QG model. Comparisons of qualitatively similar periodic orbits have shown that the periods and the amplitudes of the orbits in the PE and QG models have considerable quantitative differences. Thus, the behavior of the QG model is qualitatively similar to that of the PE model concerning certain chaotic and periodic regimes though the correspondence of the values of F_1 between the two models is not good.

However, the behavior of the BE model is found to be remarkably closer to that of the PE model when $F_1 < 0.243$. The range of values of F_1 corresponding to the different chaotic and periodic regimes from C_1 to P_4 are almost the same for the PE and BE models as shown in Tables 3.1 and 3.3. In Fig 3.18 we present 20-day time evolutions of x_1, y_1 and z_1 at F_1=0.055, 0.1 and 0.12 when the BE model has reached the corresponding attractors. At these values of F_1, the attractors are chaotic and the variations of x_1, y_1 and z_1 are quite similar to the corresponding evolutions in the PE model (compare Fig. 3.18 with 3.2, 3.4 and 3.6). The projection of the chaotic attractor of the BE model at F_1=0.12 is shown in Fig. 3.19 as several Poincare cross-sections and should be compared with the corresponding PE attractor given in Fig. 3.7. The similarity between the two models is quite striking. As mentioned earlier, the states of the PE attractors can be well approximated by the balance equation (2.16).

The xy orbits of the periodic regime P_4 in the PE and BE models

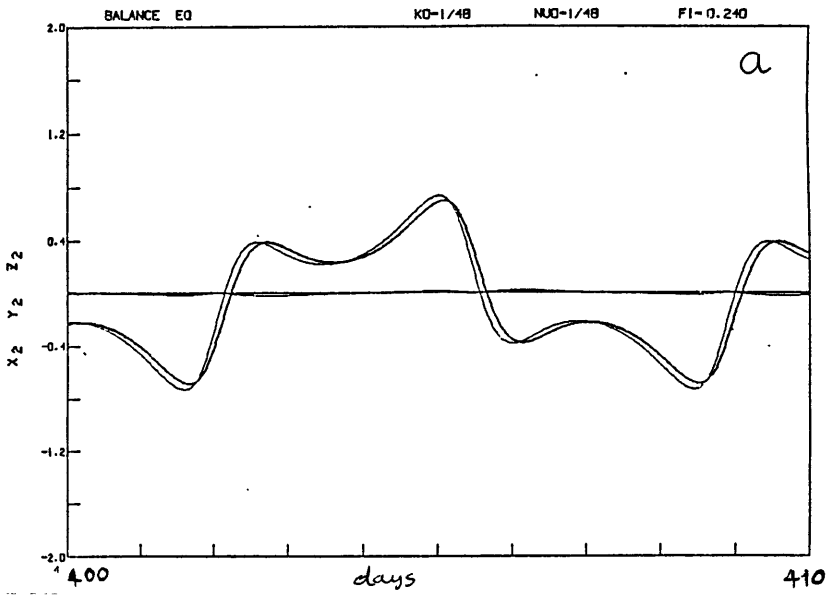

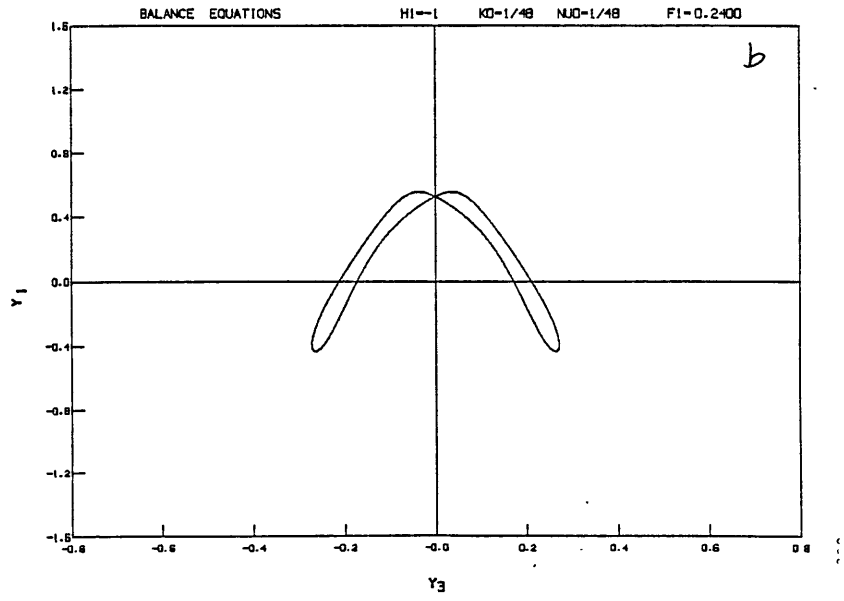

Figure 3.20. BE model at h_1=-1.0: xy orbit at F_1=0.24.

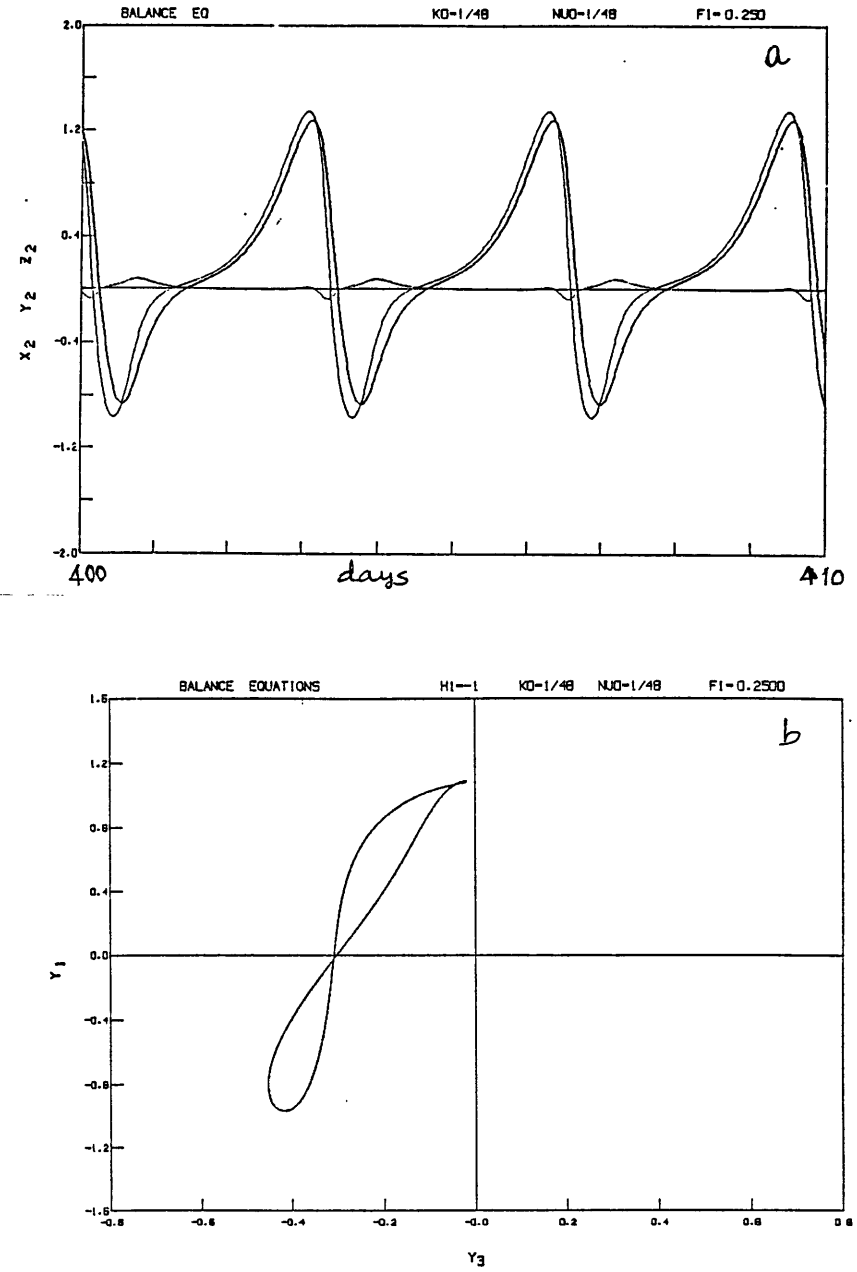

Figure 3.21. BE model at h_1=-1.0: x orbit at F_1=0.25.

resemble each other closely in the range $0.123 < F_1 < 0.243$. The xy orbit at $F_1=0.24$ in the BE model is shown in Fig. 3.20 and looks very much like the xy orbit of the PE model shown in Fig. 3.8. Unlike in the QG model, the periodic regime P_4 of the BE model ends in a saddle-node bifurcation at $F_1=0.246$ where the stable xy orbit merges with an unstable xy orbit. With this bifurcation, the BE model reproduces the behavior of the PE model at $F_1=0.2437$. Thus the symmetric xy orbit ceases to exist beyond certain value of F_1 in the PE and BE models whereas it remains a stable solution in the QG model as $F_1 \to \infty$.

The similarity in the behavior of the PE and BE models ends with the saddle-node bifurcation of the xy orbit. For all values of $F_1 > 0.246$ until the orbits go to infinity at $F_1=1.72$, the attractor of the BE model is a periodic x orbit (and a y orbit by symmetry). In Fig. 3.21 we show such a y orbit at $F_1=0.25$. Comparing with the xy orbit at $F_1=0.24$ in Fig. 3.20, we notice that the maxima of the variables in the y orbit have increased considerably and the period of the y orbit has almost halved. As F_1 increases, the period of the y orbits decreases while the amplitude continue to increase. Looking again at the PE model, the x orbit in the periodic regime P_5 (Fig. 3.15) appears like an x orbit of the BE model with superposed gravity waves. We will discuss more about the gravity waves and the x periodic orbits of the PE model later.

An interesting property exhibited by the BE model is the hysterisis effect if F_1 is decreased slowly while following the x orbit. Let us start from an x orbit at $F_1=0.25$ and decrease F_1 slowly while using point on the attractor of the previous F_1 as the initial condition for the

new integration. As F_1 decreases, the x orbits continue to be attractors of the BE model even when xy orbits are also attractors of the model for $F_1 < 0.246$. For a small range of F_1, both x and xy orbits are attractors of the BE model. When F_1 is further decreased, the x orbit undergoes period doubling bifurcations culminating in chaos. These chaotic attractors exist for a small range of F_1. If this second branch of attractors is followed by further decreasing F_1, we find that there are other periodic orbits like x^2y^2, x^3y^3 and other chaotic windows. Finally the second branch ceases to exist for $F_1 < 0.2293$. Between F_1=0.2293 and F_1=0.246, depending on the initial condition, the BE model can reach either the xy periodic orbit or an attractor in the second branch belonging to the x orbit. When the x orbit undergoes period doubling bifurcation, it continues to exist as an unstable periodic solution as F_1 is decreased. By following this unstable x orbit with decreasing F_1, we have concluded that it shows all signs of being created as a homoclinic orbit at $F_1 \approx 0.23$. Thus we can distinguish two branches of solutions in the BE model. The first branch is equivalent to the solutions of Lorenz's convection model (or the QG model) but with the end of the xy orbit. The second branch is born at $F_1 = 0.23$, undergoes its own sequences of behavior and bifurcations and ends in an x orbit. We will discuss the possibility of extending similar arguments to the PE model later.

3.3. ALL MODELS WITH DIFFERENT h_1

From the previous discussions of the attractors of the PE and BE models one might get an impression that the saddle-node birfucation of the xy orbit (i.e., the end of the P_4 regime) is somehow responsible for the

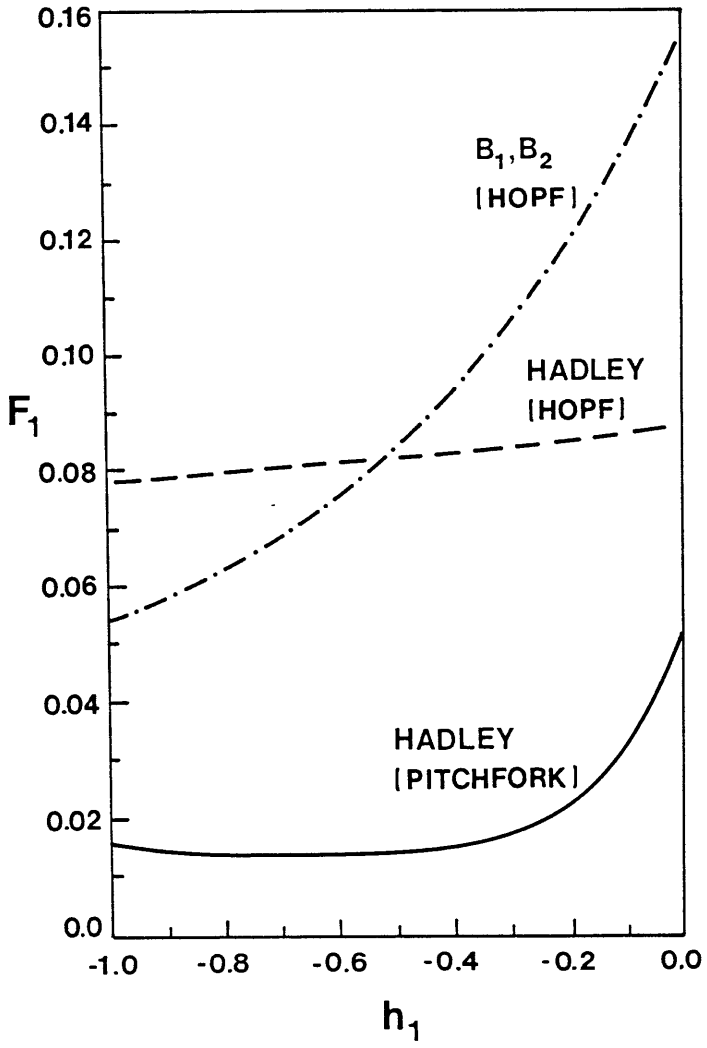

Figure 3.22. Bifurcations of the steady states in the PE model.

persistence of the gravity waves in the attractors of the PE model as F_1 is increased. When h_1=-1.0, the topography varies from +2 to -2 km, and the slow Rossby motion is enhanced while the gravity waves are damped out for up to moderate values of F_1. We now describe the behavior of the model as the variation of the topography is decreased (i.e., as $|h_1|$ is decreased). The PE and BE models have been studied at h_1=-0.5, -0.25, -0.1 and 0.0. We will, however, present a summary of the behavior of the models when h_1=-0.5 and h_1=0 and discuss the nature of some attractors for h_1=0 with particular interest in persisting gravity waves.

For all values of h_1, the Hadley fixed point and the branch equilibria B_1 and B_2 are solutions of the PE and BE models and they are stable for small values of F_1. The bifurcations of these fixed points are similar to the case when h_1=-1.0 and are represented in Fig. 3.22 for $-1.0 < h_1 < 0.0$. We notice that the Hopf bifurcation of the Hadley fixed point (involving gravity wave frequency) occurs before the Hopf bifurcation of B_1 or B_2 when $h_1 > 0.54$.

The complete behaviors of the PE and BE models are summarized in Table 3.4 for h_1=-0.5 and h_1=0. In Table 3.4, we have listed the values of F_1 corresponding to the different regimes of behavior. The time-dependent solutions of the two models follow the same sequences of the behavior as found in the case with h_1=-1.0. However, as $|h_1|$ decreases, the entire sequence of different regimes is shifted in the increasing direction of the forcing parameter space. Concerning the nature of the solutions, the labels of the different regimes in Table 3.4 have the same meaning as in Fig. 3.1; for example, the P_4 regimes consist of periodic

Regime	Range of F_1 (h_1=-0.5)	Range of F_1 (h_1=0.0)
Hadley fixed point	0.00.. - 0.013	0.0.. - 0.0504
Fixed points B_1 and B_2	0.014 - 0.083	0.0505 - 0.1523
Chaotic C_1	0.084 -	0.156 - 0.287
Periodic P_1 (x^2y)	-	0.288 -
Chaotic C_2	- 0.154	0.289 - 0.297
Periodic P_2 (x^2yxy^2xy)	0.155 -	0.298 - 0.299
Chaotic C_3	0.156 - 0.159	0.300 - 0.303
Periodic P_3 (x^2y^2)	0.160 - 0.167	0.304 - 0.316
Chaotic C_4	0.168 - 0.175	0.317 - 0.323
Periodic P_4 (xy)	0.176 - 0.3469	0.324 - 0.5657
Chaotic C_5	0.347 - 0.700	0.566 - 0.734

Table 3.4a. PE model (h_1=-0.5 & 0.0): F_1 for different regimes

Regime	Range of F_1 (h_1=-0.5)	Range of F_1 (h_1=0.0)
Hadley fixed point	0.00.. - 0.013	0.0.. - 0.0504
Fixed points B_1 and B_2	0.014 - 0.083	0.0505 - 0.1523
Chaotic C_1	0.084 -	0.158 -
Periodic P_1 (x^2y)	-	-
Chaotic C_2	- 0.154	- 0.308
Periodic P_2 (x^2yxy^2xy)	0.155 -	0.308 - 0.309
Chaotic C_3	0.156 - 0.159	0.310 - 0.313
Periodic P_3 (x^2y^2)	0.160 - 0.168	0.314 - 0.324
Chaotic C_4	0.169 - 0.176	0.326 - 0.333
Periodic P_4 (xy)	0.177 - 0.367	0.334 - 0.716
Periodic P_5 (x)	0.368 - 0.700	0.722 - 1.0+
P_5, C_5 (Hysterisis)	0.356 -	0.717 - 0.721

Table 3.4b. BE model (h_1=-0.5 & 0.0): F_1 for different regimes

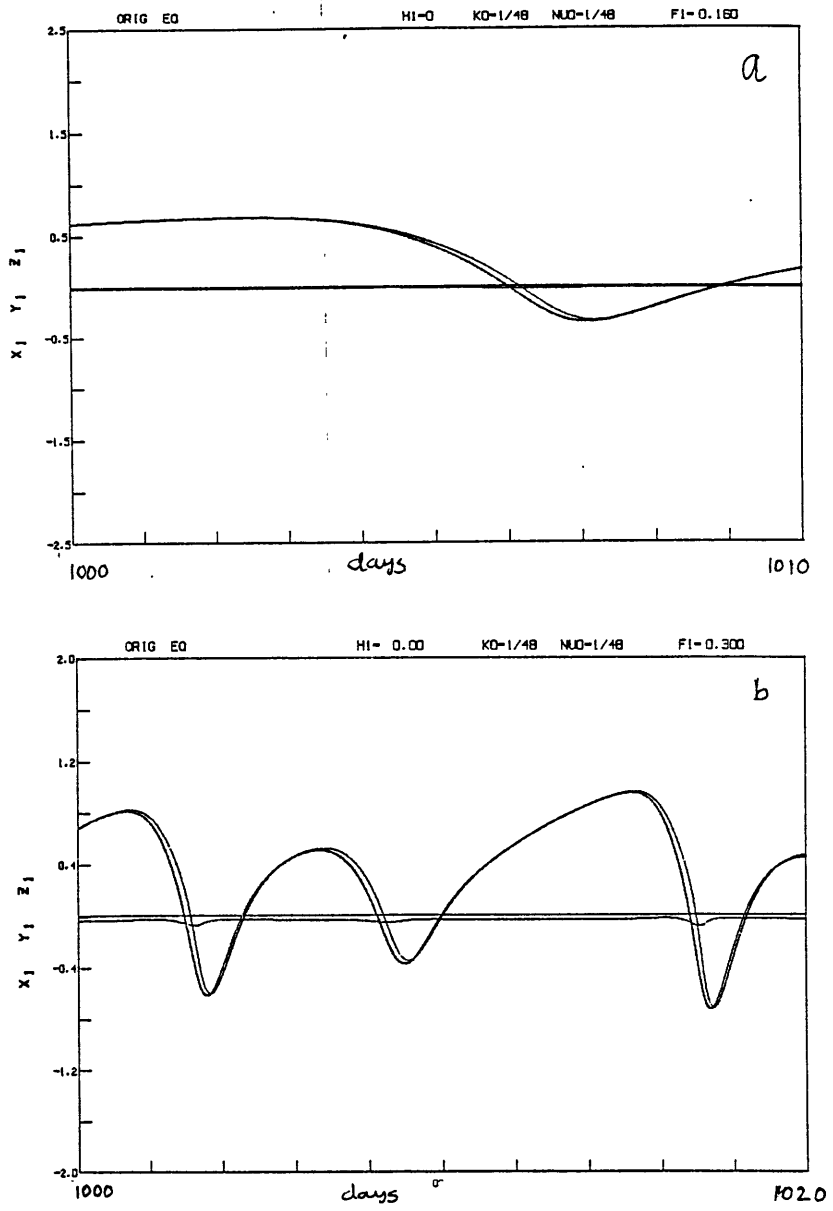

Figure 3.23. PE model (h_1=0.0): variations of x_1, y_1, z_1 at (a) F_1=0.16, (b) F_1=0.3.

xy orbit as was the case with h_1=-1.0.

The various bifurcations occuring between the regimes C_1 and P_4 are the same for all the values of h_1 we have studied. We will discuss the bifurcations beyond P_4 later. When h_1=0, the Hadley fixed point is the only attractor for the QG model for all values of F_1. For other values between h_1=-1 and h_1=0, the QG model has the same type of behavior seen when h_1=-1, though the different regimes occur at different values of F_1. As h_1 approaches zero, the QG model becomes less and less of an approximation to the PE and BE models.

The values of F_1 corresponding to the different regimes from C_1 to P_4 in the BE model are close to those of the PE model even when h_1=0. However, there are some important differences in the nature of the attractors between the PE model at h_1=0 and the PE model at h_1=-1 or the BE model at h_1=0. We will show that these differences are related to the presence of persisting gravity waves in the attractors.

We now discuss the attractors of the PE model with h_1=0. In Fig. 3.23, we show the variations of x_1, y_1 and z_1 for 20 days within the attractor at F_1=0.16 and 0.3 in the chaotic C_1 and C_3 regimes respectively. We have examined long time series of many attractors in these regimes and have found that they are qualitatively similar to those of the BE model at h_1=0 and of the PE model at h_1=-1. However, a more detailed numerical examination of the maxima of any variable, say z_1, has shown the presence of high-frequency oscillations superposed on the slow variations in many attractors belonging to regimes from C_1 to P_4. These

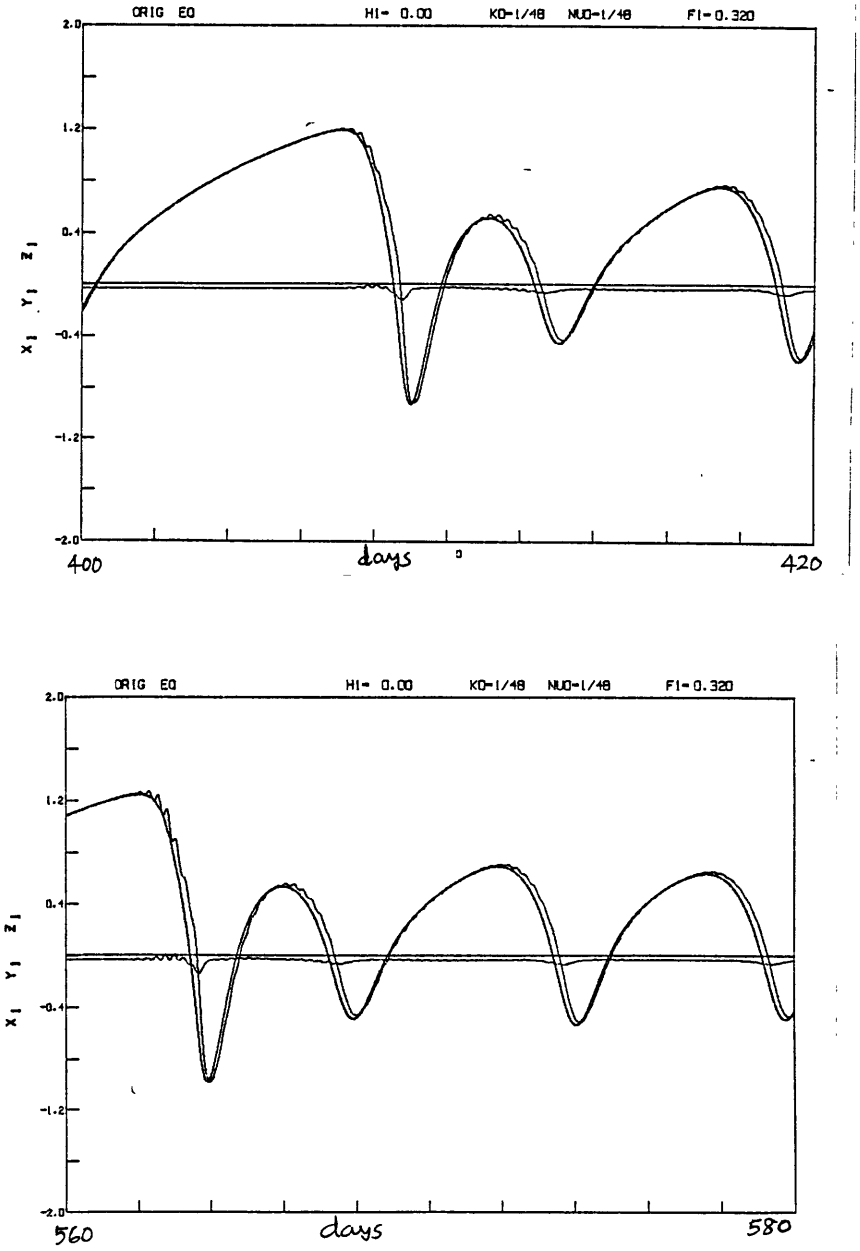

Figure 3.24. PE model (h_1=0.0): Variations of x_1, y_1, z_1 at F_1=0.32.

F_1	λ_1	λ_2	λ_3	λ_4	λ_5	λ_6	λ_7	λ_8	λ_9	d
0.32	0.008	0.0	-0.009	-0.009	-0.023	-0.023	-0.065	-0.065	-0.128	2.95

Table 3.5. Spectrum of Lyapunov exponents (λ's) and Fractal dimension (d) ($h_1 = 0.0$)

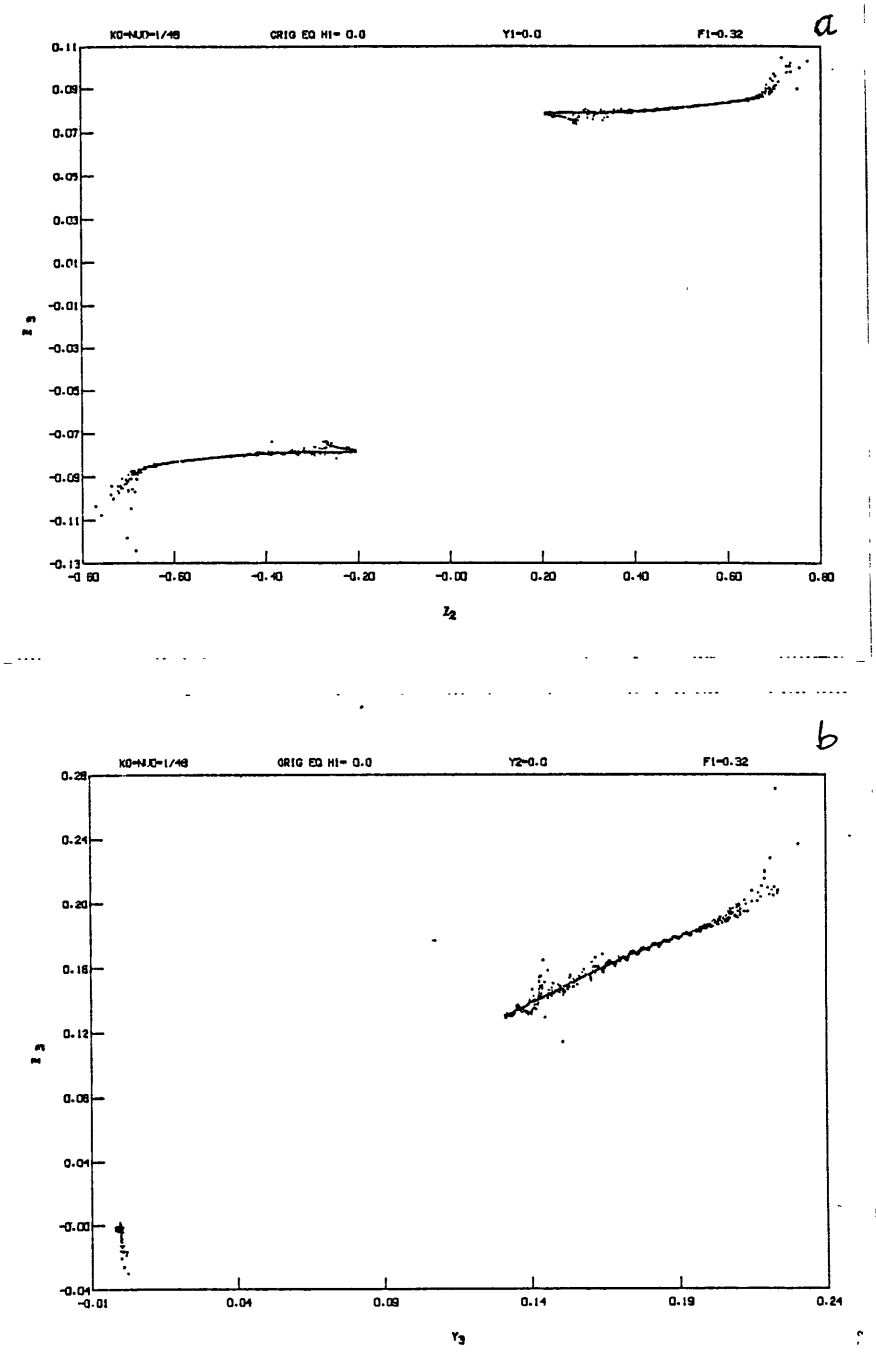

Figure 3.25. Poincare cross-sections (y_1=0 and y_2=0) at F_1=0.32 in the PE model (h_1=0.0).

gravity waves, however, have very small amplitudes and seem to appear infrequently for lower values of F_1. At such values of F_1, most of the points on the attractor are quasi-geostrophic or nearly satisfied by the balance equation.

For values of $F_1 > 0.3$, the presence of persisting gravity waves becomes more evident when the time series of the attractors are examined. One such case, at F_1=0.32, in the C_4 regime is shown in Fig. 3.24 which consists of 10-day variations of x_1, y_1 and z_1. By examining a long time series of the variables of the attractor at F_1=0.32, we have found that the intensity of the gravity waves superposed on the slow motion is always as weak as we see in Fig. 3.24. This behavior is much different from the attractors with gravity waves of the PE model in the C_5 regime when h_1=-1.0 (Fig. 3.14). Though the attractor represented in Fig. 3.24 is nonperiodic, it appears to be less chaotic. The spectrum of Lyapunov exponents for this case is given in Table 3.5 and the corresponding fractal dimension is found to be 2.95. It is even possible to examine the structure of this attractor by projecting it onto to a three-dimensional subspace as shown in Fig. 3.25 which consists of different Poincare cross-sections. These projections do not fill up the phase space, but yet cannot be approximated by smooth curves as in Fig. 3.7 (for F_1=0.12, h_1=-1.0). The presence of gravity waves is clearly evidenced in the scattering of the points around a smooth curve. When y_2=0 the geostrophic and the balance relations are both given by $y_3 = z_3$. Thus, a corresponding projection of the attractor of the BE model would be represented by points on the $y_3 = z_3$ line.

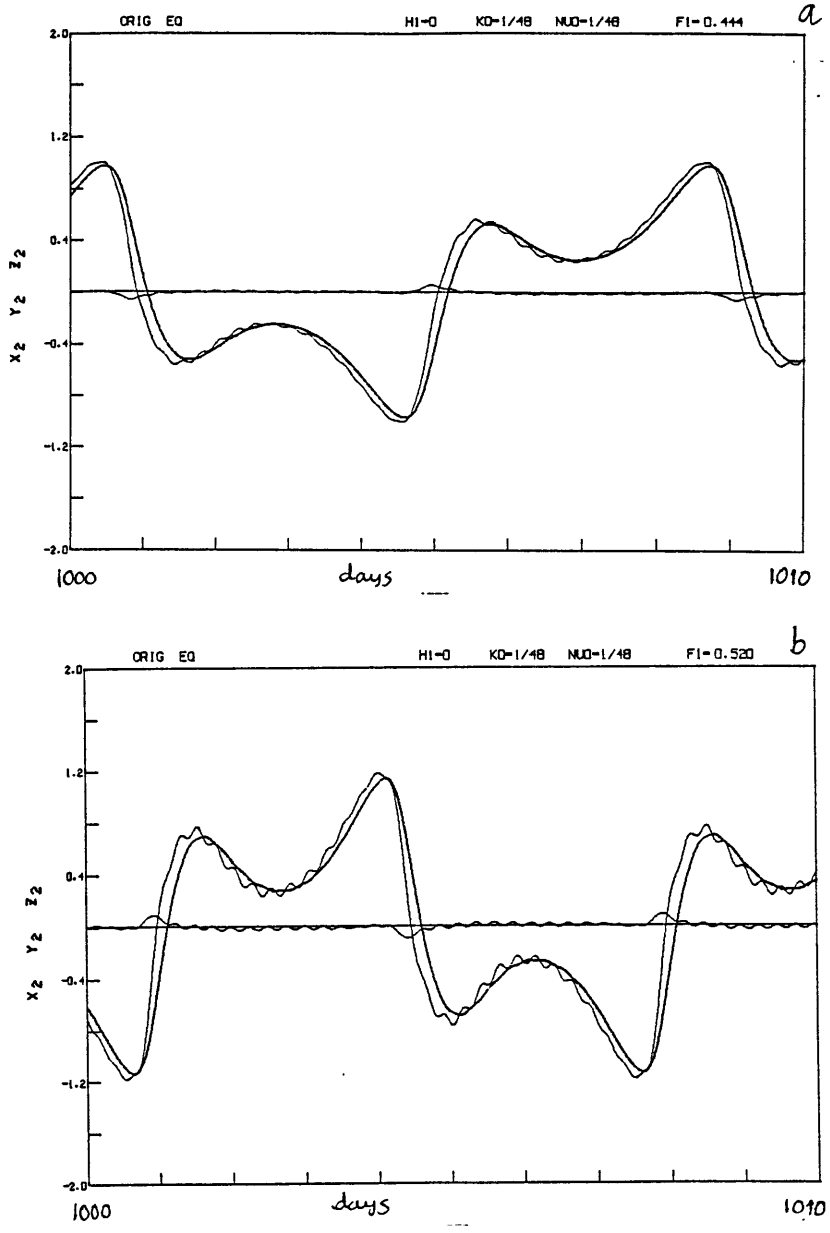

Figure 3.26. xy orbits at (a) F_1=0.444 and (b) F_1=0.52 in the PE model with h_1=0.0.

In the entire periodic regime P_4 for h_1=-1.0, the xy orbits did not reveal the presence of high-frequency oscillations. However, when h_1=0, we have found that the xy orbits consists of gravity waves superposed on slow oscillations. Figure 3.27 shows the xy orbits at F_1=0.444 and 0.52. The intensity of the gravity waves increases with F_1. The manner in which the gravity waves are phase locked with the slow motion also changes as F_1 is varied. The number of maxima corresponding to the gravity waves in one period varies with F_1. The xy orbit becomes unstable at F_1=0.5658 due to a Hopf bifurcation. It must be remembered that the xy orbit was annihilated in a saddle-node bifurcation for h_1=-1.0. After the Hopf bifurcation, as F_1 is increased, the PE model exhibits chaotic behavior with persisting gravity waves. The xy orbit remains an unstable solution for a range of values of F_1 after the Hopf bifurcation. It is possible for the unstable xy orbit to be part of the chaotic attractors in such cases. In the BE model, the xy orbit still undergoes a saddle-node bifurcation and the model follows a behavior similar to the case with h_1=-1.0 as F_1 is increased.

It was found that a periodic orbit with gravity wave period (6 hours) was created as a result of the Hopf bifurcation of the Hadley fixed point in the PE model with h_1=-1.0. The periodic orbit was an unstable solution for all values of F_1 after the bifurcation. As seen in Fig. 3.22, the Hopf bifurcation of the Hadley fixed point occurs for all values of h_1. When h_1=0, the periodic orbit G created at the Hopf bifurcation exists as an unstable solution in the $0.087 < F_1 < 0.22$. From F_1=0.22 to F_1=0.604, the periodic orbit G is found to be stable and hence becomes a

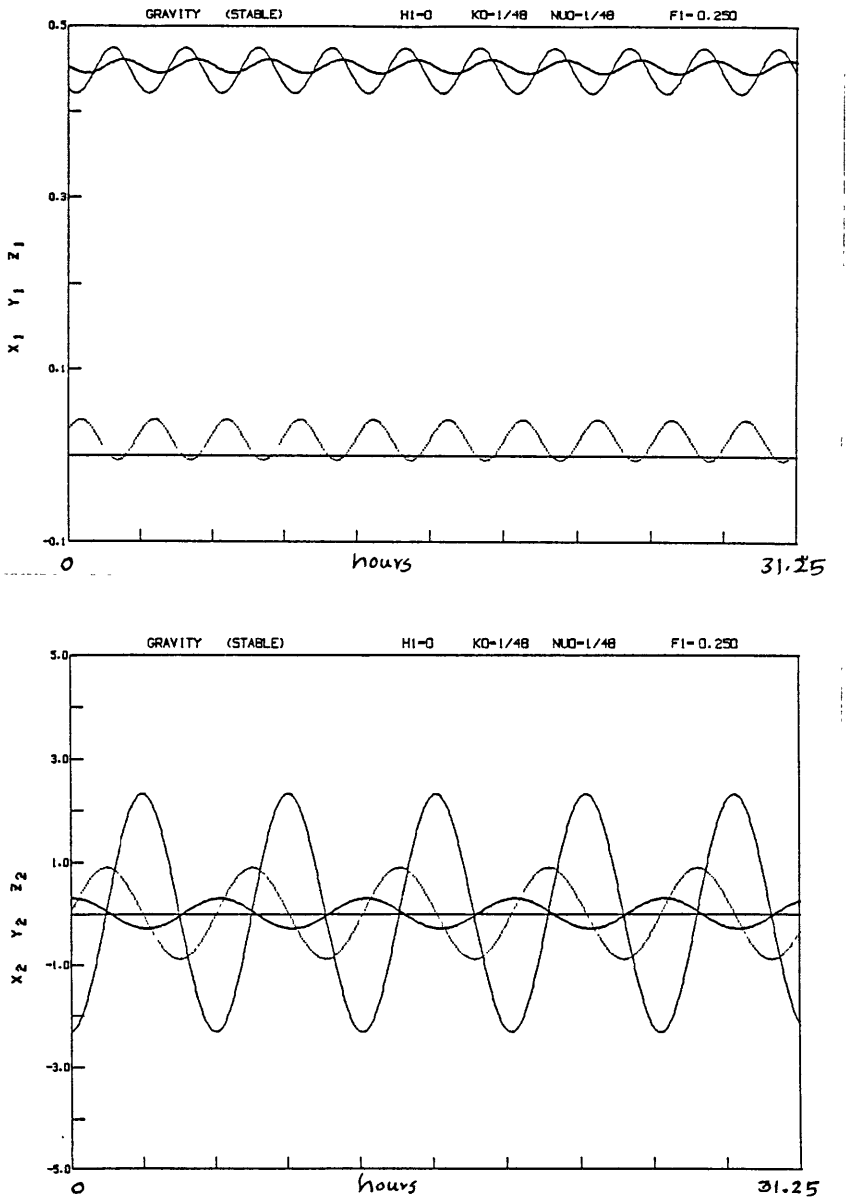

Figure 3.27. Stable periodic orbit G at F_1=0.25 (PE model with h_1=0.0).

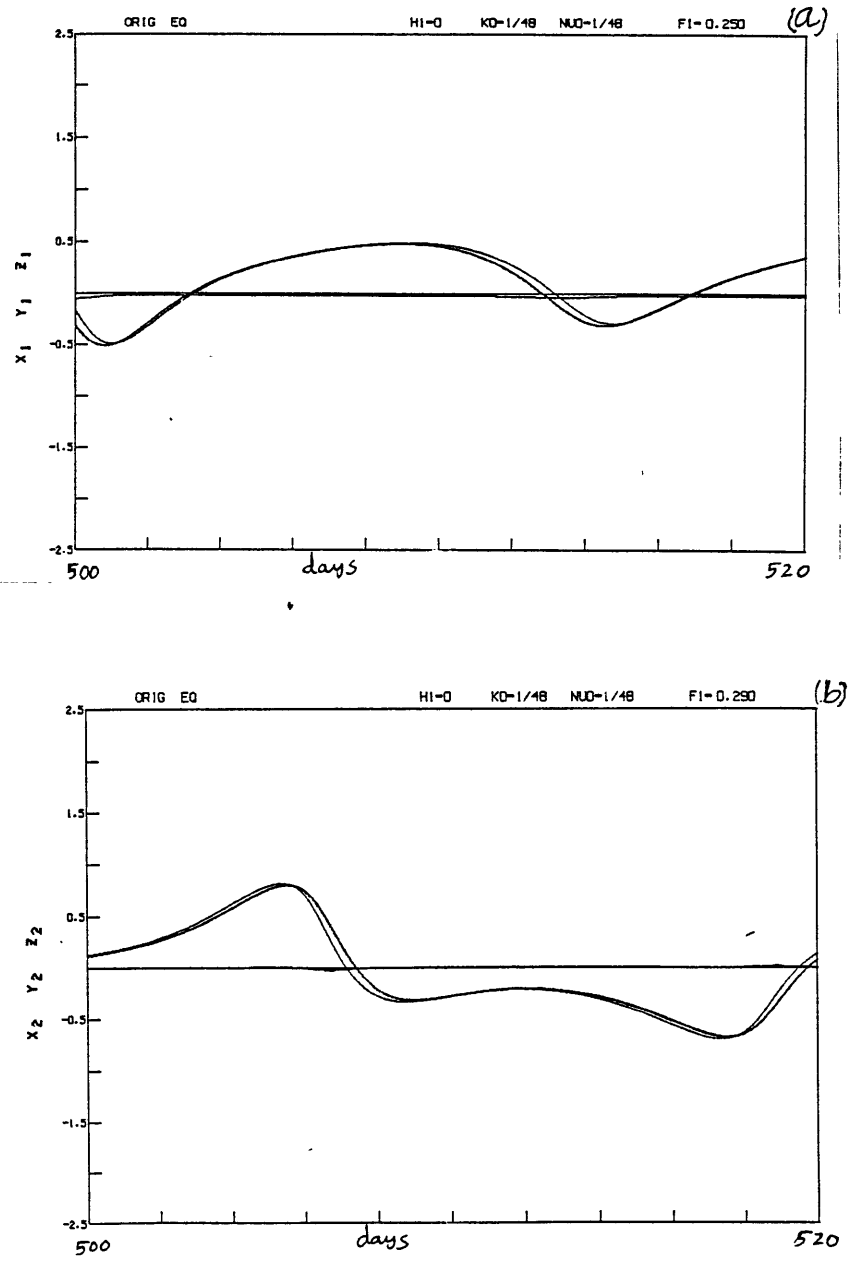

Figure 3.28. Variations of x_1, y_1, z_1, and x_2, y_2, and z_2 of the chaotic attractor at F_1=0.25 in the C_1 regime of PE model with h_1=0.0.

second attractor of the PE model. In Fig. 3.27 we present such an attractor for F_1=0.25. At F_1=0.604, the orbit G looses stability due to a Hopf bifurcation, but remains as an unstable solution until the PE model blows up at a higher value of F_1. The amplitudes of the variables increase considerably with increasing F_1 while the period of the orbits increases by a very small value.

At a particular value of F_1, depending on the initial conditions, the PE model will reach either the orbit G or one of the corresponding attractors given in Fig. 3.1. We have also found that, keeping the same arbitrary initial condition and varying F_1, the model reaches either G or the regimes in Fig. 3.1 for different values of F_1. Thus, when F_1=0.25, it is possible to reach either the gravity attractor G as in Fig. 3.27 or the chaotic attractor in C_1 (Fig. 3.28) whose states are mostly quasi-geostrophic or balanced. The initial points to reach the two attractors may in fact be quite near in the phase space.

The orbits in the periodic regime G are found to be stable for other values of h_1 also. As h_1 approaches from 0.0 to -1.0, the range of values of F_1 for which the orbits in G are attractors shrinks. At h_1=-0.8, the periodic orbit in G is unstable for all values of F_1. When the periodic orbit G is an attractor, it looses stability by Hopf bifurcation as F_1 is increased.

3.4. GRAVITY WAVES

From the discussions of the previous sections it is clear that the

gravity waves are present in the attractors of the PE model when the forcing is strong for all values of topography h_1. When the forcing is weak or moderate, the gravity waves do not seem to persist in the attractor for h_1=-1.0 though they are present at h_1=0 and other values. We now offer some discussion relating these facts to some properties of the Hadley fixed point. Another point of discussion in this section is concerned with the attractors (with gravity waves) of the PE model beyond the P_4 regime. In the BE model we have seen that the x periodic orbit of the P_5 regime follows a hysterisis path as F_1 is decreased. The x orbit is created as a homoclinic orbit and forms a second branch of solutions. This is true for all values of h_1. We will examine the possibility of having analogous behavior in the PE model.

In his study of the PE model at F_1=0.1, Lorenz (1980) stated that the Hadley fixed point was part of the chaotic attractor. He showed that the orbits within the attractor came close to the Hadley fixed point often. Such close encounters of the orbits with H also occur at other values of F_1 for which the attractors are chaotic. The Hadley fixed point is not part of any periodic attractor. We recall that H undergoes a Hopf bifurcation at F_1=0.0775. A small departure from H oscillates with gravity wave frequency near H for any value of F_1. We now discuss the evolutions of such orbits initiated from near H. When the Hadley solution is stable, the gravity waves decay and the orbit spirals into H after a short time. When the attractor is chaotic, the Hadley fixed point is unstable also with respect to slow mode because of the pitchfork bifurcation. For $F_1 < 0.0775$, the initial gravity waves damp out after a few days and the orbit reaches the chaotic attractor containing slow

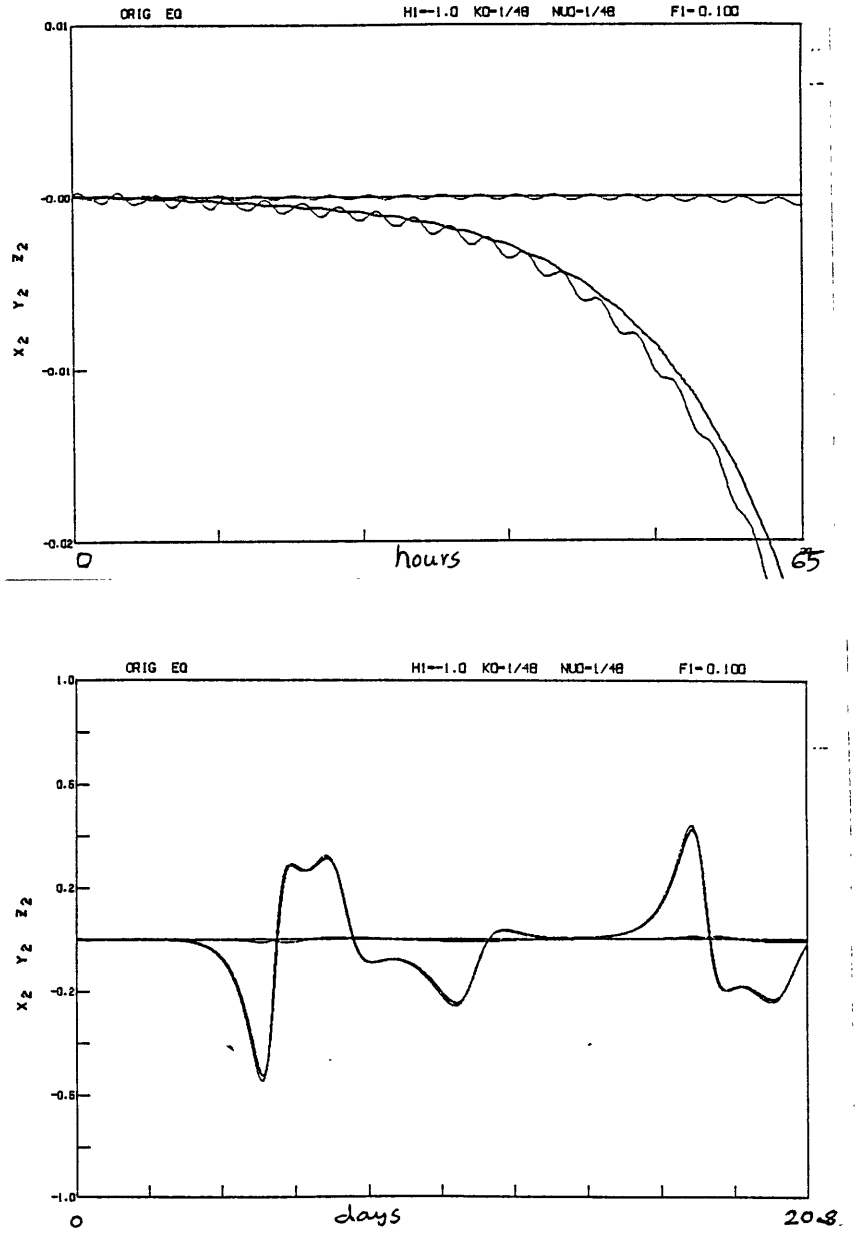

Figure 3.29. Orbit from near Hadley point at F_1=0.1 (PE model with (h_1=-1.0).

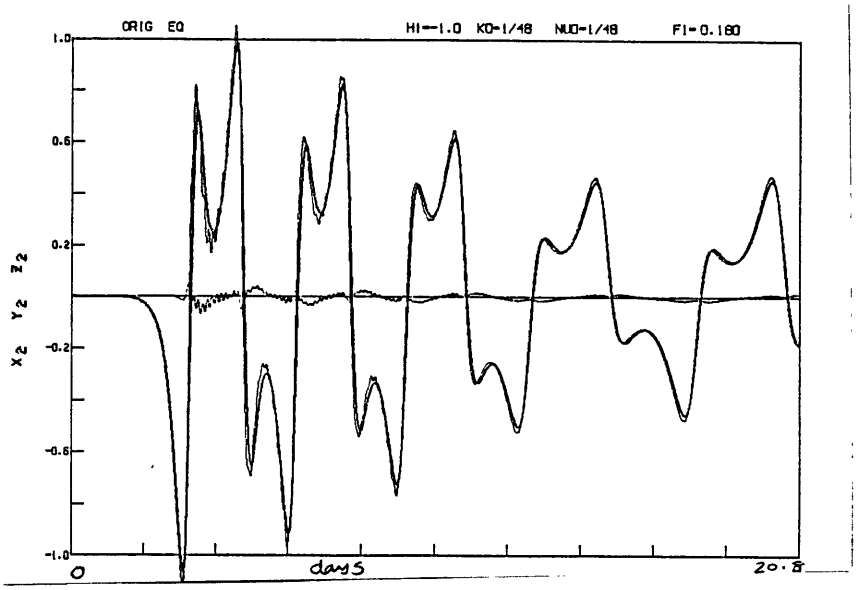

Figure 3.30. Same at Fig. 3.29 at F_1=0.18.

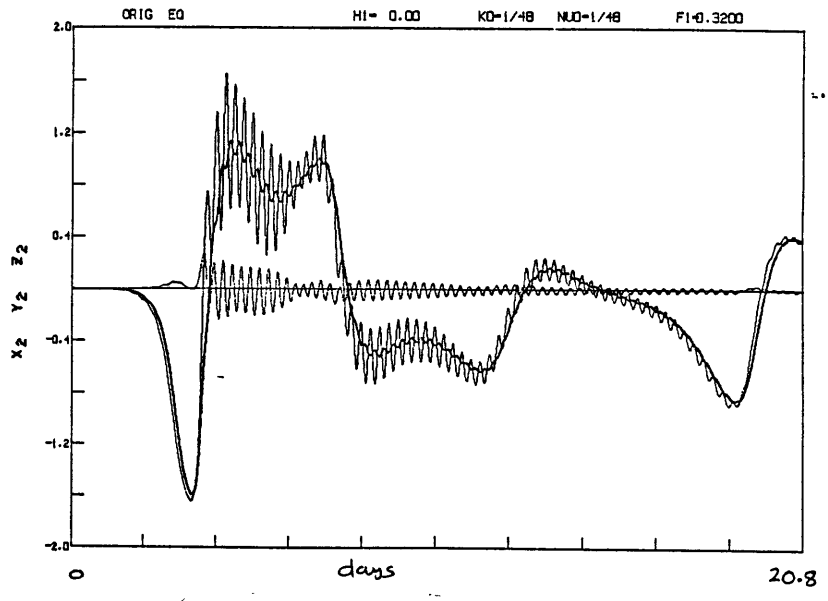

Fig. 3.31 contd...

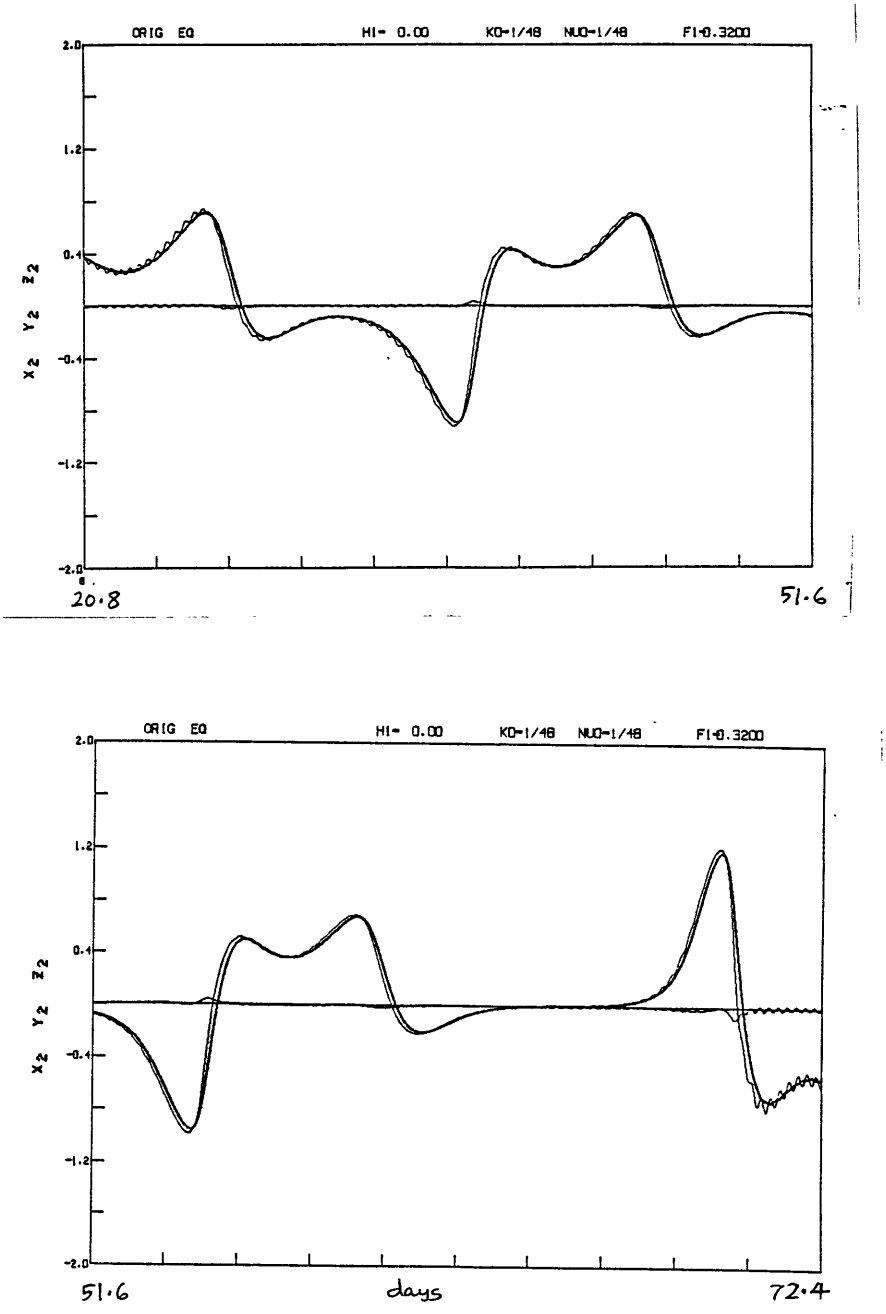

Figure 3.31. Orbit from near Hadley point at F_1=0.32 (PE model with (h_1=0.0).

motion. Let us now increase F_1 and consider some cases after the Hopf bifurcation of H has occured. In Fig. 3.29 we show the behavior of the orbit emanating from near H when F_1=0.1. The orbit spirals away from H with gravity wave frequency while also moving with slow motion, and the gravity waves decay after a few days. The subsequent evolution consists of only slow motion, the orbit having entered a region of phase space away from H where gravity waves are damped. We have examined long time series and have found that, though the encounters of the orbit with H are many, they are not close enough to excite gravity waves.

As F_1 is further increased, longer time is required for the initial gravity waves to be damped as shown for F_1=0.18 in Fig. 3.30. It is also possible that as F_1 increases, regions around H, where the gravity waves are not damped, may become larger. Thus we cannot identify the Hopf bifurcation of the Hadley fixed point as the bifurcation that causes the attractors to contain persisting gravity waves.

We discussed earlier the chaotic attractor at F_1=0.32 and h_1=0.0 (Sec. 3.3, Fig. 3.24) which consisted of gravity waves. For a given value of F_1, the Hadley solution is located at the same point in the phase space for all the values of h_1. However, its stability property changes with h_1. Even though the attractor in Fig. 3.24 is in regime C_4, the stability of H is quite different. In Fig. 3.31 we show the behavior of an orbit initiating as a small departure from the Hadley fixed point. In this case, we notice that the gravity waves do not completely die out and that they are present in the attractor. It is clear that, in certain regions of phase space visited by the orbit, the gravity waves are not damped.

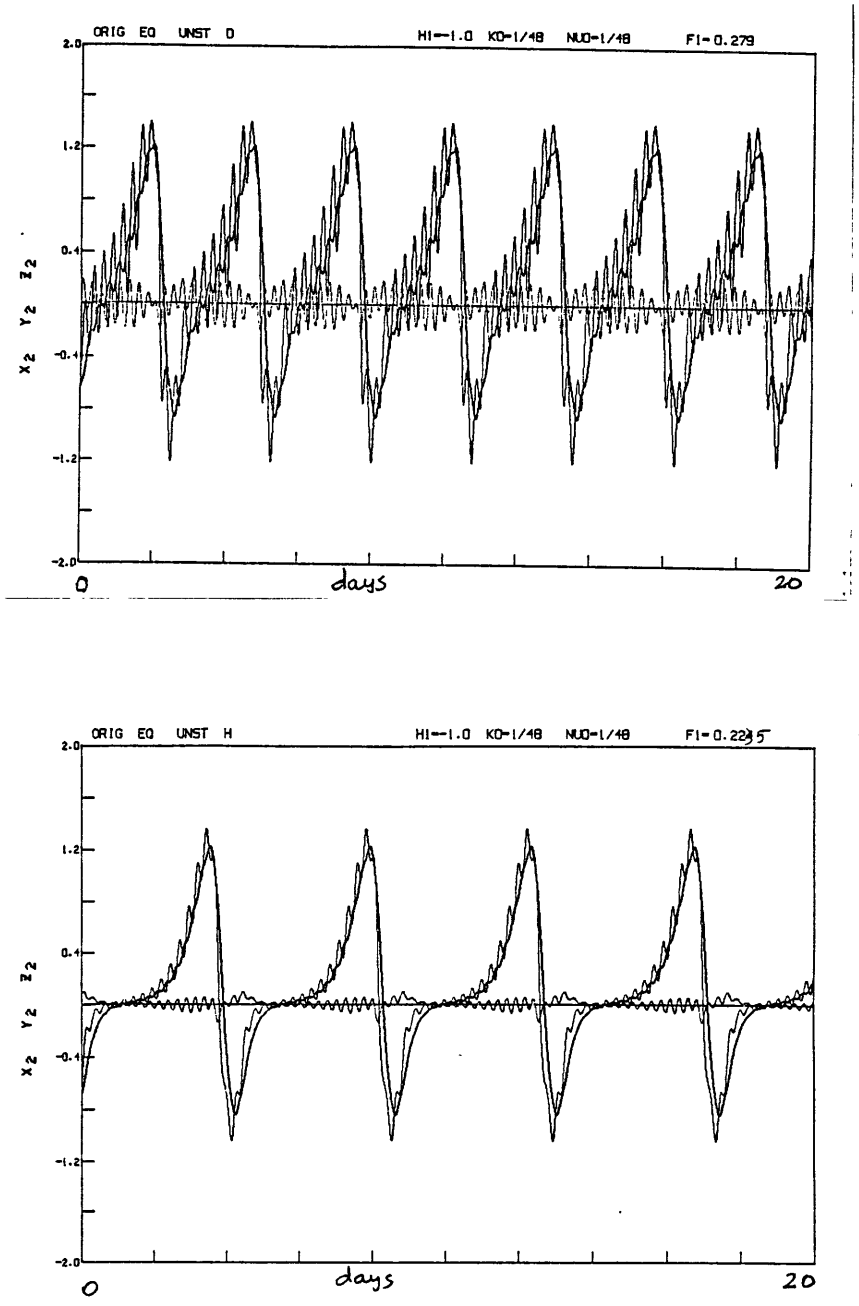

Figure 3.32. Unstable x orbit of PE model with h_1=-1.0 at (a) F_1=0.279, and (b) F_1=0.2235.

Beyond the P_4 regime, for all values of h_1, the presence of the gravity waves in the attractors is quite evident. In the BE model, x or y orbits are the attractors (Fig. 3.21) after the P_4 regime ends. As we saw earlier when h_1=-1.0, the x orbits of P_5 regime (Figs. 3.15) can be considered to be x orbits of the BE model with superposed gravity waves. In the PE model, beyond the P_4 regime, we have found other unstable periodic orbits, resembling the x orbits of the P_5 regime, exist over a large range of values of F_1. At a given value of F_1, these unstable periodic solutions have slightly different periods and the orbits are close to each other.

Starting with one such unstable x orbit in the C_5 regime of the PE model, we decreased F_1 slowly and determined that the x orbit existed even at those values of F_1 corresponding to P_4 regime. In Fig. 3.32, three such orbits at F_1= 0.279 and 0.2235 are shown. The period of these orbits increases as F_1 decreases. The orbit is also approaching the Hadley fixed point as seen from the maxima of y_1 and z_1 and the corresponding y_2 and z_2 in Fig. 3.32. In the BE model, such an x orbit was stable for some values of F_1, underwent period doubling bifurcation and was created as a homoclinic orbit of the Hadley fixed point. We have found similar behavior for other values of h_1. For certain values of h_1, the xy orbit in P_4 regime of the PE model ends in saddle-node bifurcation, while for other values of h_1, it undergoes Hopf bifurcation. We do not know the extent to which the analogy between the PE and BE models can be drawn. The x orbits of the PE model are unstable and the gravity waves certainly seem to play an important role in their instability and the subsequent behavior of the PE model as F_1 is increased.

Chapter 4 THE SLOW MANIFOLD

From the description of the behavior the PE model in Chapter 3 the gravity waves appear to be completely absent in the attractors corresponding to weak forcing. When h_1=-1.0, in the range $0 < F_1 < 0.24$, the BE model reproduces the solutions of the PE model in a very close manner. If the gravity waves die out completely by the time the attractor is reached, the solutions of the PE model should vary with three degrees of freedom. For such cases, as Lorenz (1980) has discussed, the attractor should be embedded in a three-dimensional stable invariant slow manifold. Under the action of the flow represented by the primitive equations, the slow manifold is said to be invariant if a point on it evolves in time remaining on the slow manifold. The slow manifold is stable if a point near it eventually reaches points on it. Lorenz's study shows that the chaotic attractor at F_1=0.1 is contained in a stable invariant slow manifold.

A point on the slow manifold is defined by three variables which determine the other six so that the orbits with initial states on the slow manifold do not have gravity waves. In this chapter we will describe the method used by Lorenz (1980) to calculate the values of the six variables as functions of three variables, say the y's, of a point on the slow manifold. The results of applying Lorenz's method on various points of the attractors at different values of F_1 will be discussed. We will determine whether or not the attractors are embedded in the slow manifold as F_1 is varied. We will specifically be interested to know the nature of

the attractors in this regard in the range $0 < F_1 < 0.243$. If the attractor at any value of F_1 is not contained in the slow manifold, the initialization procedure with the states of slow manifold will be carried out. The resulting orbits will be examined to determine whether gravity waves are reexcited. Based on these results, we will discuss whether or not a stable invariant slow manifold exists for any value of F_1. We must emphasize that all our results and conclusions are based on the particular definition that the states of the slow manifold are determined by Lorenz's method.

4.1. SUPERBALANCE STATES: LORENZ'S ALGORITHM

The determination of the states of the slow manifold consists of finding a function that relates three fixed variables with the remaining six. Lorenz (1980) devised a method to calculate such a function based on complete separation of the frequencies of the gravity waves and the quasi-geostrophic oscillations. The frequencies of the two motions differ by one order of magnitude. In the PE model being studied, the gravity waves oscillate with a period of about six hours whereas the slow motion varies on the order of a few days depending on F_1.

Consider one of the variables of the solution of the PE model and assume that it can be separated into quasi-geostrophic and gravity wave components. With such a decomposition, the ratio of the gravity wave to quasi-geostrophic components of the variable will be about n order of magnitude less than the corresponding ratio of the n^{th} time derivative of the same variable. Hence, if there are no gravity waves in the

solution, the value of the n^{th} time derivative of any variable, for large n, should be close to zero compared to the value of the variable. Lorenz used this criterion to devise an algorithm to find the points on the slow manifold.

Lorenz's method consists of considering the values of three variables y_1, y_2 and y_3 to be fixed and then determining the remaining six variables. We will follow Lorenz's notation and define X and Y to be six- and three-dimensional vectors with components $(x_1,x_2,\ldots,x_6)$ and (y_1,y_2,y_3) respectively. In vector X, we have kept x_1, x_2 and x_3 unchanged and have defined $x_{i+3} = y_i - z_i$ for i=1,2,3. Thus, to find the points on the slow manifold, we have to determine a converged value of X such that $dX/d\tau=0$, $d^2X/d\tau^2=0$, etc., in successive approximations. The geostrophic relation X=0 is chosen to be the starting approximation.

To find the solutions of the algorithm, Lorenz suggested a double approximation procedure. For each n, the value of X which satisfies $d^nX/d\tau^n=0$ is determined by iteration. If $X_{n,k}$ denotes the k^{th} approximation of X within such an iteration cycle, the starting approximation is the geostrophic relation $X_{1,0}=0$. Then $X_{n,k}$ is determined by solving

$$[\partial(d^nX_{n,k}/d\tau^n)/\partial X_{n,k}](X_{n,k+1} - X_{n,k}) = -d^nX_{n,k}/d\tau^n. \qquad (4.1)$$

The solution of (4.1) involves inverting a sixth order square matrix consisting of partial derivatives. It is not difficult to evaluate the elements of the matrix by explicitly writing the expressions for the partial derivatives. They can be evaluated approximately by perturbing

the components of X one at a time and finding the differences of the corresponding components of $d^nX/d\tau^n$. When the iteration procedure has converged at k=K(n) for a particular n, we use $X_{n,K(n)}$ as the starting approximation for the iteration cycle at n+1 (i.e., by letting $X_{n+1,0} = X_{n,K(n)}$). If there is a solution for Lorenz's algorithm, the entire procedure should converge at some n.

We can also use other forms of the algorithm. One variation of the algorithm, suggested by Lorenz, consists of finding X such that $d^{n-1}x_i/d\tau^{n-1} = 0$, $d^nx_i/d\tau^n = 0$, for i=1,2,3 in the n^{th} approximation. It is also possible to use the first algorithm with fixed values of z_1, z_2 and z_3 and determine the remaining six variables. Lorenz called the equation that would describe the invariant manifold the superbalance equation. Therefore, we will refer to the solutions determined by Lorenz algorithm as superbalance states.

The free normal modes of the linearized PE model consist of three slow Rossby modes and six fast gravity modes. We can rewrite the model equations in normal mode form using normal mode expansion procedure (Daley, 1981). The variables of the transformed equations will be the coefficients of the normal mode expansion. If Y now denotes the vector with the three slow modes and X the vector with the fast modes, then we can rewrite the equations of the model as

$$dX/d\tau = -i\Lambda_X X + R_X(X,Y)$$

$$dY/d\tau = -i\Lambda_Y Y + R_Y(x,y) \qquad (4.2)$$

where Λ_X and Λ_Y are diagonal matrices with the eigenfrequencies of the

normal modes and R_X and R_Y represent the projections of the nonlinear terms on the normal modes. R_X and R_Y can also include forcing and dissipation terms.

The normal mode initialization scheme consists of determining the initial state such that $d^nX/d\tau^n$ is set to zero for increasing n. Thus a higher order normal mode initialization method is equivalent to Lorenz's algorithm where X is determined keeping Y fixed. Machenhauer's (1977) scheme is equivalent to Lorenz's method at n=1 and consists of solving

$$-i\Lambda_X X = R_X(X,Y) \tag{4.3}$$

In large PE models used in weather forcasting, the initialization is usually limited to Machenhauer's scheme.

4.2. SUPERBALANCE STATES AND ATTRACTORS

According to the definition of the superbalance state, it is obvious that any steady state solution of the PE model is a point on the slow manifold. In this section we will apply the superbalance algorithm to the points on the periodic and chaotic attractors of the PE model. We wish to determine whether a well converged solution of the algorithm can be obatined for all the cases. The procedure will be tested at various points in the phase space of the attractors for different values of F_1. In those cases where the method converges, the superbalance states will be compared with the corresponding points on the attractor. When h_1=-1.0, we do not expect the attractor to be embedded in a slow manifold for

$F_1 > 0.2437$ where the attractors are certainly known to contain persisting gravity waves.

Our discussion begins with the attractors in the range $0.054 < F_1 < 0.2437$ when $h_1=-1.0$. In these studies, we have performed the integration of the model with a higher accuracy by including more terms in the Taylor series and using a time step of $\Delta\tau=0.001$. In this way, the convergence property of the superbalance algorithm and the agreement of the superbalnce states with the points on the attractor can be tested more precisely. All our discussions will be based on using the first form of the algorithm in which x_1, x_2, x_3, z_1, z_2 and z_3 are determined with fixed values of y_1, y_2 and y_3.

Let us begin with a discussion of the case $F_1=0.1$ which was also studied by Lorenz. We applied the algorithm at many points along the orbit after it had reached the attractor. In Table 4.1 we present the numerical values of z_1 found by the algorithm at each n. Here, a point on the attractor near a maximum of y_1 was chosen, and, keeping y_1, y_2 and y_3 fixed, the algorithm was solved up to n=15 (i.e., until $d^{15}X/d\tau^{15}=0$). For each n, the algorithm needs about four or five k to converge. The value of z_1 given in Table 4.1 is such a converged value at each n. As n increases we notice that the value of z_1 begins to converge at n=10 to about 16 decimal places. The other components of X behave in an identical manner. We have ensured that the integration of the model and the numerical solutions of the algorithm are more accurate than presented in

n	z_1
1	0. 2308421334332639
2	0. 2308533787816541
3	0. 2308513956074159
4	0. 2308513654813103
5	0. 2308513703568660
6	0. 2308513704610300
7	0. 2308513704473180
8	0. 2308513704469897
9	0. 2308513704470298
10	0. 2308513704470301
11	0. 2308513704470303
12	0. 2308513704470303
13	0. 2308513704470303
14	0. 2308513704470303
15	0. 2308513704470303
B	0. 2308513704470303
A	0. 2308513692073461

Table 4.1a. Solution (B) of superbalance algorithm and its comparison to the corresponding point (A) on the attractor (A is near a maximum of y_1). F_1=0.1

n	z_1
1	−0. 0889739891618238
2	−0. 0896386235284091
3	−0. 0897411318883115
4	−0. 0897444838151129
5	−0. 0897465011190397
6	−0. 0897464802305036
7	−0. 0897465318080562
8	−0. 0897465276061630
9	−0. 0897465288403853
10	−0. 0897465284988065
11	−0. 0897465284571988
12	−0. 0897465284371997
13	−0. 0897465284211325
14	−0. 0897465284220598
15	−0. 0897465284194444
B	−0. 0897465284194444
A	−0. 0897465281024586

Table 4.1b. Same as 4.1a at a different point A (near a minimum of y_1).

Table 4.1. The procedure has converged already to eight decimal places at n=4. The value of z_1 obtained by numerical integration (i.e., the chosen point on the attractor), which is also given in Table 4.1, agrees with the solution of the algorithm up to eight decimal places. The other components of X also agree up to eighth place. This is a better agreement than the result stated by Lorenz (1980) who examined only five decimal places. However, we consider the difference of about 10^{-8} in the values of the components of X between the point on the attractor and its superbalance state as significant.

In Table 4.1, the result of a similar procedure at a point near a minimum of y_1 on the orbit in the attractor is also presented. The convergence of the procedure is seen to occur slowly as n increases. The convergence up to eight decimal place takes place at n=8. The time derivatives of the points on the attractor are possibly larger and decrease slowly. Even at n=15, the solution does not converge to 16 decimal places, but oscillates in the 11th decimal place. We found that the algorithm did not show any trend towards convergence by extending n beyond 15. Thus, in the region of phase space being considered, there is possibly no solution to the algorithm with a starting geostrophic approximation.

We have repeated this entire procedure at many points on the attractor. In general, at points where $y_1 > 0$, the algorithm converges faster, and a satisfactory solution is always found. Referring to Fig. 3.4, which shows the variation of y_1 and z_1 at F_1=0.1, the behavior just described is found to be at those points where the variation occurs slowly and where y_1 and z_1 are very close. The classical balance equation (2.16)

n	z_1		
	$F_1 = 0.08$	$F_1 = 0.077$	$F_1 = 0.055$
1	0. 2108258091362817	0. 1620707286531861	0. 1559923303916878
2	0. 2109249503632194	0. 1620997642850243	0. 1559924525274842
3	0. 2109149425371350	0. 1620983017096619	0. 1559924795369959
4	0. 2109148097787461	0. 1620982535423184	0. 1559924788642786
5	0. 2109147922253699	0. 1620982508234939	0. 1559924787233440
6	0. 2109147914754173	0. 1620982509308133	0. 1559924787256018
7	0. 2109147917084809	0. 1620982509485902	0. 1559924787259375
8	0. 2109147917194928	0. 1620982509489533	0. 1559924787259390
9	0. 2109147917199159	0. 1620982509491012	0. 1559924787259411
10	0. 2109147917199756	0. 1620982509490915	0. 1559924787259411
11	0. 2109147917199311	0. 1620982509490878	0. 1559924787259410
12	0. 2109147917199263	0. 1620982509490879	0. 1559924787259410
13	0. 2109147917199268	0. 1620982509490880	0. 1559924787259410
14	0. 2109147917199268	0. 1620982509490880	0. 1559924787259410
15	0. 2109147917199268	0. 1620982509490880	0. 1559924787259410
B	0. 2109147917199268	0. 1620982509490880	0. 1559924787259410
A	0. 2109147917199156	0. 1620982509491491	0. 1559924787259403

n	z_1		
	$F_1 = 0.08$	$F_1 = 0.077$	$F_1 = 0.055$
1	-0. 0294792236792425	-0. 0967261697362129	0. 0666556709081366
2	-0. 0297921465700416	-0. 0973972773179095	0. 0666746523576187
3	-0. 0298088618226867	-0. 0974670481261490	0. 0666991272635301
4	-0. 0298103797105473	-0. 0974715273511506	0. 0666995027533074
5	-0. 0298106836785250	-0. 0974731043531153	0. 0666996093979034
6	-0. 0298106964336877	-0. 0974731316147518	0. 0666996146726704
7	-0. 0298107031004929	-0. 0974731802852199	0. 0666996152347165
8	-0. 0298107031584130	-0. 0974731781359443	0. 0666996153291202
9	-0. 0298107033592316	-0. 0974731800183924	0. 0666996153245548
10	-0. 0298107033512109	-0. 0974731797191567	0. 0666996153265880
11	-0. 0298107033587499	-0. 0974731797786304	0. 0666996153260504
12	-0. 0298107033578240	-0. 0974731797454609	0. 0666996153260922
13	-0. 0298107033581097	-0. 0974731797406394	0. 0666996153260597
14	-0. 0298107033580182	-0. 0974731797373609	0. 0666996153260595
15	-0. 0298107033580197	-0. 0974731797352519	0. 0666996153260577
B	-0. 0298107033580197	-0. 0974731797352519	0. 0666996153260577
A	-0. 0298107033580096	-0. 0974731797347714	0. 0666996153260564

Table 4.2. Same as 4.1 at F_1=0.08, 0.077, 0.055

is also a better approximation at these points compared to the points with $y_1 < 0$. This separation of the phase space is done for identification purpose only, and the zero crossing of y_1 has no special property. Along the orbit from a maximum of y_1 to its minimum, where y_1 (and other variables also) varies rapidly, the convergence of the algorithm begins to fail gradually as y_1 approaches negative values. There is no sudden change in the behavior of the model at any particular point. The points on the attractor where the algorithm yields converged solutions, the two differ by about 10^{-8} in the values of the components of X. By considering only eight decimal places, one might conclude that the algorithm has converged and that the attractor is identical to the slow manifold at F_1=0.1. However, our numerical results are accurate enough to show that the attractor at F_1=0.1 is not embedded in a slow manifold. Next, we will describe the behavior of the model for other values of F_1.

First, we will discuss the results of the application of the algorithm as F_1 is decreased. In Table 4.2 we present the values of z_1 determined by superbalance algorithm at F_1=0.08, 0.077, and 0.055. The values of z_1 of the corresponding points on the attractors, all of which are chaotic, are also given in Table 4.2. These points are located near a maximum and a minimum of y_1 on the orbits in the attractors. As shown in Table 4.2, the algorithm yields convergent solutions for points near the maximum of y_1. The agreement between the points on the attractor and their corresponding superbalance states increases steadily as F_1 decreases. At F_1=0.08, they agree to 11th decimal place, and are almost indistinguishable at F_1=0.055.

n	Z_1 at $F_1 = 0.12$
1	0. 2329822518354727
2	0. 2331331943912453
3	0. 2331208495079067
4	0. 2331203618702545
5	0. 2331203208593536
6	0. 2331203220945261
7	0. 2331203227862736
8	0. 2331203228219029
9	0. 2331203228236188
10	0. 2331203228227473
11	0. 2331203228224650
12	0. 2331203228224614
13	0. 2331203228224681
14	0. 2331203228224692
15	0. 2331203228224694
B	0. 2331203228224694
A	0. 2331204111641617

n	Z_1 at $F_1 = 0.12$
1	−0. 1932222966547914
2	−0. 1949225514173099
3	−0. 1953384832963322
4	−0. 1953475638325675
5	−0. 1953605901243149
6	−0. 1953598260122497
7	−0. 1953602820428687
8	−0. 1953601722599429
9	−0. 1953601664747032
10	−0. 1953601567234973
11	−0. 1953601496804834
12	−0. 1953601503028397
13	−0. 1953601488345076
14	−0. 1953601496146872
15	−0. 1953601496439877
B	−0. 1953601496439877
A	−0. 1953600863968104

TABLE 4·3a

n	Z_1		
	$F_1 = 0.15$	$F_1 = 0.2$	$F_1 = 0.243$
1	0. 3177891918762174	0. 3961556188185622	0. 6020652891454712
2	0. 3178699276832260	0. 3963195699273742	0. 6023793138856653
3	0. 3178532469639378	0. 3962971067344172	0. 6022758786531404
4	0. 3178528696234273	0. 3962957647360574	0. 6022692491051185
5	0. 3178529246352638	0. 3962957666275243	0. 6022694302658312
6	0. 3178529278176108	0. 3962957827749106	0. 6022696601801777
7	0. 3178529279019110	0. 3962957830963452	0. 6022696797769480
8	0. 3178529278794913	0. 3962957830376422	0. 6022696763349351
9	0. 3178529278738207	0. 3962957831118955	0. 6022696772444310
10	0. 3178529278735019	0. 3962957831061368	0. 6022696768904311
11	0. 3178529278736161	0. 3962957831023621	0. 6022696766805454
12	0. 3178529278736440	0. 3962957831025616	0. 6022696767136614
13	0. 3178529278736421	0. 3962957831025517	0. 6022696767247847
14	0. 3178529278736411	0. 3962957831025581	0. 6022696767266304
15	0. 3178529278736411	0. 3962957831025817	0. 6022696767300527
B	0. 3178529278736411	0. 3962957831025817	0. 6022696767300527
A	0. 3178529253059390	0. 3962972606759417	0. 6032800810647768

n	Z_1		
	$F_1 = 0.15$	$F_1 = 0.2$	$F_1 = 0.243$
1	-0. 1213944474655779	-0. 2585946520678371	-0. 4819068399031398
2	-0. 1234176267487021	-0. 2621793506789717	-0. 4929792184540862
3	-0. 1232923141138469	-0. 2632885190264890	-0. 4972422809771439
4	-0. 1233340106137698	-0. 2633083412836047	-0. 4972070765604623
5	-0. 1233333109278920	-0. 2633623686173869	-0. 4976551923103604
6	-0. 1233353424660765	-0. 2633563451507808	-0. 4975118929727332
7	-0. 1233355268691175	-0. 2633588173212987	-0. 4975282146931877
8	-0. 1233357051416706	-0. 2633576156344048	-0. 4974817440695838
9	-0. 1233357552042017	-0. 2633573347667887	-0. 4974505439903953
10	-0. 1233357790660053	-0. 2633572205304909	-0. 4974543308300819
11	-0. 1233357931974009	-0. 2633570547817916	-0. 4974382881856343
12	-0. 1233357973850244	-0. 2633571097626024	-0. 4974508276594125
13	-0. 1233358022525015	-0. 2633570845905909	-0. 4974584453506636
14	-0. 1233358029783321	-0. 2633571277059317	-0. 4974477011712729
15	-0. 1233358050155205	-0. 2633571529332542	-0. 4974625086685203
B	-0. 1233358050155205	-0. 2633571529332542	-0. 4974625086685203
A	-0. 1233358138435986	-0. 2633594868606575	-0. 4967804930953956

Table 4.3*b*. Same as 4.1 at F_1=0.15, 0.2, 0.243

The convergence of the algorithm near the minimum of y_1 shows steady improvement as F_1 decreases. At F_1=0.055, the oscillatory behavior of the procedure is still evidenced, though in the 13th decimal place. The points on the chaotic attractor at F_1=0.055 thus appear to be extremely close to superbalance states, if not identical. For all the values of F_1, we have applied the algorithm at many points along the orbits in the attractors. Thus, as F_1 decreases from 0.1, the attrator of the model approaches the slow manifold steadily.

We will now discuss the behavior of the model as F_1 is increased when $F_1 > 0.1$. In Table 4.3 we present the values of z_1 determined by superbalance algorithm and the corresponding values on the attractors at F_1=0.12, 0.15, 0.2, and 0.243. At F_1=0.12, the attractor is chaotic and thus we must examine many points along the orbits. The general behavior of the model is similar to the case with F_1=0.1 discussed earlier. As shown in Table 4.3, near the maximum of y_1, the algorithm converges well; however, the solution of the algorithm agrees with the point on the attractor only up to seventh decimal place. Again, near the minimum of y_1, there are clear indications that the algorithm may not produce convergence beyond the eighth decimal place. If we accept it as a solution (up to eighth place), then we notice that its agreement with the point on the attractor is also limited to the same accuracy.

As discussed in Sec. 3.1, between F_1=0.123 and F_1=0.243, the attractors of the PE model are xy periodic orbits. On these periodic orbits, the superbalance algorithm has been applied at many points covering one complete period. The trend in the behavior of the solution

of the algorithm found until F_1=0.12, discussed earlier, continues as F_1 is increased. As shown in Table 4.3, there are indications that the algorithm is not converging well at all points on the orbits (see especially at F_1=0.243). At those points where the convergence is relatively better, the difference in the value of z_1 between the attractor and the superbalance state has increased from about 10^{-7} at F_1=0.15 to about 10^{-4} at F_1=0.243.

We have performed all the above experiments on many points on the attractors for many different values of F_1. For all values of F_1, there are many points, mainly with positive values of y_1, where the algorithm converges to some solution. The degree of convergence decreases as F_1 increases. At all other points on the attractors, the algorithm fails to converge with varying degree depending on the region of the phase space and on F_1. Along the orbits where y_1 is decreasing rapidly, the higher order time derivatives of the variables of the model become larger. Wherever the convergent solutions are found for the algorithm, there has always been some difference between the points on the attractor and the corresponding superbalance states. For the smallest values of F_1 in the chaotic regime C_1, these differences are quite insignificant and, perhaps, nonexistant. However, these differences increase steadily with F_1 reaching a value of about 10^{-3} at the end of the periodic regime P_4 (at about F_1=0.243).

Our experiments have been performed with such small increments in F_1 as to indicate that the changes occuring in the behavior of the model, as F_1 is varied, are gradual. We have not found any kind of bifurcation

n	Z_1		
	$F_1 = 0.2439$	$F_1 = 0.244$	$F_1 = 0.25$
1	0. 6197604169171008	0. 6095902002102905	1. 0233440797161376
2	0. 6202963888490974	0. 6099137417134837	1. 0232266378128271
3	0. 6203374581344663	0. 6098218625600073	1. 0231782787584126
4	0. 6203271132239483	0. 6098150461627540	1. 0231817509639495
5	0. 6203241415363901	0. 6098149717499009	1. 0231829852874340
6	0. 6203242131415147	0. 6098151975551351	1. 0231829159130485
7	0. 6203242094773569	0. 6098152197888890	1. 0231828879803011
8	0. 6203242276958325	0. 6098152171912382	1. 0231828866260380
9	0. 6203242413395511	0. 6098152186667810	1. 0231828864724654
10	0. 6203242406794438	0. 6098152182757881	1. 0231828868765179
11	0. 6203242395656798	0. 6098152179888355	1. 0231828869880783
12	0. 6203242392694990	0. 6098152180136546	1. 0231828869415563
13	0. 6203242391342855	0. 6098152180280972	1. 0231828869285015
14	0. 6203242391850450	0. 6098152180323469	1. 0231828869320893
15	0. 6203242392482654	0. 6098152180371124	1. 0231828869328399
B	0. 6203242392482654	0. 6098152180371124	1. 0231828869328399
A	0. 6239662934318130	0. 6075625574469508	0. 8050799353785482

n	Z_1	
	$F_1 = 0.2439$	$F_1 = 0.244$
1	-0. 5326092999582324	-0. 4572679834434672
2	-0. 5450333384812045	-0. 4719020826322220
3	-0. 5504865684113412	-0. 4749474729163730
4	-0. 5502861560752100	-0. 4755358269458527
5	-0. 5508557434708762	-0. 4761796140029036
6	-0. 5506274230220750	-0. 4761065071041217
7	-0. 5506212946507664	-0. 4762348532307346
8	-0. 5505613995060224	-0. 4761356862451151
9	-0. 5505037445948511	-0. 4761159351132563
10	-0. 5505226932014657	-0. 4760674756614846
11	-0. 5505030959972540	-0. 4760192080134139
12	-0. 5505139515510034	-0. 4760429674212711
13	-0. 5505420551668189	-0. 4760303817118531
14	-0. 5505083474790801	-0. 4760585736225042
15	-0. 5505098128840313	-0. 4760954503849284
B	-0. 5505098128840313	-0. 4760954503849284
A	-0. 5487651406809868	-0. 4808544710926718

Table 4.4. Same as 4.1 at F_1=0.2439, 0.244, 0.25

concerning the relation between the attractors and the slow manifold. An examination of the two cases at F_1=0.077 and F_1=0.08, shown in Table 4.2, indicates that the Hopf bifurcation of the Hadley fixed point has not introduced any abrupt change in our results.

We recall that, after the saddle-node bifurcation at F_1=0.2437, as F_1 is increased, the attractors of the PE model are known to contain persisting gravity waves. It was also mentined that, for some values of F_1, the solutions consisted of long intervals of laminar behavior interrupted by more chaotic bursts with gravity waves. It is interesting to find what the superbalance algorithm will generate when $F_1 > 0.2437$. In the range $0.2437 < F_1 < 0.25$, during the laminar phases of the orbits, the behavior of the model is simply an extension of its behavior at F_1=0.243 which was discussed earlier. The solutions of the algorithm and their comparisons with the points on the attractor at F_1=0.2439 and 0.244 are shown in Table 4.4. When $F_1 > 0.25$, the gravity waves appear to persist all the time along the orbits in the attractor. For such values of F_1, there are only a few points on the attractors where the superbalance algorithm yields solutions converging up to tenth decimal places as shown in Table 4.4. The difference between the solutions of the algorithm and the integration (attractor) is quite large.

For strong forcing ($F_1 > 0.25$), the algorithm fails completely in producing a solution for most of the points on the attractor. On the periodic orbit such as the x orbit at F_1=0.315 (Fig. 3.15), we have not found a single point, covering an entire period, where the algorithm yielded a convergent solution. In many cases, it has not been possible

to obatin a solution within the iteration cycle for each n in the algorithm. In all these cases, the points on the attractors are strongly ageostrophic. The algorithm fails to yield a solution converging to some value close to the geostrophic state with fixed y's on the attractor which is used as the starting approximation.

At F_1=0.055, the attractor appeared to be almost embedded in a slow manifold. Therefore, the actual time derivatives of the variables must be closer to zero as n becomes large. We have examined the time derivatives at many points on the attractor and have found that they become smaller as n increases. Depending on the point on the attractor considered, the values of the tenth derivatives are about 10^{-9} - 10^{-10}; and between n=10 and n=15, they decrease from about 10^{-11} to about 10^{-17}. The exact order of magnitude depends on the location of the point in the phase space of the attractor. The sign of the derivative of any particular variable need not be same for all n. Even when they are becoming small, they oscillate about zero. In almost all the cases, for n > 15, the absolute values of the time derivatives show an increasing trend as n increases. For example, in one case, they are about 10^{-12}, 10^{-10} and 10^{-7} at n=20, 25 and 30 respectively. Any of our computations beyond n=30 may not be accurate. As F_1 increases, we have found that same trend continues except that the values of the derivatives become larger. Even for small values of F_1, the higher derivatives have large values. At these values of F_1, the time derivatives certainly do not exhibit the kind of behavior we demand of a superbalance state as n increases.

We have performed similar experiments applying the superbalance

algorithm at other values of the topography h_1. In all the cases, the general behavior of the model is very similar to the case with h_1=-1.0.

Thus, we have found that the superbalance algorithm does not produce converged solutions at all points of the phase space of the attractor. When the forcing is very small (e.g., F_1=0.055), it appears as though the attractor is embedded in a slow manifold. As F_1 increases, we are certain that the attractor is not contained in a slow manifold. However, for smaller values of F_1, the points on the attractors are very close to the states of the slow manifolds. At such values of F_1, one can argue that, upto a certain accuracy (say 10^{-10}), the attractor is in a slow manifold. For moderate values of F_1 (0.12 to 0.243), the differences between the points of the attractor and the corresponding subperbalance states increase. It is certain that the attractors with the gravity waves are not embedded in any slow manifolds when $F_1 > 0.243$. Therefore we conclude that as F_1 decreases from 0.243, the attractor of the model approaches the states of a slow manifold. For the smallest values of F_1, in the regime C_1, it is almost impossible to distinguish between the slow manifold and the attractor. Of course, when F_1 is further decreased, the PE model reaches steady state attractors which are exactly superbalanced.

4.3. STABILITY AND INVARIANCE OF THE SLOW MANIFOLD

In the previous section we argued that the attractors of the PE model were not embedded in the slow manifold. The attractor is an invariant set, and we have not yet discussed whether or not the slow

manifold is invariant under the PE flow. If the slow manifold does not contain the attractor, then it is unstable. A point not on the slow manifold, even when close to it, will always reach the attractor. In this section we will discuss the invariance of the slow manifold with the help of the results of the initialization procedure with superbalance states. Even if the slow manifold is found to be invariant in the PE model, it has already been proved to be unstable for almost all the values of F_1 for which the attractors are not fixed points.

The numerical determination of the invariance property of the slow manifold is straightforward. With a superbalance state as the initial condition, the PE model will be integrated and the superbalance algorithm will be applied to the states of the subsequent evolution. If the points on the orbit for all future times are identical to their corresponding superbalance states, then the slow manifold is invariant under the PE flow.

We begin our discussion of the numerical results again with F_1=0.1. With an arbitrary initial condition, the PE model is integrated until it is certain that the orbit is in the attractor. We choose a point A_0 on the attractor for which the superbalance algorithm yields a convergent solution, and the corresponding superbalance state B_0 is determined. A second integration is performed with the superbalance state B_0 as the new initial condition. The superbalance algorithm is applied at points along the orbit initiating from B_0. The resulting superbalance states are compared with their corresponding points on the orbit.

HOURS (after initialization)		Z_1 (after initialization)
3	A	0.3244307000016084
	B	0.3244307000016055
6	A	0.3300421568710208
	B	0.3300421568710210
9	A	0.3345668556022824
	B	0.3345668556022798
12	A	0.3378496002437578
	B	0.3378496002437580
15	A	0.3396958895860521
	B	0.3396958895860516
18	A	0.3398664463418197
	B	0.3398664463418212
21	A	0.3380711524733596
	B	0.3380711524733602
24	A	0.3339629060509610
	B	0.3339629060509595
144	A	0.3257601781415628
	B	0.3257601739349813

Table 4.5a. Initialization procedure at F_1=0.15. The points (A) on the new orbit are compared to their corresponding superbalance states (B) periodically.

$F_1 = 0.2$		
HOURS	z_1	
3	A	0. 4075732568205671
	B	0. 4075732568205679
6	A	0. 4169163355887530
	B	0. 4169163355887557
9	A	0. 4241616305278962
	B	0. 4241616305279041
12	A	0. 4290227484110067
	B	0. 4290227484110379
15	A	0. 4310836899045811
	B	0. 4310836899046350
18	A	0. 4297854259913612
	B	0. 4297854259914457
21	A	0. 4244073204517836
	B	0. 4244073204517862
24	A	0. 4140451630848336
	B	0. 4140451630843764
120	A	0. 4293020530328756
	B	0. 4293021434447597

$F_1 = 0.25$		
HOURS	z_1	
3	A	1. 0280072597561558
	B	1. 0280072597542530
6	A	1. 0318193304182852
	B	1. 0318193304086768
9	A	1. 0340232273118430
	B	1. 0340232272857345
12	A	1. 0336461924573628
	B	1. 0336461924877608
15	A	1. 0291371724837974
	B	1. 0291371732143652
18	A	1. 0181171840048597
	B	1. 0181171859775718
21	A	0. 9971794909421370
	B	0. 9971794758618909
24	A	0. 9620122509984175
	B	0. 9620122621081228
72	A	0. 8868630278544651
	B	1. 0276228607838069

Table 4.5b. Initialization procedure at F_1=0.2, 0.25.

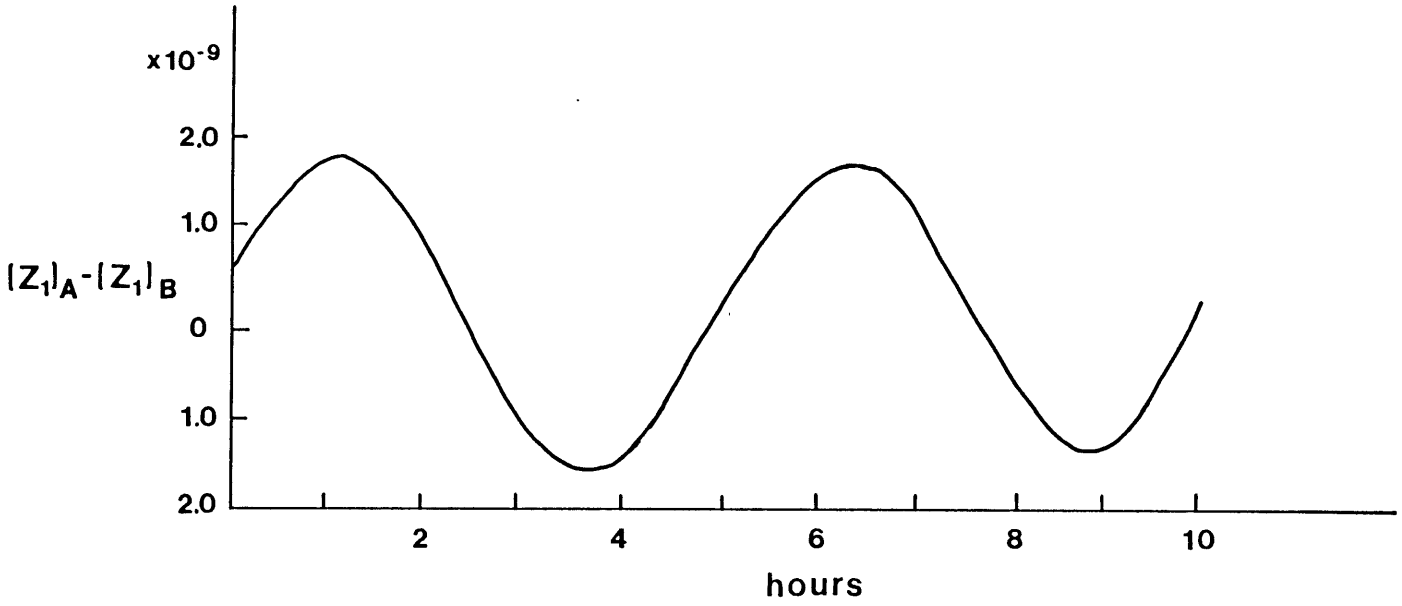

Figure 4.1. Difference in the values of z_1 on an orbit in the attractor and on the orbit initialized with superbalance state (F_1=0.1)

In Table 4.5 we present the values of z_1 in such an integration at F_1=0.15. We note that the point A_0 is located near a maximum of y_1 and the corresponding superbalance state B_0 agrees with A_0 up to seven decimal places. Shown in Table 4.5 are the values of z_1 at several points along the orbit from B_0 in the second integration. These points are separated in time by two hours. The values of z_1 of the corresponding superbalance states at those points are also given. We notice that, in the new integration, the points on the orbits are extremely close to the superbalance states for first few days. This behavior continues until the orbit reaches the region of phase space with $y_1 < 0$ where the superbalance algorithm does not yield convergent solutions. When the orbit enters the region with $y_1 > 0$ again, the points on the orbits are no longer close to the corresponding superbalance states. The difference in the value of z_1 between the two integrations starting from points A_0 and B_0 is plotted in Fig. 4.1 for the first two days. The difference is oscillating with a period of gravity waves. We obtain a similar figure if we plot the difference between the points on the orbits from A_0 (i.e. the attractor) and their corresponding superbalance states. If we follow the orbit from B_0 further, we find that it reaches the attractor whose states are not contained in a slow manifold. Similar behavior was found by repeating this procedure with many other points on the attractor.

We have performed similar numerical experiments at numerous points for all values of F_1. As shown in Table 4.5, the experiments at higher values of F_1 reveal even more clearly the behavior found at F_1=0.15. A plot of the difference between the integrations from A_0 and B_0 looks very much like Fig. 4.1 with the difference that the amplitudes are about 10^{-7}

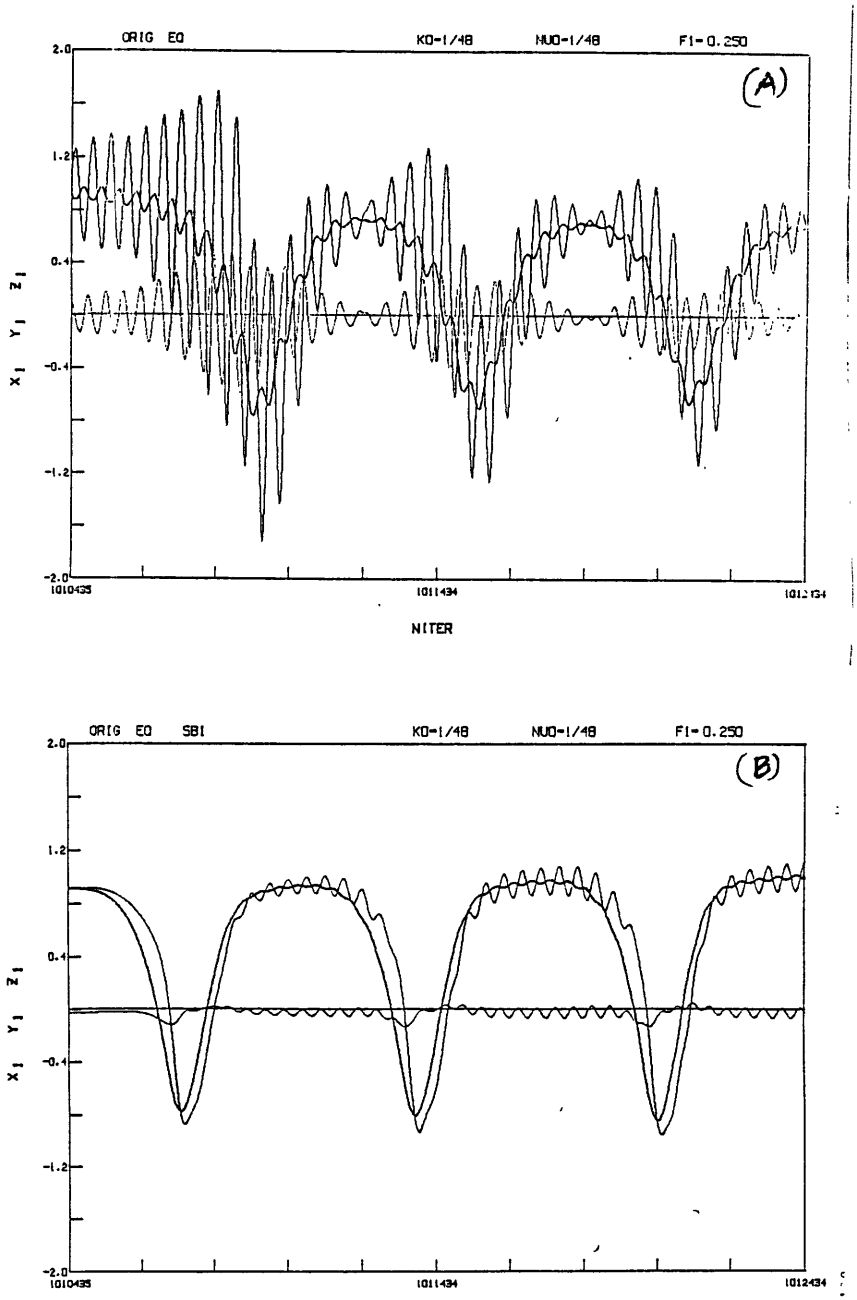

Figure 4.2a. F_1=0.25: (A) an orbit in the attractor (B) the orbit initialized with a superbalance state on the attractor.

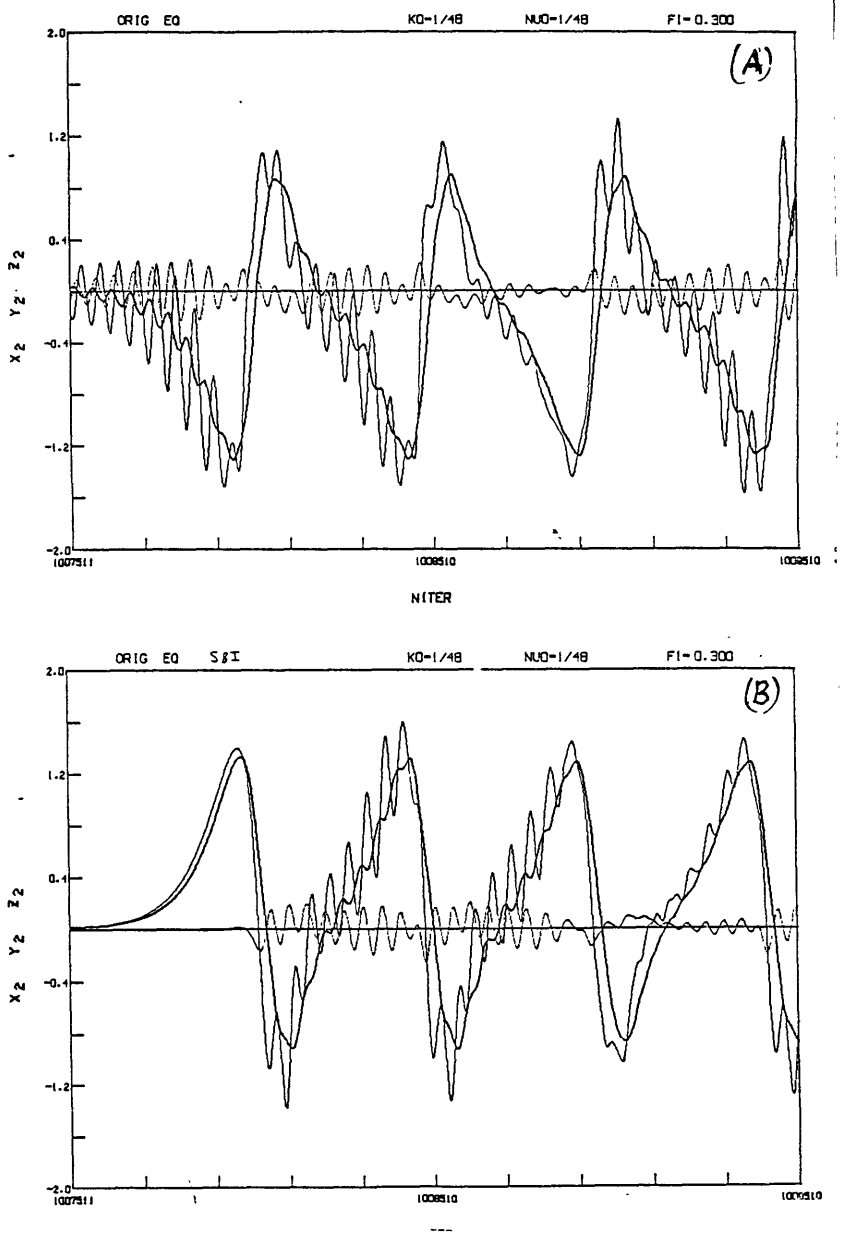

Figure 4.2b. F_1=0.3 (same as 4.2a).

and 10^{-5} at F_1=0.12 and F_1=0.2 respectively. This amplitude increases with F_1. Identical behavior was found for all values of F_1 we have studied. Thus, the slow manifold is not found to be invariant under the PE flow. For very small values of F_1 in the chaotic regime C_1 where the attractor and the slow manifold are extremely close, we can perhaps state that the slow manifold is almost invariant.

The orbits of the second integration originating from B_0 reach the attractor after some days. For weak and moderate values of F_1 (<0.243), the superbalance states can be considered to be small departures from the corresponding points on the attractor. Therefore, the orbits of the two integrations (from A and B) appear to be close to each other as time evolves. If the attractor is periodic, the orbit from B_0 reaches the periodic orbit after a few days. If the attractor is chaotic, after a specified period of time, the points of the orbits (from A_0 and B_0) within the attractor will be as different as two randomly chosen points in the attractor.

We now discuss the initialization experiments with superbalance states for $F_1 > 0.243$. For these values of F_1, the attractors contain persisting gravity waves with considerable intensity. There are only a few points in the phase space of the attractor where the superbalance algorithm yields reasonably well converged solutions. We chose a few such points and performed integrations with their superbalance states as initial conditions. In Fig. 4.2 we present the evolution of the orbits in the two integrations for F_1=0.25 and 0.3. In the second integration, the gravity waves appear to be completely absent in the first cycle of the

slow variations. However, the gravity waves reappear with considerable intensity by the time the second cycle is reached after a few days. Eventually, the orbit initiating from the superbalance state reaches the attractor. After a certain time has elapsed, the points from the two orbits will be completely different. In Fig. 4.2, for F_1=0.3, we notice that even after a few hours the two orbits are completely different. In an initialization procedure such as Machenhauer's scheme, using a state generated by lower order superbalance algorithm (stopping at low n), the gravity waves reappear even faster.

Chapter 5 SUMMARY AND CONCLUSIONS

We have studied a simple nonlinear primitive-equation model consisting of nine dependent variables as a forced dissipative dynamical system. With fixed values for the dissipation parameters that we have considered, the forcing in the model can be interpreted to be a measure of the Rossby number. The solutions of the PE model have been studied as a function of forcing.

Due to the presence of the nonlinearities, forcing and dissipation, the solutions of the system (the attractors) are confined to a region of the phase space with zero volume. The model exhibits a variety of behaviors as a parameter, such as forcing, is varied. The attractors of the PE model are found to be stationary, periodic or chaotic depending on the value of forcing. The steady states exist as stable solutions for very small values of forcing. Once all the steady states become unstable, the behavior of the model alternates between periodicity and chaos. The transitions from one kind of attractor to another occur in many different ways and are similar to some of the typical ones found in many simple dynamical systems.

The stable steady solutions of the PE model, which exist for very small values of forcing, are zonally uniform and nearly geostrophic. The other steady state attractors, which are created when the Hadley solution becomes unstable, are also nearly geostrophic though not zonally uniform. For a range of weak forcing, where the attractors are either periodic or

chaotic, the solutions vary with a time scale of a few days. The states of these attractors are either in approximate geostrophic equilibrium or satisfied by the the classical balance equation to a good approximation. There is no apparent sign of the presence of the gravity waves in these attractors.

For moderate values of forcing, the attractors of the model still do not appear to contain gravity waves. The motion is on a slow time scale, and some of the periodic orbits oscillate with a period of about four days. The classical balance relation is still a good approximation for many points on the attractor. Within the weak and moderate forcing range, the sequence of different behaviors and the bifurcations of the PE model are found to be qualitatively similar to those of Lorenz's convection model.

The similarity with the convection model ends in the PE model when a particular periodic orbit ceases to exist beyond a particular moderate value of forcing. In the convection model, the corresponding orbit exists for all values of a certain parameter after it is created. We have found that there is a drastic change in the nature of the attractors of the PE model after this bifurcation occurs. For all values of forcing beyond this bifurcation, the solutions of the PE model consist of gravity waves with considerable amplitude superposed on slowly varying motion. Both periodic and chaotic attractors consisting of gravity waves exist at different values of forcing. However, the periodic windows are narrow, and the behavior is predominently chaotic. Many points on these attractors are strongly ageostrophic.

We have also studied the solutions of the PE model for different values of the topography. The general behavior of the model is similar in all the cases although the various regimes of behavior occur at different values of forcing. When the topography was suitably chosen, we found that the gravity waves could be present in the attractors corresponding to the regimes without gravity waves for the case discussed earlier. However, the amplitudes of the gravity waves are rather small. For all values of topography, in the strong forcing regime, the gravity waves with considerable intensity are present along with the slow motion in the attractors. The attractors are mostly chaotic.

Another result due to nonlinearity is the Hopf bifurcation of the Hadley steady state which creates a gravity wave periodic orbit. This periodic solution oscillates with a period of about six hours and is not superposed on any slow variation. For certain values of topography, the gravity wave periodic orbit exists as a second attractor. In such cases, depending on the initial condition, an orbit can reach either the attractor with nearly balance motion or the gravity wave attractor.

We have also studied two other models, the BE and QG models, which are constructed by replacing the divergence equation with the classical balance equation or the geostrophic equation. Both the BE and QG models are three-dimensional. For all values of topography, the BE model is an extremely good approximation to the PE model for weak and moderate forcing. The sequence of different behaviors and the bifurcations of the PE and BE models are found to be remarkably similar for a certain range of forcing. At some value of forcing, the behavior of the BE and PE models

diverge completely. The attractors of the PE model then have gravity waves with considerable amplitude. In a qualitative sense, the solutions of the PE model, in the weak and moderate forcing range, appear to vary with three degrees of freedom, much like the solutions of the BE model.

The QG model, however, is not found to be such a good approximation to the PE model for any value of topography. In certain cases, the solutions of the QG model and its bifurcation are qualitatively similar to those of the PE and BE models. However, the various regimes of behavior occur at higher values of forcing. For some values of topography, the behavior of the QG model is completely different from those of the PE and BE models.

We examined whether the attractors of the PE model, for the weak and moderate forcing, with no apparent presence of gravity waves are embedded in a stable invariant slow manifold. The states of the slow manifold are determined by Lorenz's algorithm which is based on complete separation of quasi-geostrophic and gravity wave frequencies. For very small values of forcing, after the steady states become unstable, the algorithm yields convergent solutions at most of the points on the attractors. The attractors in this range of forcing appear to be extremely close to the slow manifold.

However, the closeness between the points on the attractor and their superbalance states gradually disappears as the forcing increases. At moderate values of forcing also, the superbalance algorithm fails to

generate convergent solutions at many points on the attractor. In such cases it is also clear that the points on the attractors are considerably different from the superbalance states whenever such solutions can be obtained. In the strong forcing range, which consists of solutions with known presence of gravity waves, the superbalance algorithm fails to yield a solution at most of the points on the attractors. There is no doubt that the points on the attractors are rather different from the states of the slow manifold.

We have concluded that the attractor is not embedded in a slow manifold for almost all the values of the forcing for which the attractors are not fixed points. The slow manifold is found to be unstable. With the help of the initialization procedures, we have determined that the slow manifold is not invariant under the PE flow for most values of forcing. At any particular value of forcing, the orbit initiating from a state on the slow manifold remains on the slow manifold for a few hours. However, after it has completed one slow oscillation (usually a few days), the points on the orbits are found to be no longer on the slow manifold. In some cases the reappearance of the gravity waves is quite evident in a plot of the time series.

We present the following picture of the relation between the attractors and the slow manifold. For strong forcing, the attractor is definitely not embedded in any slow manifold. For moderate forcing, the attractor is still not contained in the slow manifold, but the states of the attractor and of the slow manifold are not too far apart. However, the slow manifold is not invariant under the PE flow. As the forcing

decreases, the slow manifold and the attractor move closer to each other, and the slow manifold becomes almost invariant. At some values of forcing, it is difficult to distinguish between the slow manifold and the attractor. We have not found any abrupt change in the relation between the states of the attractor and the slow manifold as the forcing is varied. The gradual change in the behavior of the model is one reasons why we cannot be certain that any attractor, other than fixed points, is embedded exactly in a slow manifold.

Our initialization experiments have shown that the gravity waves can reappear after a few days of integration even it we initiaize with a higher order superbalance state. If a low order procedure such as Machenhauer's scheme is used, the gravity waves will reappear in the solutions even faster.

Though we have studied the low-order PE model analyzing large ensembles of solutions and bifurcations in great detail, our results are meant to provide a qualitative picture of the atmospheric dynamics. It must be emphasized that the features of the atmosphere are not reproduced in a quantitative manner by the low-order model. We consider it interesting and helpful to know that the solutions of the PE model consist of quasi-geostrophic-like solutions for certain cases and persisting gravity waves for others. Our detailed study with high accuracy computations is necessary to understand the complicated behaviors of nonlinear forced dissipative system. We can clearly appreciate its advantages by our understanding that the BE model closely reproduces the behavior of the PE model and is better than the QG model.

Even with our simple PE model, we have chosen the values of the physical constants in a such way that the model exhibits interesting behavior. Other combinations of the values of the physical constants may produce a more complicated behavior or may show no interesting behavior at all. For example, different combinations of the lengths of the basis vectors used in the spectral expansion have resulted in the PE model possessing a global steady state attractor. In a similar manner the PE model possesses a steady state attractor for a large range of forcing when the topography or the forcing is chosen to be nonzonal. However, choosing a case which exhibits complex behavior has helped us to determine the existene of solutions with different behaviors such as the nearly balanced states and the gravity waves superimposed on slow motions.

The superbalance algorithm was expected to generate a converged solution close to a state satisfying the classical balance equation. We do not fully understand the failure of the convergence in certain regions of the phase space. In a higher order algorithm it is possible that there is no unique solution. It is interesting to examine whether there are other solutions for the algorithm in some regions of phase space and whether they are relevant to the atmosphere. One should investigate whether any other algorithm produces states identical to those of the attractor corresponding to moderate forcing. We should also examine the possibility of reformulating the equations is such a way that the invariant manifolds are easier to determine.

The physical system we have studied consists of homogeneous fluid, and, hence, the model consists of only external gravity waves. A

more realistic atmospheric model, such as a global circulation model, consists of thousands of variables. In such a model internal gravity waves with lower frequency can also be excited. We do not know whether the attractor of a large model will be embedded in an invariant slow manifold. However, it is possible that many modes of motion will decay. A more realistic low-order model that can be studied easily is a two-layer model. This model admits internal gravity waves of lower frequency; it will be interesting to determine what the attractors with persisting gravity waves look like. If the attractors of a two-layer model do not have gravity waves, then we must find whether the attractor is embedded in lower dimensional invariant manifold. The definition of slow manifold should also be reexamined since Lorenz's algorithm is based on complete separation of quasi-geostrophic and gravity wave frequencies.

A more realistic atmospheric model would be represented by the full partial differential equations similar to eqs. 2.1 and 2.2 and would include all the appropriate physical features and processes. The purpose of studying the idealized low-order model is to provide a necessary step in qualitative understanding of atmospheric dynamics. The developments in the understanding of the behavior of the nonlinear forced dissipative systems are fairly new (Guckenheimer and Holmes, 1983); these studies are still concerned with simple systems. Only recently have attempts been made to understand the behavior of the dynamical systems represented by the full partial differential equations. In this regard, Curry et al. (1984) have studied two- and three-dimensional Benard convection and have examined the effect of increasing the order of the spectral model from three (Lorenz's convection model) to the full system. Though Curry

et al. do not observe strong chaos in the full two-dimensional system for the chosen values of physical parameters, they state that the low-order models are often representative of the real solutions which vary slowly in space. They also mention that it is possible to observe chaotic behavior by considering other values of certain parameters in the system. However, their study shows that the three-dimensional system undergoes transitions from steady states to periodic states and then to chaotic states in a manner similar to the finite-mode model of certain order. This process is one of the typical scenarios of transition to chaos in many simple dynamical systems.

A realistic spectral model of the full primitive equations (2.1 and 2.2) will consist of thousands of variables. It still can be considered as a system consisting of nonlinear interactions between the Rossby and gravity modes with forcing and dissipation. Even in the full model we should expect many modes to decay because of the dissipative nature of the system. If many of the gravity modes decay, it is possible for the solutions of the system to vary on a slow time scale and be close to quasi-geostrophic equilibrium. The existence of chaotic behavior and attractors with persisting gravity waves will be determined by the relative strength of forcing compared to dissipation. Because of dissipation we expect the system to be represented by a lower dimensional subspace. In such a case, the interesting question is whether a slow manifold exists for certain values of the physical parameters.

Our results of the low-order model concerning the initialization procedure with superbalance states can be of direct relevance to

predictability in the full system. We have shown that the gravity waves can be suppressed for a few days by initializing with superbalance states. Such orbits do not stay on slow manifold, but reach the attractors after some time. Whatever the nature of the attractor may be, the predicted states from the reinitialized orbits will always be different from true solutions. If the attractor is periodic, after the reinitialized orbit reaches the attractor, there will be a definite phase lag between the true solution and the predicted state. However, if the attractor is chaotic, the divergence of the reinitialized orbit from the true orbit depends on the degree of chaos. For all completely chaotic cases, eventually, the difference between the points on the two orbits will be equal to that between any two randomly chosen points in the attractor. The short-term predictability depends not only on the degree of chaos but also on the location of the initial point on the true orbit. This is clearly evident in the cases presented in Figs. 4.2. In some cases (as in Fig. 4.2b), the reinitialized orbit is completely different from the true orbit even from the beginning. In such cases, though the gravity waves are suppressed initially, the predicted states, even after a few hours, are drastically different from the true states. If a low-order procedure like Machenhauer's scheme is used, the gravity waves will reappear even faster. Thus we may severely compromise the predictability by concentrating on suppressing the gravity waves.

Note: During the writing of this thesis, the author came across a preprint entitled "Invariant manifolds, quasi-geostrophy and initialization" by R. Vautard and B. Legras. This preprint discusses some aspects of the concepts of the slow manifold and its relation to Lorenz's primitive equation model. Their discussion includes the bifurcations of the steady states, but does not give any numerical results of the behavior of the model that we have found. They show an example where the superbalance algorithm fails to converge. But they do not discuss any numerical results of the application of superbalance algorithm to the primitive equation model, nor any other aspects of numerical experiments with slow manifold. They present a different procedure which expresses the fast variables as analytic function of the slow variables to find the states of the slow manifold, but they do not apply it specifically to the primitive equation model.

Appendix A STATIONARY SOLUTIONS AND THEIR STABILITY

Consider a dynamical system to be represented by

$$dX/dt = F(X), \tag{A1}$$

where X and F are N-dimensional vectors. The steady states or the fixed points of the system are the solutions to

$$F(X) = 0. \tag{A2}$$

Newton's method of solving eq. A2 consists of an initial guess X_0 and an expansion about X_0 to first order as

$$X = X_0 - [D_X F(X_0)]^{-1} F(X_0), \tag{A3}$$

where $D_X F$ is a matrix with partial derivatives as its elements. The solution X in eq. A3 is used as the initial guess in the next step of iteration and the procedure is repeated until convergence is achieved.

The linear stability analysis of a fixed point X_s is performed by evaluating the eigenvalues of the matrix $D_X F(X_s)$. If the real parts of all the eigenvalues are negative, the fixed point is stable. The fixed point is unstable if the real part of any eigenvalue becomes positive.

We now discuss two particular bifurcations of the fixed points as some parameter μ of the system is varied. Consider a fixed point to be stable for $\mu < \mu_0$. Let one of the real eigenvalues of the fixed point

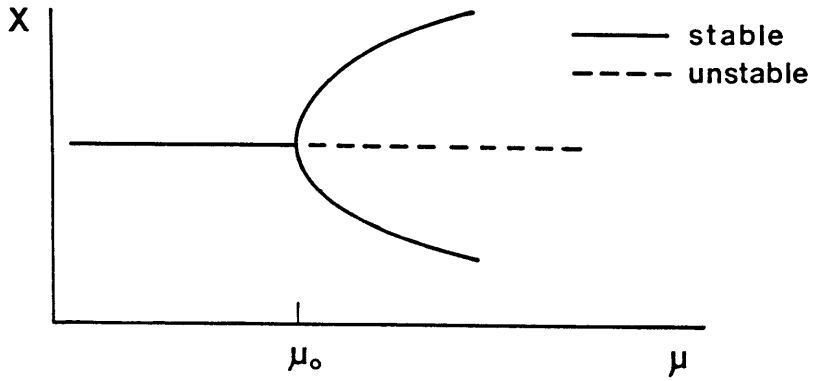

Figure A1. Pitchfork bifurcation.

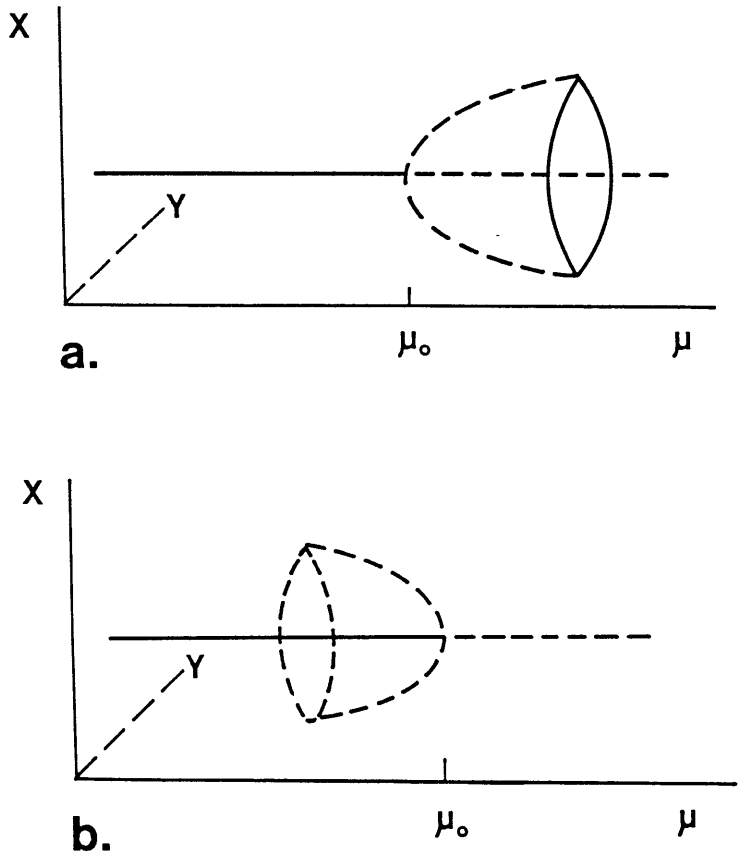

Figure A2. Hopf bifurcation (a) supercritical and (b) subcritical.

become positive for $\mu > \mu_0$. If the system possesses certain symmetry (e.g., invariance under reflection of certain coordinates), usually two new fixed points come into existence at μ_0. This is known as a pitchfork bifurcation and is schematically represented in Fig. A1.

A fixed point can also become unstable if a pair of complex conjugate eigenvalues crosses the imaginary axis from left to right. This is known as Hopf bifurcation, and a periodic orbit is either created or destroyed at the point of bifurcation. If the fixed point looses stability by creating a stable periodic orbit which exists for $\mu > \mu_0$, then the Hopf bifurcation is said to be supercritical. In a subcritical bifurcation, an unstable periodic orbit which exists for $\mu < \mu_0$ is absorbed at μ_0. These two cases are shown schematically in Fig. A2. The period of the periodic orbits depends on the imaginary part of the complex conjugate eigenvalue. Other kinds of bifurcations of a fixed point are discussed by Guckenheimer and Holmes (1983).

Appendix B PERIODIC SOLUTIONS AND THEIR STABILITY

In this appendix we will describe the numerical technique to locate the periodic orbits. This is based on Newton's method, and the theory is discussed by Curry (1979). We will also discuss the stability of the periodic orbits.

Consider an N-dimensional dynamical system to be described by

$$dX/dt = F(X), \tag{B1}$$

where X and F are N-dimensional vectors. Let the flow of the system be represented by $\phi(X_0,\tau)$ where X_0 is the initial position and τ is the time elapsed. Therefore, we have

$$d\phi(X_0,\tau)/dt = F(\phi(X_0,\tau)). \tag{B2}$$

We choose a local cross-section Σ of dimension N-1 such that the flow is transverse to it everywhere. If an orbit starts at a point X_0 on Σ, it will intersect Σ again at a point $X_1=\phi(X_0,\tau)$ after a time τ. Then $\phi(X_0,\tau)$ is the first return or Poincare map.

Thus, locating a periodic orbit is equivalent to finding a fixed point on the Poincare map. If the periodic orbit intersects Σ at X_p and has period τ_p, then we must solve

$$\phi(X_p,\tau_p) = X_p \tag{B3}$$

to locate the periodic orbit. Let X_0 and τ_0 be the initial guesses for

the position and the period of the orbit. A small change dX_0 in the initial position will result in a small change dX_1 in the first return map and $d\tau_1$ in the return time. The location of the periodic orbit thus reduces to determining dX and $d\tau$ such $X_p = X_0 + dX$ and $\tau_p = \tau_0 + d\tau$. With a first order expansion around X_0 and τ_0, we must solve

$$X_0 + dX = \phi(X_0, \tau_0) + [D_X\phi(X_0, \tau_0)]dX + F(\phi(X_0, \tau_0))d\tau, \qquad (B4)$$

where $D_X\phi$ is a matrix with partial derivatives as its elements. The elements of $D_X\phi$ are evaluated by integrating

$$d(D_X\phi)/dt = (D_\phi F)(D_X\phi). \qquad (B5)$$

The solution of eq. B4 yields dX and $d\tau$ which are corrections to the initial guesses X_0 and τ_0. With X_0+dX and τ_0+$d\tau$ as new initial guesses, the procedure is repeated until it converges. Sparrow (1982) has given many practical hints that are useful in locating the periodic orbits with this method.

The stability of the periodic orbit also reduces to the stability of the fixed point on the corresponding Poincare map (Guckenheimer and Holmes, 1983). The stability analysis is thus performed by examining the eigenvalues of the linearized map, $D_X\phi(X_p, \tau_p)$, obtained by integrating eq. B5. One of the eigenvalues is always equal to one, corresponding to the direction of the flow. If the periodic orbit is stable, then all other eigenvalues have modulus less than one. If we have one or more eigenvalues with modulus greater than one, then the periodic orbit is unstable. As any particular parameter of the system is changed,

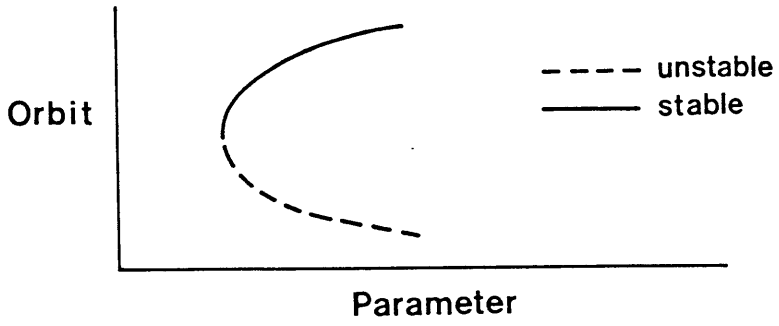

Figure B1. Saddle-node bifurcation.

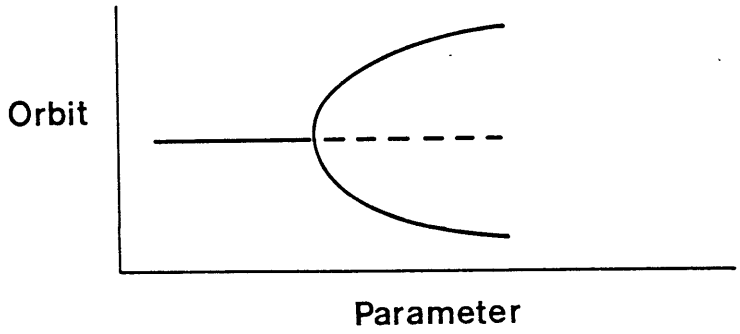

Figure B2. Symmetric saddle-node bifurcation.

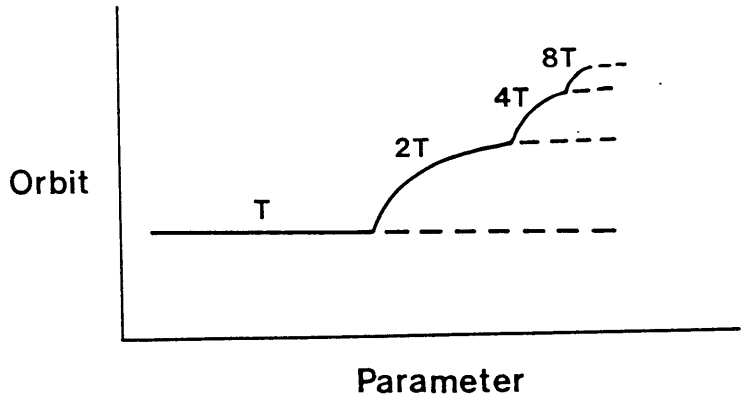

Figure B3. Period-doubling birfucation.

there are three ways in which the instability can occur: an eigenvalue may become greater than +1, less than -1 or a complex conjugate pair may have modulus greater than one. Each of these possibilities is usually associated with one particular bifurcation of the periodic orbit.

We now briefly describe four different bifurcations that can occur with a periodic orbit as a parameter is varied. The first one, known as the saddle-node bifurcation, involves a stable and an unstable periodic orbit (Fig. B1). As the parameter is varied, the two orbits, either both symmetric or both nonsymmetric, move closer and merge at the point of bifurcation. If we examine the eigenvalues of the linearized map, $D_X \phi$, we find that, for the stable orbit, a real positive eigenvalue increasingly approaches +1 at the bifurcation point. For the unstable orbit, a positive real eigenvalue greater than one decreases to exactly +1 at the bifurcation point.

The second bifurcation is analogous to the pitchfork bifurcation of the fixed point. This is called the symmetric saddle-node bifurcation in which a symmetric stable orbit looses stability (with a real positive eigenvalue of $D_X \phi$ becoming greater than +1) at the bifurcation point. Simultaneously, two non-symmetric stable orbits come into existence as shown in Fig. B2. The symmetric orbit continues to exist as an unstable solution after the bifurcation.

The third bifurcation is known as the period doubling bifurcation in which a stable periodic orbit of period T looses stability by creating a stable orbit with period 2T (Fig. B3). The loss of stability of the

orbit with period T involves a real eigenvalue of $D_x\phi$ becoming less than -1. The unstable orbit continues to exist as a solution beyond the bifurcation point. As the parameter is varied, the orbit with period 2T looses stability to an orbit with period 4T, and this sequence of period doubling continues until it culminates in chaos. The range of values of the parameter for each periodic window decreases after each period doubling bifurcation according to a universal relation discovered by Feigenbaum (1978).

The last bifurcation to be discussed is associated with a pair of complex conjugate eigenvalues of $D_x\phi$ having modulus greater than one after the bifurcation. This is the Hopf bifurcation of the periodic orbits. Guckenheimer and Holmes (1983) have discussed this and other bifurcations.

Appendix C LYAPUNOV EXPONENTS

A useful way of analyzing the chaotic behavior of a system quantitatively is to study the growth rate of small initial errors by comparing orbits originating from closely located points (Lorenz, 1965). The average divergence or convergence of nearby orbits are characterized by their Lyapunov exponents (Shimada and Nagashima, 1979).

Consider a dynamical system whose time evolution is described by

$$dX/dt = F(x), \tag{C1}$$

where X and F are N-dimensional vectors. The time evolution of an infinitesimal deviation Y from X is given by

$$dY/dt = GY. \tag{C2}$$

The matrix G has N rows and N columns and its elements are the partial derivatives $\partial f_i/\partial x_j$, where f_i and x_i are elements of F and X respectively. The solution of (C2) at time t_1 depends on the initial condition at t_0 and is given by

$$Y(t_1) = AY(t_0), \tag{C3}$$

where A is a square matrix. The elements of A are evaluated by integrating eq. C2 numerically.

As Lorenz (1965) has shown, an infinitesimal sphere of initial condition, given by $Y^TY=\varepsilon^2$, becomes an ellipsoid given by $Y^T(AA^T)^{-1}Y=\varepsilon^2$ at

time t_1. if $\varepsilon\gamma_1,\ldots,\varepsilon\gamma_N$ are the lengths of the semi-axes of the ellipsoid, then the Lyapunov exponents of the orbits are defined as

$$\lambda_i = \lim_{t_1\to\infty} (\log\gamma_i)/(t_1 - t_0) \qquad (C4)$$

where $\lambda_1 > \ldots\ldots > \lambda_N$. They are also the Lyapunov exponents of the system if the limits in eq. C4 are the same for all orbits.

The positive exponents correspond to axes which are expanding whereas the negative exponents correpsond to contracting directions. The sum $\sum \lambda_i$ is the time-averaged divergence of the vector field (equal to the exponential damping rate $-\sum b_i$ in eq. 2.23). Any attractor with at least one positive exponent is chaotic. If $\lambda_1=0$ and $\lambda_2<0$, the attractor is periodic. If the system has a fixed point as its attractor, then $\lambda_1<0$.

Lyapunov exponents have been used to estimate the fractal dimensions of chaotic attractors (Farmer et. al., 1983). A conjecture by Kaplan and Yorke (1979) gives a relation for the fractal dimension as

$$d = L + \sum_{i=1}^{L} \lambda_i / \lambda_{L+1} \qquad (C5)$$

where L is defined by the condition

$$\sum_{i=1}^{L} \lambda_i > 0 \qquad \text{and} \qquad \sum_{i=1}^{L+1} \lambda_i < 0.$$

The numerical techniques for computing all the Lyapunov exponents are described by Shimada and Nagashima (1979) and Benettin et al. (1980).

REFERENCES

Arnold, V. I., 1973: Ordinary Differential Equations. The MIT Press, Cambridge, Massachusetts, 280 pp.

Baer, F., 1977: Adjustments of initial conditions required to supress gravity oscillations in nonlinear flows. Contrib. Atmos. Phys., 50, 350-366.

Baer, F., and J. J. Tribbia, 1977: On complete filtering of gravity waves through nonlinear initialization. Mon. Wea. Rev., 105, 1536-1539.

Benettin, G., L. Galgani, A. Giorgilli, and J. -M. Strelcyn, 1980: Lyapunov characteristic exponents for smooth dynamical systems and for Hamiltonian systems: a method of computing all of them. Meccanica, 15, 9-30.

Charney, J. G., 1948: On the scale of atmospheric motions. Geofys. Publ., 17(2), 1-17.

------, 1955: The use of the primitive equations of motion in numerical prediction. Tellus, 7, 22-26.

------, 1973: Planetary fluid dynamics. In Dynamic Meteorology (P. Morel, ed.). Reidel, Dordrecht, Holland, 97-352 pp.

Curry, J. H., 1979: An algorithm for finding closed orbits. In Lecture Notes in Mathematics, 819, Springer-Verlag, Berlin, 111-120.

------, J. R. Herring, J. Loncaric, and S. A. Orszag, 1984: Order and disorder in two- and three-dimensional Benard convection. J. Fluid Mech., 147, 1-38.

------, and D. Winsand, 1985: Low-order intermediate models: Bifurcation, recurrence and solvability. Preprint, University of Colorado, Dept. of Mathematics.

Daley, R., 1981: Normal mode initialization. Rev. Geophys. Sp. Sci., 19, 450-468.

Errico, R. M., 1981: An analysis of interactions between geostrophic and

ageostrophic modes in a simple model. J. Atmos. Sci., 38, 544-553.

------, 1982: Normal mode initialization and the generation of gravity waves by quasi-geostrophic forcing. J. Atmos. Sci., 39, 573-586.

Farmer, J. D., E. Ott, and J. A. Yorke, 1983: The dimension of chaotic attractors. Physica D, 7, 153.

Feigenbaum, M. J., 1978: Quantitative universality for a class of nonlinear transformations. J. Stat. Phys., 19, 25-52.

Gent, P. R., and J. C. McWilliams, 1982: Intermediate model solutions to the Lorenz equations: Strange attractors and other phenomena. J. Atmos. Sci., 37, 1685-1699.

Guckenheimer, J., and P. Holmes, 1983: Nonlinear Oscillations, Dynamical Systems, and Bifurcations of Vector Fields. Springer-Verlag, New York, 453 pp.

Hirsch, M., and S. Smale, 1974: Differential Equations, Dynamical Systems, and Linear Algebra. Academic Press, Orlando, Florida, 359 pp.

Hoffman, R., 1981: Alterations of the climate of primitive equation model produced by filtering approximations and subsequent stochastic tuning and stochastic forcing. J. Atmos. Sci., 39, 3-13.

Kaplan, J., and J. Yorke, 1978: Chaotic behavior of multidimensional difference equations. In Lecture Notes in Mathematics, 730, Springer-Verlag, Berlin, 204-227.

Kasahara, A., 1982: Nonlinear normal mode initialization and the bounded derivative method. Rev. Geophys. Sp. Sci., 20, 385-397

Kopell, N., 1985: Invariant manifolds and the initialiation problem for some atmospheric equations. Physica D, 14, 203-215.

Kreiss, H.-O., 1979: Problems with different time scales for ordinary differential equations. SIAM J. Numer. Anal., 16, 980-998.

Leith, C. E., 1980: Nonlinear normal mode initialization and quasi-geostrophic theory. J. Atmos. Sci., 37, 958-968.

Lorenz, E. N., 1960: Maximum simplification of the dynamic equations. Tellus, 12, 243-254.

------, 1963: Deterministic nonperiodic flow. J. Atmos. Sci., 20, 130-141.

------, 1964: The problem of deducing the climate from the governing equations. Tellus, 16, 1-11.

------, 1965: A study of the predictability of a 28-variable atmospheric model. Tellus, 17, 321-333.

------, 1980: Attractor sets and quasi-geostrophic equilibrium. J. Atmos. Sci., 37, 1685-1699.

------, 1982: Low-order models of atmospheric circulations. J. Meteor. Soc. Jap., 60, 255-267.

Machenhauer, B., 1977: On the dynamics of gravity oscillations in a shallow water model, with application to normal mode initialization. Beitr. Phys. Atmos., 50, 253-271.

McWilliams, J. C., and P. R. Gent, 1980: Intermediate models of planetary circulations in the atmosphere and ocean. J. Atmos. Sci., 37, 1657-1678.

Pedlosky, J., 1979: Geophysical Fluid Dynamics. Springer-Verlag, New York, 624 pp.

Shimada, I., and T. Nagashima, 1979: A numerical approach to ergodic problem of dissipative dynamical systems. Prog. Theor. Phys., 61, 1605-1616.

Sparrow, C., 1982: The Lorenz equations: Bifurcations, Chaos, and Strange Attractors. Springer-Verlag, New York, 269 pp.